

Amphiboles: Crystal Chemistry

Frank C. Hawthorne

*Department of Geological Sciences
University of Manitoba, Winnipeg, Manitoba R3T 2N2, Canada
frank_hawthorne@umanitoba.ca*

Roberta Oberti

*Istituto di Geoscienze e Georisorse, Consiglio Nazionale delle Ricerche
I-27100 Pavia, Italy
oberti@crystal.unipv.it*

INTRODUCTION

This chapter provides an introduction to the crystal structure, crystal chemistry and chemical composition of the amphiboles. It is not an exhaustive treatment; it is intended as an introduction to the material discussed in the following chapters. More extensive discussion of many points is given in Hawthorne (1981, 1983a), although all later developments are discussed in some detail here. Published crystal-structure refinements are listed in Appendix I.

CHEMICAL FORMULA

The general chemical formula of the amphiboles can be written as



where A = Na, K, □, Ca, Li;
B = Na, Li, Ca, Mn²⁺, Fe²⁺, Mg;
C = Mg, Fe²⁺, Mn²⁺, Al, Fe³⁺, Mn³⁺, Ti⁴⁺, Li;
T = Si, Al, Ti⁴⁺;
W = (OH), F, Cl, O²⁻.

Minor elements such as Zn, Ni²⁺, Co²⁺, V³⁺, Sc, Cr³⁺ and Zr are also observed as C cations. In a mineral group as chemically complicated as the amphiboles, there are many problems connected with (1) the measurement of chemical composition, and (2) calculation of the chemical formula.

SOME ASPECTS OF CHEMICAL ANALYSIS

Chemical composition

The chemical composition of an amphibole is most commonly produced by electron microprobe analysis (EMPA). Instrumentation is very reliable and data reduction (including matrix corrections) are accurate. The main source of error is almost certainly errors in standards, a problem that can be dealt with in a simple but tedious fashion by cross-analyzing all standards. A more serious problem involves the components that cannot be analyzed (or analyzed accurately) by EMPA. Of particular relevance with regard to amphiboles are FeO vs. Fe₂O₃, Li₂O and H₂O, all of which occur commonly as highly variable constituents in amphiboles. We

will focus on microbeam methods of analysis where possible as these avoid heterogeneity and contamination problems.

Li_2O and H_2O . Li can be analyzed by Secondary-Ion Mass Spectrometry (SIMS) and Laser-Ablation Inductively Coupled Mass Spectrometry (LA-ICP-MS). Both these techniques are generally used for trace- and minor-element analysis, but procedures are now available which allow reasonably accurate ($\leq \pm 10\%$) quantification of Li at the major-element level. The presence of significant matrix effects (i.e., the various factors distorting the direct proportionality of secondary-ion intensity to element concentration) in SIMS analysis has been overcome using the voltage-offset technique (Ottolini et al. 1993) and by the construction of reliable matrix-matched calibration curves (Ottolini et al. 1993; Ottolini and Oberti 2000). LA-ICP-MS does not suffer from matrix effects, and thus allows more straightforward quantification of Li (also Be, B) with almost the same precision and accuracy as SIMS (Tiepolo et al. 2005). However, LA-ICP-MS analysis is more destructive than SIMS analysis, and the beam diameter used (20–40 μm) is not ideal for the determination of compositional zoning. Extensive work in the last 15 years has shown that Li is a much more common constituent in amphiboles that had hitherto been realized (e.g., Hawthorne et al. 1992, 1993, 1994, 1996b,c; Caballero et al. 1998, 2002; Oberti et al. 2000, 2003a,b, 2004). In particular, the results of structure refinement offer a rather straightforward way to detect the presence of both ^6Li and ^7Li . In the first case, the occurrence of Li lowers the refined site-scattering at the $M(4)$ site below 22 electrons per formula unit (epfu) (^6Li always being in solid solution with Na). In the second case, the refined site-scattering values at the $M(1)$ and $M(3)$ sites can be used in a diagnostic plot (Fig. 1), where samples falling in the area below the solid line contain ^7Li . If these tests are positive, and in the absence of the oxo component [namely, $^{\text{w}}\text{O}^{2-}$], more quantitative evaluations can be obtained

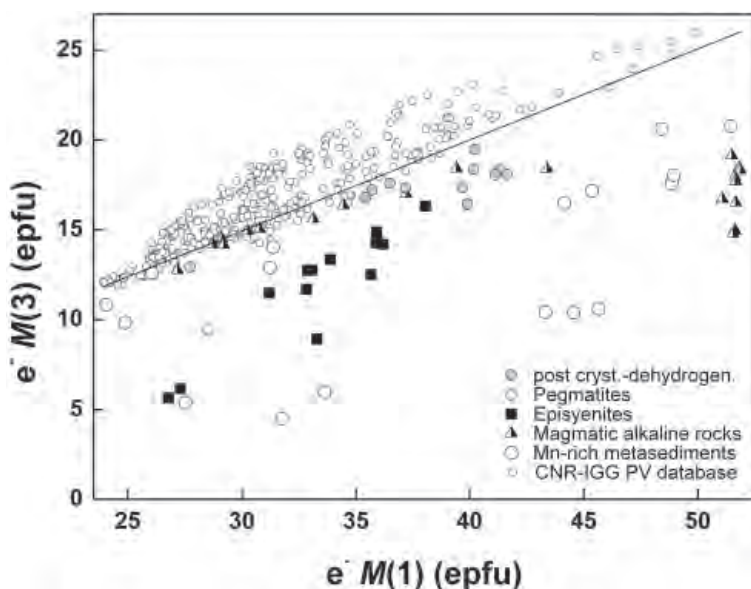


Figure 1. Diagnostic plot for the presence of ^7Li based on the results of structure refinement. Amphiboles fall in the upper left part of the plot, and their distance from the line represents Fe^{2+} -Mg order between the $M(1)$ and $M(3)$ sites. All ^7Li -bearing amphiboles fall well below the line by an amount proportional to the ^7Li content. Oxo-amphiboles, where the loss of H occurred after crystallization via oxidation of Fe^{2+} to Fe^{3+} at the $M(1)$ site, also plot slightly below the line (anti-order). This is an updated version of the plot first proposed by Hawthorne et al. (1994).

by a procedure of formula recalculation which takes into account chemical constraints based on present knowledge of Li crystal-chemistry in amphiboles (no Al at the *T* sites, highly charged cations ≤ 2.0 atoms per formula unit (apfu), and ${}^{\text{C}}\text{Li} \leq A$ -site occupancy; Oberti et al. 2003b).

H can be analyzed by SIMS (e.g., Ottolini et al. 1995; Ottolini and Hawthorne 2001), although matrix effects are quite large and the standard and sample matrices must match very closely, and by hydrogen-line extraction (e.g., Cosca et al. 1991). Considerable work has been done on microbeam analysis of H in amphiboles (e.g., Zanetti et al. 1996; Hawthorne et al. 1998, 2000, 2001; King et al. 1999, 2000; Oberti et al. 2000, 2003a,b, 2004; Caballero et al. 2002; Tait et al. 2005). Because SIMS analysis for H requires much analytical time (each sample must be degassed overnight) and careful check of matrix-matched standards, there have been attempts to relate H content (determined by SIMS) with changes in the structural parameters obtained by structure refinement of the same crystals. Work done at CNR-IGG-PV has shown that H content is inversely related to the *M*(1)-*M*(2) separation, a structural response to avoid repulsive interactions between the high-charge cations at these sites. However, the *M*(1)-*M*(2) distance is sensitive to the type of amphibole (e.g., it is different in richterite than in pargasite-kaersutite), but the methods work well within a given type of amphibole. More details are given in Oberti et al. (2007a).

FeO vs. Fe_2O_3 . Both FeO and Fe_2O_3 are often major constituents in amphiboles, and the absence of $\text{Fe}^{2+}:\text{Fe}^{3+}$ determination must be considered as a major deficiency in a chemical analysis of an amphibole. It is common to calculate the $\text{Fe}^{2+}:\text{Fe}^{3+}$ ratio in an amphibole using the method introduced by Stout (1972) which relies on the fact that expressing Fe as FeO introduces a different amount of oxygen into the formula calculation than expressing Fe as Fe_2O_3 .

The calculation of the unit-cell content of an amphibole is based on a fixed number of anions [e.g., 24 (O,OH,F), 23 (O)] or a fixed number of cations [e.g., 13 (Si,Al,Ti,Mg, $\text{Fe}^{2+},\text{Fe}^{3+},\text{Mn}^{2+}$), 15 (Si,Al,Ti,Mg, $\text{Fe}^{2+},\text{Fe}^{3+},\text{Mn}^{2+},\text{Ca}$)]. The corresponding number of cations or anions results from the requirement of electroneutrality. Alternatively, we can normalize the anions to a fixed number, normalize the cations to a fixed number, and then adjust the $\text{Fe}^{2+}:\text{Fe}^{3+}$ ratio for electroneutrality. Thus we can calculate the formula for 24 (O, OH, F) anions, and vary the $\text{Fe}^{2+}:\text{Fe}^{3+}$ ratio to get a specific number of cations (1) 13 (Si,Al, Ti,Mg, $\text{Fe}^{2+},\text{Fe}^{3+},\text{Mn}^{2+}$) and (2) 15 (Si,Al,Ti,Mg, $\text{Fe}^{2+},\text{Fe}^{3+},\text{Mn}^{2+},\text{Ca}$). Calculation (1) provides a maximum 'estimate' of the amount of Fe^{3+} and calculation (2) provides a minimum 'estimate' of the amount of Fe^{3+} ; normally, the mean is taken as the optimum value. Hawthorne (1983a) examined the efficacy of this method using the superior analysis of Leake (1968); the results are shown in Figure 2. There is no correlation at all between the observed and calculated values for Fe_2O_3 , indicating that no reliance can be placed on this type of calculation. Is there any point in doing such a calculation? Yes: while recognizing that the values are very inaccurate, inspection of Figure 2 indicates that the calculation does provide a better estimate than the alternative of not doing such a calculation: $\text{Fe}_2\text{O}_3 = 0.00$ wt%. Schumacher (1997, 2007) describes in detail the various methods by which such estimates may be made, and Schumacher (1991) shows the effects of the estimation of Fe^{3+} on various geothermobarometers.

What the above discussion does emphasize is the need to have a method for the determination of the $\text{Fe}^{2+}:\text{Fe}^{3+}$ ratio in an amphibole. This may be done in a variety of ways:

- (1) Crystal-structure refinement of amphiboles can determine the amount of Fe^{3+} in the structure by distinguishing between Fe^{2+} and Fe^{3+} on the basis of their different ionic radii ($r[\text{Fe}^{3+}] = 0.645 \text{ \AA}$, $r[\text{Fe}^{2+}] = 0.78 \text{ \AA}$) and their effect on the mean bondlength of the site(s) at which they occur. Useful constraints are based on electroneutrality, where H is determined analytically (or evaluated from some structural parameters) and the content of the *A* site is quantified based on EMP analysis and site-scattering refinement.

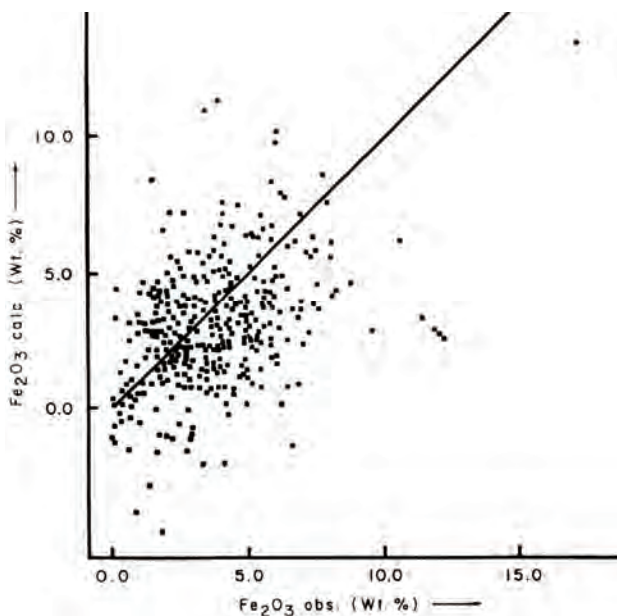


Figure 2. Observed and calculated contents of Fe₂O₃ using the superior analyses of Leake (1968); the diagonal line indicates a 1:1 relation (from Hawthorne 1983a).

- (2) Mössbauer spectroscopy (Bancroft 1973; Hawthorne 1983b, 1988; Murad and Cashion 2004; Dyar et al. 2006) is responsive to the valence state of Fe (Fig. 3) and has been used extensively for determining the Fe²⁺:Fe³⁺ ratio in amphiboles (e.g., Bancroft and Brown 1975; Dyar et al. 1993; Enders et al. 2000; Gunter et al. 2003). Milli-Mössbauer spectroscopy (McCammon 1994) can determine the Fe²⁺:Fe³⁺ ratio of a single grain of a mineral, and this method has been used for amphiboles (Sokolova et al. 2000a,b, 2001; Uvarova et al. 2005). A significant problem with the Mössbauer method is lack of information on the recoil-free fractions of Fe²⁺ and Fe³⁺ in minerals (see discussion by Dyar et al. 2006). Eeckhout and De Grave (2003) report measurements on riebeckite indicating that the recoil-free fraction for Fe³⁺ is significantly larger than that for Fe²⁺. As the recoil-free fractions of the Fe²⁺ and Fe³⁺ are usually assumed to be unity, this assumption introduces errors in the determination of Fe²⁺:Fe³⁺ ratios that may be of the order of 10%. However, determination of the recoil-free fractions in amphiboles will remove this error.
- (3) Milli-XANES (X-ray Absorption Near-Edge Structure) spectroscopy can measure the Fe²⁺:Fe³⁺ ratio (Fig. 4) with a spot size of a few microns, although reasonably good results on amphiboles have been obtained with a beam size of ~ 50 μm (Delaney et al. 1996). Dyar et al. (2002) have shown that orientation effects are a major source of error in determining Fe²⁺:Fe³⁺ ratios in amphiboles, and quote a probable accuracy of ± 20% in randomly oriented crystals. However, by using oriented samples and standards, they suggest that an accuracy of < 2-3% absolute is possible.
- (4) EELS (Electron Energy Loss Spectroscopy) - ELNES (Energy Loss Near-Edge Spectroscopy) can determine Fe²⁺:Fe³⁺ ratios (Fig. 5) at a submicron scale (Garvie and Buseck 1998; van Aken and Liebscher 2002) with quoted accuracies of 0.02. However, electron-beam damage can be a problem, but good values can be obtained at low beam intensity (Garvie et al. 2004).

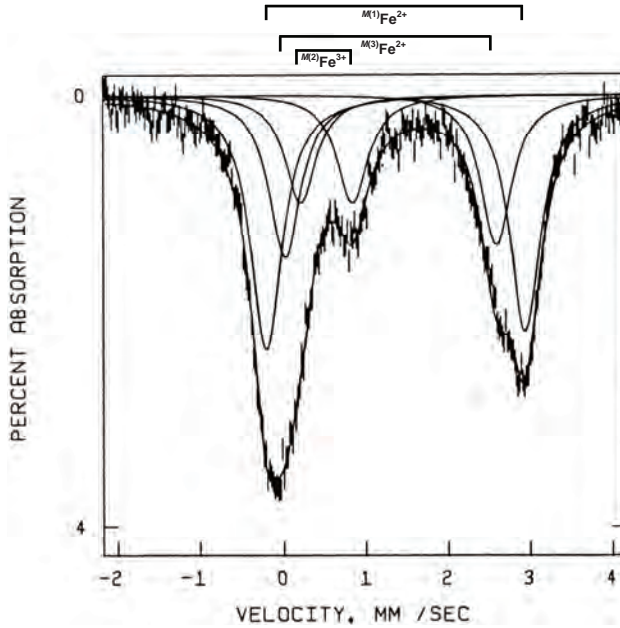


Figure 3. The Mössbauer spectrum of ferrotschermakite, with the absorptions marked (from Hawthorne 1988).

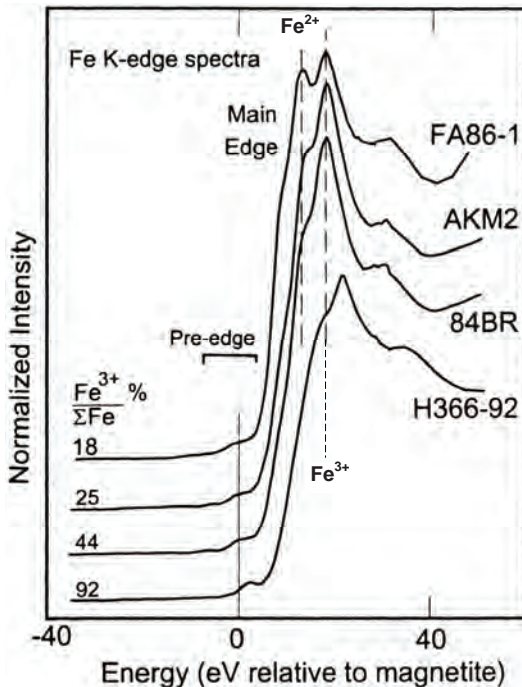


Figure 4. Milli-XANES spectra of several amphiboles, showing the absorptions due to Fe^{3+} and Fe^{2+} and the Fe^{3+}/Fe value for each amphibole. [Used by permission of The Geochemical Society, from Delaney et al. (1996), Special Publication No 5 (Mineral Spectroscopy: A Tribute to Roger G. Burns), Fig. 1, p. 167.]

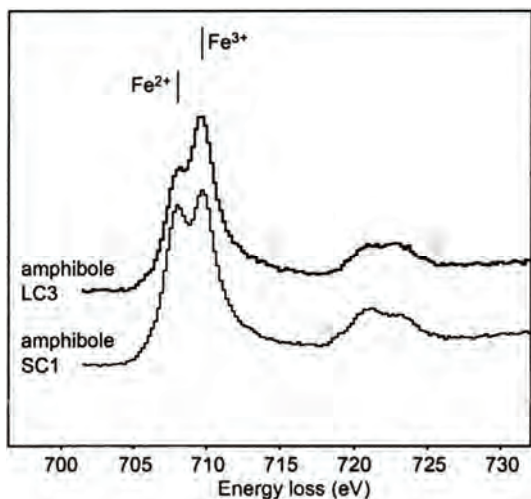


Figure 5. EELS spectra of two amphiboles, showing the absorptions due to Fe^{3+} and Fe^{2+} . [Used by permission of Macmillan Publishers Ltd, from Garvie and Buseck (1998), *Nature*, Vol. 396, Fig. 3, p. 669].

- (5) The Flank method optimizes use of the electron microprobe to use X-ray spectroscopy to determine $\text{Fe}^{2+}:\text{Fe}^{3+}$ ratios via the positions and intensities of the FeL_α and FeL_β peaks as a function of valence state (Höfer et al. 1994). Enders et al. (2000) have applied/tested the method extensively for sodic amphiboles, and have shown that it can be reasonably accurate down to an $\text{FeO}(\text{total})$ content of 6–8 wt%. However, they also suggest that the calibration procedures are particularly laborious and complicated, suggesting that it will not find use as a routine method for $\text{Fe}^{2+}:\text{Fe}^{3+}$ determination.

None of these methods can be considered as routine in the sense that they are widely available in the community or are simple to use. *Crystal-structure refinement* is the most widely available method, but in view of the fact that one gets a large amount of crystal-chemical information at the same time, it seems wasteful to do this just for one piece of information. Moreover, the method cannot be used for poorly crystalline, microcrystalline or noncrystalline materials, and the instrumentation is relatively expensive. *Milli-Mössbauer spectroscopy* provides a much more economical method, but facilities are very few, particularly in the Earth Science community. *Micro-XPS* currently requires access to synchrotron radiation, and unless conventional laboratory sources increase greatly in intensity, this will not become a standard facility in mineral-analysis laboratories. In our view, the most viable method is milli-Mössbauer spectroscopy. The cost of an electron microprobe is currently approaching US \$1M, and yet they produce amphibole analyses of only limited use. Addition of a milli-Mössbauer facility (approximate cost US \$50,000) to an electron-microprobe lab will result in amphibole (and other mineral) analyses that are far more accurate than anything routinely produced at the present time.

Summary

One thing to stress about the chemical composition and chemical formulae of amphiboles is the importance of complete chemical analyses. We know a lot about the crystal-chemical and chemical characteristics of amphiboles, and partial chemical compositions are no longer very useful in either Mineralogy or Petrology. To be useful, an amphibole *must* be analyzed for Fe^{3+} as well as Fe^{2+} (i.e., FeO). Indeed, in studies of kaersutite, measurement of $\text{Fe}^{3+}/(\text{Fe}^{2+} + \text{Fe}^{3+})$ (e.g., McGuire et al. 1989, 1991; Dyar et al. 1992, 1993; King et al. 1999; Popp et al. 1995, 2006; Nasir and Al-Rawas 2006) has long been considered essential. Furthermore, if it is suspected that Li is present and/or H is not given by $[\text{OH} + \text{F} + \text{Cl}] = 2$ apfu (either from the paragenesis or unusual aspects of the calculated formula), Li and H should be measured

too. Facilities to do this type of analysis are not common; however, this is an indication that we should be pushing for funding for such instrumentation (electron microprobes were rare commodities once upon a time, as for example, SIMS and Mössbauer instruments are today).

CALCULATION OF THE CHEMICAL FORMULA

This is one of the most important issues connected with deriving an accurate chemical formula for an amphibole, and the details of how it is done are often poorly understood. The chemical composition of a mineral is presented as weight % of the oxides of the elements (except for the halogens) present. Classically, the contents of the unit cell were normalized on the density of the mineral; this procedure is not followed now due to the difficulty of measuring accurately the density of most minerals. Present methods are all based on scaling the ratios of the cations and/or anions to some quantity that one believes is constant and known within the unit cell. Current methods are outlined below; Hawthorne (1983a) and Schumacher (1997) give a more detailed discussion of these methods.

24 (O, OH, F, Cl)

This method assumes an anion content of 24 apfu (atoms per formula unit). Presuming that there are no anion vacancies in amphiboles, this method either (1) requires that H (as H₂O) is determined, or (2) assumes that (OH,F,Cl) = 2 apfu. A slightly more complicated variation has been introduced where (OH,F,Cl) < 2 apfu and an amount of O²⁻ occurs at the O(3) site, entering the structure *via* the substitution $M^{(1)}Ti^{4+} + O^{(3)}O^{2-} = M^{(1)}(Mg, Fe^{2+}) + O^{(3)}(OH)^-$. Here, the formula is still normalized on 24 (OH,F,Cl) anions, but (OH,F,Cl) = 2 - 2 × $M^{(1)}Ti^{4+}$ apfu; the issue is whether or not all ⁶⁷Ti occurs at the M(1) site or not, and this is not currently known (see Oberti et al. 2007a).

The effect of the occurrence of O²⁻ at the O(3) site in the unit formula of an amphibole is illustrated in Table 1 for a strongly dehydrogenated sodic amphibole rich in Ti (which will be soon presented to IMA-CNMMN for approval as “ferri-obertiite”) (Hawthorne et al. 1998) in which the H content was determined by SIMS and the Fe³⁺ content was determined from the crystal structure. Where all components

Table 1. Normalization of a Ti-rich oxygenian sodic amphibole* formula (1) using all components determined and a 24 (O,OH,F) normalization, and (2) using OH + F = 2.0 apfu and Fe³⁺ estimated after the method of Papike et al. (1974).

SiO ₂		52.47
Al ₂ O ₃		0.09
TiO ₂		6.51
Fe ₂ O ₃		4.54
FeO		18.43
MnO		0.15
MgO		5.74
CaO		0.90
Na ₂ O		8.70
K ₂ O		1.51
Li ₂ O		0.17
F		0.51
H ₂ O		0.58
O=F		<u>-0.21</u>
Total		100.09
	(1)	(2)
Si	7.993	7.874
Al	<u>0.007</u>	<u>0.016</u>
ΣT	8.000	7.890
Al	0.009	—
Fe ³⁺	0.520	—
Fe ²⁺	2.348	2.815
Mn	0.019	0.019
Ti	0.746	0.746
Mg	1.303	1.284
Li	<u>0.104</u>	<u>0.103</u>
ΣC	5.049	4.967
Ca	0.147	0.145
Na	<u>1.853</u>	<u>1.855</u>
ΣB	2.000	2.000
Na	0.716	0.702
K	<u>0.293</u>	<u>0.289</u>
ΣA	1.009	0.991
OH	0.589	1.8
F	0.246	0.2
Σ	0.835	2.0
O	1.163	—

* crystal 745 of Hawthorne et al. (1998)

were determined, formula (1), calculated by anion normalization to 24(O,OH,F), has A-, C- and T-cation sums that are in accord with the crystal structure (i.e., $\Sigma T = 8$, $\Sigma C \geq 5$, $\Sigma \leq 1$), and the high Ti content is accompanied by a high O^{2-} content at O(3) as occurs in this type of amphibole (Hawthorne et al. 1998). Assuming $OH + F = 2.0$ apfu, normalizing to 24(O,OH,F) anions and calculating the Fe^{3+} content by the method of Papike et al. (1974) gives formula (2) in Table 1. For formula (2), the T- and C-sums are too low, and no Fe^{3+} was calculated as present. Of course, the example shown in Table 1 is extreme, as it is an oxygenian amphibole; however, the formula still appears reasonable when compared to formulae given in the literature, indicating that major errors can be introduced by inappropriate normalization schemes.

23 (O)

This calculation assumes that $(O,OH,F,Cl) = 2$ apfu and is similar to the 24 (O,OH,F,Cl) where it is also assumed that $(OH,F,Cl) = 2$ apfu. The difference between these two calculations [in which each assumes that $(O,OH,F,Cl) = 2$ apfu] is that the 24 (O,OH,F,Cl) calculation also produces the required wt% of H_2O and allows evaluation of the total wt% oxide of the chemical composition.

13 cations

This method assumes that $[Si + Al + Ti + Fe^{3+} + Fe^{2+} + Mn^{2+} + Mg + (Cr, V \dots)] = 13$ apfu [i.e., that these cations occupy the $T(1)$, $T(2)$, $M(1)$, $M(2)$ and $M(3)$ sites that contain the T and C cations]. The assumption that Fe^{2+} , Mn^{2+} and/or Mg do not occupy the $M(4)$ site (i.e., are not B cations) is obviously not appropriate for the magnesium-iron-manganese-lithium amphiboles (Hawthorne and Oberti 2007). However, it is also not appropriate for the other groups of amphiboles either, as detailed structural and chemical characterization of many calcic and sodic amphiboles (as well as in clinopyroxenes) has shown the common presence of small divalent cations at $M(4')$ [a site occurring in the $M(4)$ cavity with local [6+2]-coordination similar to that of the $M(4)$ cation(s) in the magnesium-iron-manganese-lithium amphiboles; for more detail, see Rossi et al. (1987) and Oberti and Ghose (1993)]. This method of formula calculation is not recommended.

15 cations

This method assumes that either $[Si + Al + Ti + Fe^{3+} + Fe^{2+} + Mn^{2+} + Mg + Ca + Na + (Cr, V \dots)] = 15$ apfu or $[Si + Al + Ti + Fe^{3+} + Fe^{2+} + Mn^{2+} + Mg + Ca + (Cr, V \dots)] = 15$ apfu [i.e., that these cations occupy the $T(1)$, $T(2)$, $M(1)$, $M(2)$, $M(3)$ and $M(4)$ sites that contain the T, C and B cations]. The assumption is either that (1) all Na occurs at the $M(4)$ site, or that (2) all Na occurs at the A site. Neither of these assumptions are generally applicable (although they may hold for very specific compositions).

16 cations

This method assumes that all cations fully occupy all sites in the amphibole [i.e., that there are no vacancies at any sites, including the A site]. Although this condition may hold in some amphiboles, it is not a recommended scheme for formula calculation.

Summary

Amphibole formulae should always be calculated based on 24 (O,OH,F,Cl), unless justification can be given concerning the site occupancies on which any alternate scheme used is based.

AMPHIBOLES: CRYSTAL STRUCTURE

The amphibole structure consists of two principal elements, a double chain of corner-sharing tetrahedra and a strip of edge-sharing octahedra, both of which extend in the *c*-direction

(Fig. 6). Both the tetrahedrally coordinated sites and the tetrahedra themselves are denoted by T , and the octahedrally coordinated sites and the octahedra are denoted by M . There are two topologically distinct types of tetrahedra in the double chain that are designated $T(1)$ and $T(2)$, and three distinct types of octahedra that are designated $M(1)$, $M(2)$ and $M(3)$ (Fig. 6). At the junction of the strip of octahedra and the chain of tetrahedra is the $M(4)$ site, and below the hexagonal ring of tetrahedra is the A site at the center of a large cavity.

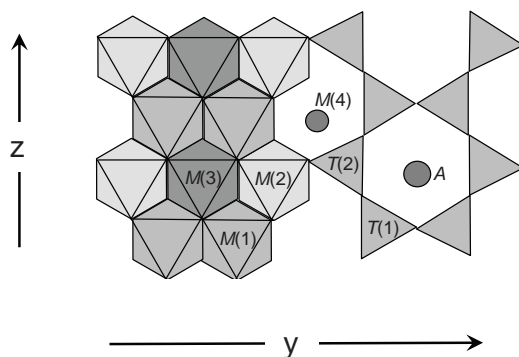


Figure 6. An idealized model of the amphibole structure *sensu lato* showing the chain of tetrahedra, the strip of octahedra, the $M(4)$ site and the A site.

Space groups

There are (currently) six known structural variants of the amphibole arrangement; the space groups and representative amphibole compositions are given in Table 2. We may divide these structures into two types: (1) those that involve different stacking sequences in the a -direction ($C2/m$, $Pnma$ and $Pnmm$), and (2) those that are derivatives of (1) and involve differences in coordination ($P2_1/m$) and/or topochemistry ($P2/a$, $C\bar{1}$). All centrosymmetric subgroups of $C2/m$, $Pnma$ and $Pnmm$ are listed in Table 3; these are possible space groups for amphiboles with the same unit cell as the structure with the parent space group. As is apparent from comparison of Tables 2 and 3, there are several structures that are symmetrically possible but have not yet been found. The triclinic $C\bar{1}$ structure has a tripled b cell-dimension relative to all other amphibole structures, and requires the presence of a third (OH) group; thus it occurs only for a very unusual synthetic-amphibole composition.

Cell dimensions

The $C2/m$, $P2_1/m$ and $P2/a$ structures have (grossly) similar (monoclinic) cell dimensions. The $P2_1/m$ structure is restricted to Mg- and possibly ^BLi -rich amphiboles of the magnesium-iron-manganese-lithium group and to $B_2 = \text{LiMg}$ and NaMg synthetic amphibole (cf. Oberti et al. 2007b); hence cell dimensions show a restricted range. The $P2/a$ structure occurs for just a single (known) composition. In contrast, the $C2/m$ structure shows a wide range of composition and a correspondingly wide range of cell dimensions. The situation is similar for the orthorhombic amphiboles; the $Pnmm$ structure is restricted to Mg-rich amphiboles of the magnesium-iron-manganese-lithium group and the cell dimensions show only a restricted range, whereas the $Pnma$ structure shows a wide range of composition. The $C\bar{1}$ structure is known only for a single (synthetic) composition and is unique among the amphibole structure-types in that it has a b axis that is tripled relative to the b axes in the other structure types. A more detailed discussion of cell dimensions is given later in this chapter.

Site nomenclature

Figure 6 shows the basic cation-site nomenclature of the amphibole arrangement. However, the different space groups of the structures give rise to sites that are crystallographically distinct from one structure to another. To facilitate comparison *between* amphibole structures, it is important to retain this distinction in the site nomenclature while maintaining some sort of congruence for analogous sites in different structures. Hawthorne (1983a) developed such a site nomenclature (Table 4) and Cámara et al. (2004) applied analogous reasoning to formulate a site nomenclature for the $C\bar{1}$ amphibole structure. Here, crystallographic sites are written in

Table 2. Observed amphibole space-groups and representative cell dimensions.

Space group	Amphibole	<i>a</i> (Å)	<i>b</i> (Å)	<i>c</i> (Å)	β (°)	<i>V</i> (Å ³)
<i>C2/m</i>	calcic amphiboles, sodic-calcic amphiboles, alkali amphiboles, monoclinic <i>C</i> -centered (Mg-Fe-Mn-Li) amphiboles	9.35–10.14	17.58–18.40	5.26–5.37	101.8–105.7	846–948
<i>P2₁/m</i>	cummingtonite	9.48–9.51	17.99–18.13	5.28–5.31	102.0–102.1	881–893
<i>P2/a</i>	joesmithite	9.92	17.95	5.24	106.0	897
<i>Pnma</i>	orthorhombic Mg-Fe-Mn amphiboles, holmquistite	18.52–18.62	17.80–18.03	5.26–5.30	–	1738–1777
<i>Pnmm</i>	protoamphibole	9.33–9.43	17.88–18.39	5.29–5.35	–	882–925
<i>C$\bar{1}$</i>	Na Na ₂ Mg ₅ Si ₈ O ₂₁ (OH) ₃	9.88	54.08	5.28	103.07*	2748

For *C $\bar{1}$* : α = 90.05, γ = 89.96°

italics (e.g., *T*(1), *M*(1), *A*, *A*(*m*)), the general formula is written in normal type, e.g., A B₂ C₅ T₈ O₂₂ W₂, and constituent cations are considered as A, B, C or T: thus in end-member tremolite, B₂ = Ca₂, whereas in calcic amphiboles, Ca, Na, Mg, Fe²⁺, Mn²⁺, Li are B cations. This will hopefully remove ambiguity when using letter symbols for the amphiboles.

The *C2/m* amphibole structure

A schematic representation of the *C2/m* structure type is shown in Figure 7. There are two distinct *T* sites that are occupied by the T cations, *T*(1) and *T*(2), that are tetrahedrally coordinated and link to form one distinct type of double-chain of tetrahedra. The *T*(1) site is coordinated by O(1), O(5), O(6) and O(7), and the *T*(2) site is coordinated by O(2), O(4), O(5) and O(6). In the double chain, adjacent *T*(1) and *T*(2) tetrahedra link through O(5) and O(6) oxygen atoms, and adjacent *T*(1) tetrahedra link through O(7) oxygen atoms. The *T*(1) and *T*(2) tetrahedra alternate along the length of the double chain, and the *T*(1) tetrahedra bridge across the double chain.

There are three distinct octahedrally coordinated *M* sites that are occupied by the C cations, and have point symmetries 1, 1 and *2/m*, respectively. The *M*(1) site is coordinated by two O(1) and two O(2) oxygen atoms, and by two O(3) W anions (OH,F,Cl,O) in a *cis* arrangement. The *M*(2) site is coordinated by two O(1), two O(2) and two O(4) oxygen atoms, and the *M*(3) site is coordinated by four O(1) oxygen atoms and two O(3) W anions in a *trans* arrangement. Within the strip of octahedra, there is extensive sharing of edges between the *M*(1), *M*(2) and *M*(3) octahedra. The double chain of tetrahedra links to the strip of octahedra in the *b*-direction through *T*(2)-*M*(2) linkage *via* common O(4) oxygen atoms, and in the *a*-direction through *T*(1) and *T*(2) linkage to the strip *via* common O(1) and O(2) oxygen atoms.

The *M*(4) site is situated at the periphery of the strip of octahedra (Figs. 6, 7), has point symmetry 2, and is occupied by B cations. It is surrounded by eight oxygen atoms arranged as a square antiprism: O(2) × 2, O(4) × 2, O(5) × 2, and O(6) × 2, not all of which necessarily bond to the central cation. Note that the cation occupancy of this site (1) is the primary feature on which the major groups of amphiboles are classified, and (2) correlates strongly with the space-group variations in amphiboles.

The *A* site occurs at the center of a large cavity between the back-to-back double-chains of the structure (Fig. 7). The center of the cavity has point symmetry *2/m*, but the *A* cations

Table 3. Subgroups of $C2/m$, $Pnma$ and $Pnmn$ *.

$C2/m$	$Pnma$	$Pnmn$
Monoclinic (Y) [†]	Orthorhombic	Orthorhombic
$P2_1/a$	$Pn2_1a$	$Pn2n$
$P2_1/m$	$Pnm2_1$	$Pnm2_1$
$P2/a$	$P2_1ma$	$P2_1mn$
$P2/m$	$P2_12_12_1$	$P2_12_12_1$
$C2$		
Cm	Monoclinic (X)	Monoclinic (X)
$P2_1$	$P2_1/n$	$P2_1/n$
$P2$	$P2_1$	$P2_1$
Pm		
	Monoclinic (Y)	Monoclinic (Y)
Triclinic [‡]	$P2_1/m$	$P2/m$
$C\bar{1}$	$P2_1$	$P2$
$C\bar{1}$	Pm	Pm
$P\bar{1}$		
$P\bar{1}$	Monoclinic (Z)	Monoclinic (Z)
$P\bar{1}$	$P2_1/a$	$P2_1/n$
	$P2_1$	$P2_1$
	Pa	Pn
	Triclinic	Triclinic
	$P\bar{1}$	$P\bar{1}$
	$P1$	$P1$

* bold = reported as amphibole space-groups

† signifies unique axis

‡ repetition of space-group symbol is indicative of different origins

Table 4. Site-nomenclature scheme for amphibole structure-types (for the $C\bar{1}$ structure, see text).

	$C2/m$	$P2_1/m$	$P2/a$	$Pnma$	$Pnmn$
tetrahedrally coordinated sites	$T(1)$	$T(1A)$ $T(1B)$	$T(1)A$ $T(1)B$	$T1A$ $T1B$	$T1$
	$T(2)$	$T(2A)$ $T(2B)$	$T(2)A$ $T(2)B$	$T2A$ $T2B$	$T2$
octahedrally coordinated sites	$M(1)$	$M(1)$	$M(1)A$ $M(1)B$	$M1$	$M1$
	$M(2)$	$M(2)$	$M(2)A$ $M(2)B$	$M2$	$M2$
	$M(3)$	$M(3)$	$M(3)$	$M3$	$M3$
cubic antiprismatic sites	$M(4)$	$M(4)$	$M(4)A$ $M(4)B$	$M4$	$M4$
[12] cavity*	A	A	$A(2)$	A	A
non-bridging anion sites	$O(1)$	$O(1A)$ $O(1B)$	$O(1)A$ $O(1)B$	$O1A$ $O1B$	$O1$
	$O(2)$	$O(2A)$ $O(2B)$	$O(2)A$ $O(2)B$	$O2A$ $O2B$	$O2$
	$O(3)$	$O(3A)$ $O(3B)$	$O(3)$	$O3A$ $O3B$	$O3$
	$O(4)$	$O(4A)$ $O(4B)$	$O(4)A$ $O(4)B$	$O4A$ $O4B$	$O4$
bridging anion sites	$O(5)$	$O(5A)$ $O(5B)$	$O(5)A$ $O(5)B$	$O5A$ $O5B$	$O5$
	$O(6)$	$O(6A)$ $O(6B)$	$O(6)A$ $O(6)B$	$O6A$ $O6B$	$O6$
	$O(7)$	$O(7A)$ $O(7B)$	$O(7)$	$O7A$ $O7B$	$O7$

* the more complex nomenclature used to describe the positional disorder of cations occupying this site is described in the section on the A site.

actually occupy off-centered sites of point symmetry 2 or m , $A(2)$ and $A(m)$, respectively. The cavity is surrounded by twelve oxygen atoms: $O(5) \times 4$, $O(6) \times 4$, and $O(7) \times 4$, but not all of these always bond to the A cations.

The $P2_1/m$ amphibole structure

A schematic representation of the $P2_1/m$ structure type is shown in Figure 8. There are four distinct T -sites that are occupied by the T cations, $T(1A)$, $T(1B)$, $T(2A)$ and $T(2B)$, that are tetrahedrally coordinated and link to form two distinct types of double-chain of tetrahedra, the A-chain and the B-chain. Coordination and linkage of these T sites is analogous to that in the $C2/m$ structure, cations labeled A always bonding to anions labeled A, and likewise for the atoms labeled B: thus $T(1A)$ is coordinated to $O(1A)$, $O(5A)$, $O(6A)$ and $O(7A)$, and the $T(1A)$ and $T(2A)$ tetrahedra link along the length of the A-chain. The A- and B-chains face each other back-to-back across the A cavity, and the B-chain is much more kinked (less extended) than the A-chain (Fig. 8).

There are three distinct M sites that are occupied by the C cations, $M(1)$, $M(2)$ and $M(3)$ with point symmetries 1, 1 and m , respectively. As can be seen in Figure 8, the oxygen atoms on one side of the octahedron strip are A-type oxygen atoms and the oxygen atoms on the other side of the octahedron strip are B-type oxygen atoms, and the $M(1,2,3)$ sites bond to both A- and B-type oxygen atoms. The $M(4)$ site has point symmetry 1 and eight adjacent oxygen atoms, however, the cations occupying this site may not bond to all of these surrounding oxygen atoms, and the existence of this structure type seems to depend on the bonding requirements of the $M(4)$ cation and the surrounding oxygen atoms, especially the aggregate ionic radius of the $M(4)$ cations. All natural amphiboles with this structure type have an unoccupied A cavity (and root composition $\square \text{Mg}_2 \text{Mg}_5 \text{Si}_8 \text{O}_{22}(\text{OH})_2$, cummingtonite). However, recent work has shown that synthetic amphiboles of the form $\text{Na B}_2 \text{Mg}_5 \text{Si}_8 \text{O}_{22}(\text{OH})_2$ with $\text{B}_2 = (\text{Na,Li})\text{Mg}$ have $P2_1/m$ symmetry at or below room temperature, and undergo a phase transition to the $C2/m$ structure at higher temperature (cf. Oberti et al. 2007b; Welch et al. 2007). In this case, the A cation occupies a site A with point symmetry 1 which is displaced $\sim 0.25 \text{ \AA}$ from the center of the cavity along a line joining the two farthest $O7A$ and $O7B$ atoms (Cámara et al. 2003).

The $P2/a$ amphibole structure

A schematic representation of the $P2/a$ structure type is shown in Figure 9. There are four distinct T sites that are occupied by the T cations, $T(1)A$, $T(1)B$, $T(2)A$ and $T(2)B$, that are tetrahedrally coordinated and link to form two distinct types of double-chain of tetrahedra, the A-chain and the B-chain. Coordination and linkage of these T sites is analogous to that in the $P2_1/m$ structure, cations labeled A always bonding to anions labeled A, and likewise for the atoms labeled B (Fig. 9).

There are five distinct M sites that are occupied by the C cations, $M(1)A$, $M(1)B$, $M(2)A$, $M(2)B$ and $M(3)$, all of which have point symmetry 2. As can be seen in Figure 9, the oxygen atoms on one side of the octahedron strip are A-type oxygen atoms and the oxygen atoms on the other side of the octahedron strip are B-type oxygen atoms, with the exception of the $O(3)$ and $O(7)$ oxygen atoms, for each of which there is only one symmetrically distinct site. There are two distinct $M(4)$ sites, $M(4)A$ and $M(4)B$, each of which has point symmetry 2 and eight adjacent oxygen atoms to which the constituent cations are bonded. The A cation occupies the $A(2)$ site, an off-centered site within the A cavity that is displaced toward the $T(1)B$ site that is occupied by Be in the only amphibole with this space-group symmetry: joesmithite, $\text{Pb}^{2+} \text{Ca}_2 \text{Mg}_5 (\text{Si}_6 \text{Be}_2) \text{O}_{22} (\text{OH})_2$.

The $Pnma$ amphibole structure

A schematic representation of the $Pnma$ structure type is shown in Figure 10. There are four distinct T sites that are occupied by the T cations, $T1A$, $T1B$, $T2A$ and $T2B$, that are tetrahedrally coordinated and link to form two distinct types of double-chain of tetrahedra, the A-chain

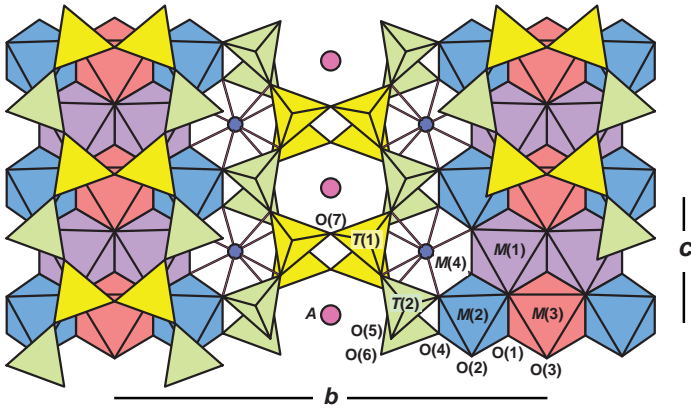


Figure 7. The $C2/m$ amphibole structure projected onto (100); polyhedra: $T(1)$ = yellow, $T(2)$ = pale green, $M(1)$ = mauve, $M(2)$ = blue, $M(3)$ = red; sites: $M(4)$ = blue circle, A = fuchsia circle.

Figure 8. The $P2_1/m$ amphibole structure projected onto (100); polyhedra: $T(1A)$ = bright yellow, $T(2A)$ = bright green, $T(1B)$ = pale yellow, $T(2B)$ = pale green, $M(1)$ = mauve, $M(2)$ = blue, $M(3)$ = red; sites: $M(4)$ = blue circle.

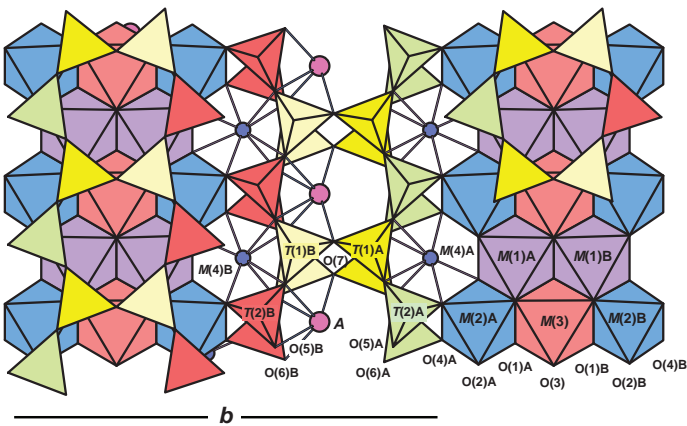
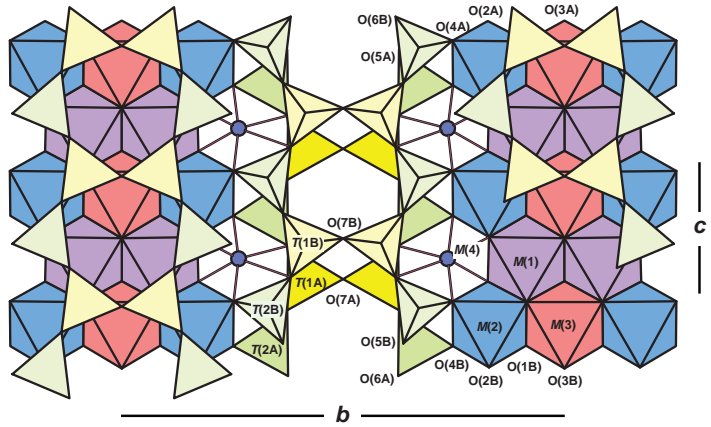


Figure 9. The $P2/a$ amphibole structure projected onto (100); polyhedra: $T(1)A$ = bright yellow, $T(2)A$ = bright green, $T(1)B$ = red, $T(2)B$ = pale green, $M(1)A$ = $M(1)B$ = mauve, $M(2)A$ = $M(2)B$ = dark blue, $M(3)$ = red; sites: $M(4)A$ = $M(4)B$ = blue circle.

and the B-chain. As with the $P2_1/m$ structure, cations labeled A always bond to anions labeled A, and likewise for the atoms labeled B.

There are three distinct M sites that are occupied by the C cations, $M1$, $M2$ and $M3$, with point symmetries 1, 1 and $2/m$, respectively. As with the $P2_1/m$ structure, the A-type cations are on one side and the B-type cations are on the other side of the strip of octahedra. The $M4$ site has point symmetry 2 and is occupied by the B cations. It is surrounded by an antiprism of eight oxygen atoms not all of which necessarily bond to the central cation. The A site occurs at the center of the cavity between the back-to-back double-chains of the structure (Fig. 10). The center of the cavity has point symmetry m , and unlike in the $C2/m$ structure, the A cations actually occupy the special position at the center of the cavity.

The $Pnmm$ amphibole structure

A schematic representation of the $Pnmm$ structure type is shown in Figure 11. There are two distinct T sites that are occupied by the T cations, $T1$ and $T2$, that are tetrahedrally coordinated

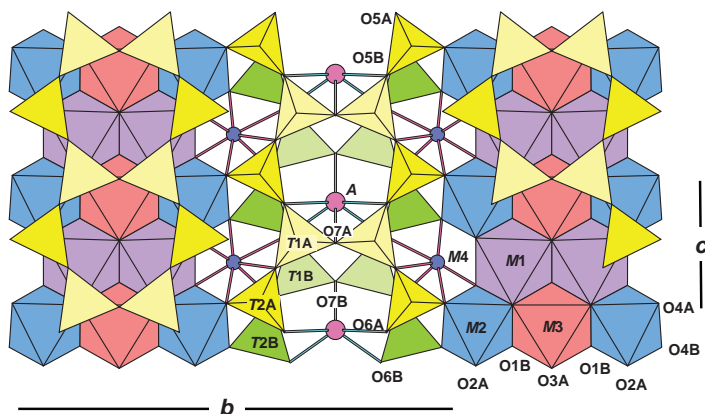


Figure 10. The $Pnma$ amphibole structure projected onto (100); polyhedra: $T1A$ = pale yellow, $T2A$ = bright yellow, $T1B$ = pale green, $T2B$ = bright green, $M1$ = mauve, $M2$ = blue, $M3$ = red; sites: $M4$ = blue circle, A = fuchsia circle.

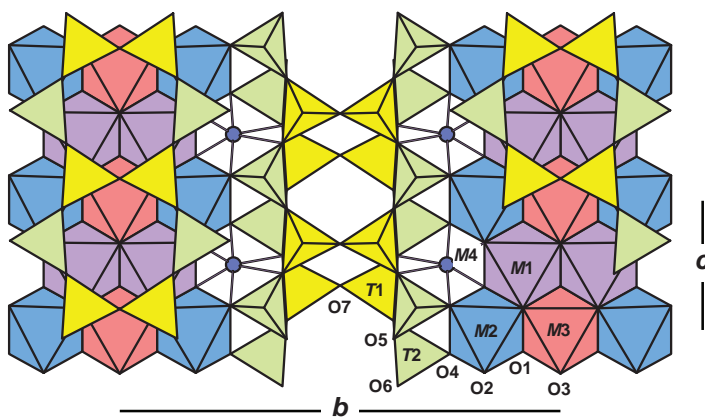


Figure 11. The $Pnmm$ amphibole structure projected onto (100); polyhedra: $T1$ = yellow, $T2$ = green, $M1$ = mauve, $M2$ = blue, $M3$ = red; sites: $M4$ = blue circle.

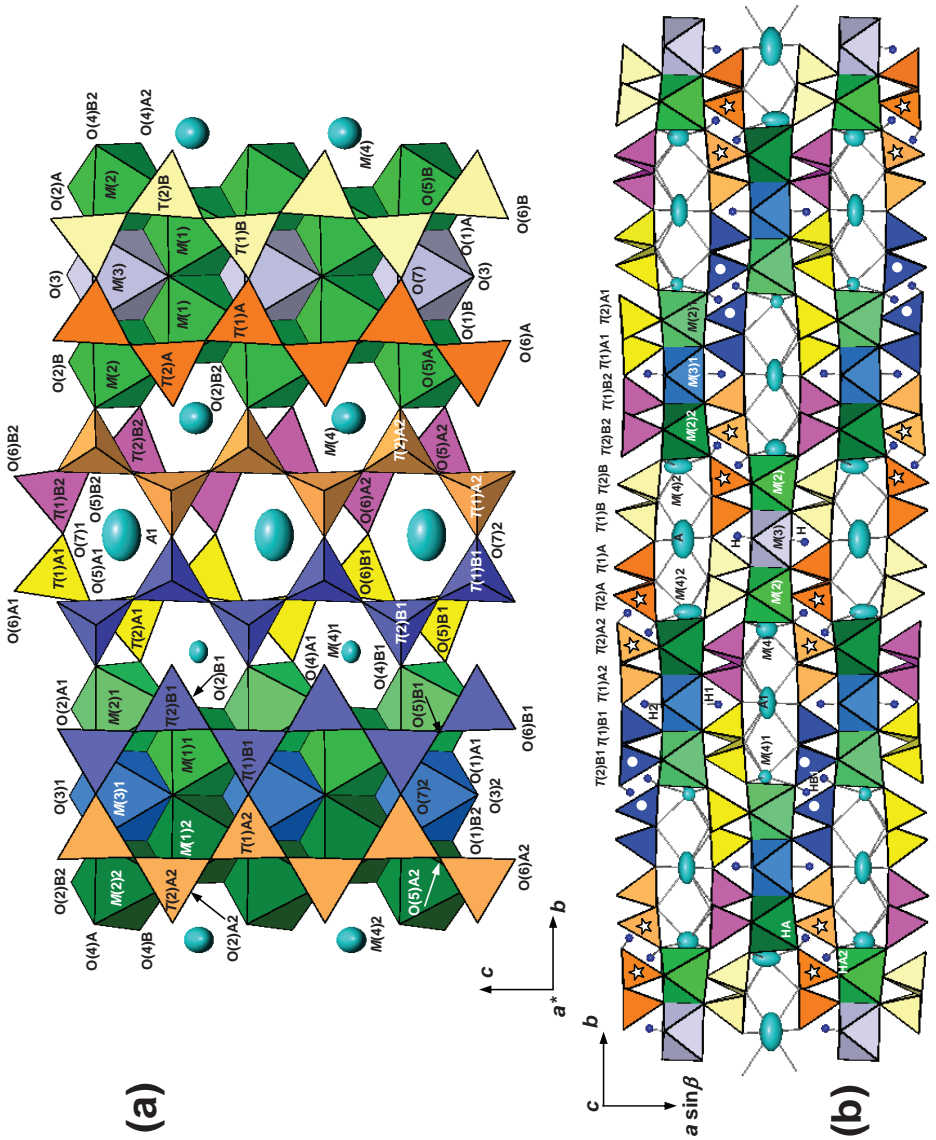


Figure 12. The $C\bar{1}$ amphibole structure ($b = 54.082 \text{ \AA}$) of synthetic $\text{Na}_2\text{Na}_2\text{Mg}_5\text{Si}_8\text{O}_{21}(\text{OH})_3$; (a) projection onto (100); (b) projection onto (001) [note the distinct positions of the $M(4)$ and A sites]. Note the calculated position for the third proton in the unit formula (modified from Cámara et al. 2004).

and link to form only one distinct type of double-chain of tetrahedra.

There are three distinct M sites that are occupied by the C cations, $M1$, $M2$ and $M3$, with point symmetries 2, 2 and $2/m$, respectively. The coordination of these sites is similar to that of the analogous sites in the $C2/m$ structure. The $M4$ site has point symmetry 2 and is occupied by the B cations. It is surrounded by an antiprism of eight oxygen atoms not all of which bond to the central cation. The A site occurs at the center of the cavity between the back-to-back double-chains of the structure (Fig. 11), it has point symmetry $2/m$.

The $C\bar{1}$ amphibole structure

This structure has only been recorded for one very peculiar composition of a synthetic amphibole: $\text{NaNa}_2\text{Mg}_5\text{Si}_8\text{O}_{21}(\text{OH})_3$ which has one H in excess with respect to the standard amphibole formula (Maresch et al. 1991; Cámara et al. 2004). The site nomenclature was derived by analogy with the monoclinic and orthorhombic structures (Fig. 12a). However, the triclinic nature of the structure, coupled with a b cell-dimension of 54.082 Å (i.e., three times the usual amphibole b edge) increases the complexity of the description. The simplest approach is to take into account the I beams (i.e., the structure module parallel to c which is formed by a strip of octahedra and the two adjacent double-chains of tetrahedra which lay above and below in the a $\sin \beta$ direction). There are two types of I-beams, and their arrangement is shown in Figure 12b.

I-beam I is centrosymmetric. The two sides of the double-chain of tetrahedra in the (100) projection (Fig. 12a) are no longer equivalent, and are named A and B in analogy with the $P2/a$ amphibole structure: $T(1)A$, $T(2)A$, $T(1)B$, and $T(2)B$. These sites repeat themselves (by the $\bar{1}$ operation) in the double chain below the strip of octahedra (cf. the center of Fig. 12b). I-beam I has three [6]-coordinated sites ($M(1)$, $M(2)$ and $M(3)$), and one [7]-coordinated $M(4)$ site. With the exception of O(3) and O(7), all anion sites are duplicated with respect to the $C2/m$ structure, and are named with regard to the T sites to which they are bonded, e.g., O(1)A and O(1)B. There is only one independent H site. The A site is [6]-coordinated and has point symmetry $\bar{1}$.

I-beam II is non-centrosymmetric. Therefore, all the T sites above and below the ribbon of octahedra are no longer equivalent, and a third index must be added to the site name: it is 1 when the tetrahedra are adjacent to I-beam I, e.g., $T(1)A1$, $T(2)A1$, $T(1)B1$ and $T(2)B1$, and 2 when they are adjacent to I-beam II, e.g., $T(1)A2$, $T(2)A2$, $T(1)B2$ and $T(2)B2$. I-beam II has five independent octahedrally coordinated sites: $M(1)1$, $M(1)2$, $M(2)1$, $M(2)2$ and $M(3)1$, and two independent [7]-coordinated $M(4)$ sites: $M(4)1$ and $M(4)2$, where the labels 1 and 2 have the same meaning as for the T sites. I-beam II has twenty-four anion sites. With the exceptions of O(3)1, O(3)2, O(7)1 and O(7)2, for which the index 1 or 2 is arbitrarily chosen, O atoms take their designations from the T site to which they are bonded. Two independent H atoms, H1 and H2, are bonded to O(3)1 and O(3)2, respectively. Above and below I-beam II, there are [8]-coordinated A(1) sites with point symmetry 1 (Fig. 12b).

The $C\bar{1}$ symmetry for the triple- b cell derives from the fact that the two distinct I-beams alternate along b in the sequence $I-II-I-II-I$, the two adjacent I-beams II being related by a center of symmetry coinciding with the A site (Fig. 12b).

The geometries of the double-chains of tetrahedra are significantly different. In I-beam I, the double chain is O-rotated, and both the A- and B-chains have O(5)-O(6)-(O5) angles similar to those found in $C2/m$ amphiboles (O(5)A-O(6)A-O(5)A = 172.8° and O(5)B-O(6)B-O(5)B = 170.4°; cf. Hawthorne 1983a for references). In I-beam II, one double chain is S-rotated (O(5)A2-O(6)A2-O(5)A2 = 183.9° and O(5)B1-O(6)B1-O(5)B1 = 184.0°), whereas the other double-chain is O-rotated (O(5)A1-O(6)A1-O(5)A1 = 162.4° and O(5)B2-O(6)B2-O(5)B2 = 163.5°). The Na atoms at the $M(4)1$ and $M(4)2$ sites have coordination [7] and are displaced significantly along the a and c axes relative to the analogous positions on the diad in the $C2/m$ structure. They have one short and one long $M(4)$ -O(4) distance, and one short and one long $M(4)$ -O(2) distance.

The third proton could not be located from difference-Fourier analysis. Bond-valence calculations [using values from Brown and Altermatt 1985) for Mg-O and Na-O, and from Brese and O'Keeffe (1991) for Si-O] shows that there are two pairs of O(4) anions which are strongly bond-valence deficient: O(4)A, O(4)B1 with 1.50 vu (valence units), and O(4)A2, O(4)B2 with 1.77 vu, and one pair with a nearly ideal value: O(4)B and O(4)A1 with 1.96 vu). Three O(2) sites, O(2)A, O(2)A2 and O(2)B1, are also slightly deficient, suggesting H-bond interactions. Stereochemical analysis shows that in the I-beam *II* modules, pairs of adjacent *M*(4)1 sites have two different and alternating spatial relations along *a* *sin* β , one with a shorter *M*(4)1-*M*(4)1 separation (4.508 Å) and the other with a longer separation (5.599 Å). In the latter case, an excess proton could occur in the pseudo-tetrahedral cavity between two *T*(2)B1 tetrahedra (marked with a white dot in Fig. 12b). A different situation is encountered where B-type sites adjacent to an I-beam *I* and to an I-beam *II* (i.e., *M*(4) and *M*(4)2) alternate along *a* *sin* β . *M*(4)2 has a very large atomic-displacement, with the major component of the ellipsoid along *a* *sin* β . It is thus possible to have a proton bonded to the O(4)A site where Na at *M*(4)2 is displaced away from the pseudo-tetrahedral cavity. Thus, the proton could protrude into the pseudo-tetrahedral cavity between two *T*(2)A and *T*(2)A2 tetrahedra (marked with a white star in Fig. 12b). With only one of the pair of H sites occupied in each cavity, the atom multiplicities for HB1, HA, and H2A are all 2, leading to one excess H pfu (*Z* = 6). Each proton would supply 0.4 vu to the O(4) donor and 0.1 vu to the O(2) acceptor, in good agreement with bond-valence calculations. Possible models for the local stereochemistry of these protons were derived from bond-lengths consideration and are given in Figure 13.

STACKING SEQUENCES AND SPACE GROUPS

Amphiboles may be considered as sheets of octahedra and tetrahedra stacked along the *a*-direction (Fig. 14). Different ordered

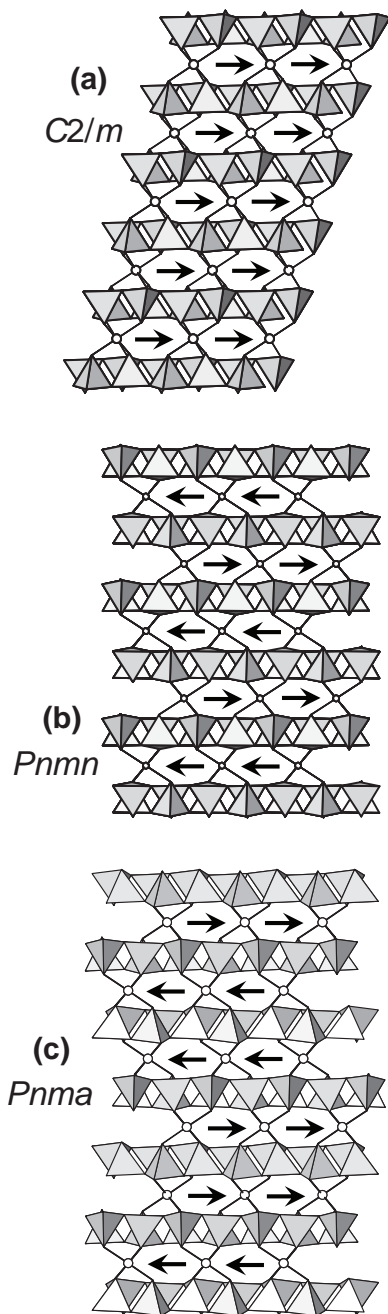


Figure 14. Schematic representation of the stacking of layers projected down the *y*-axis for the various amphibole structure types: the *P2₁/m* and *P2₁a* sequences are the same as for the *C2/m* structure type and are not shown here.

stacking sequences of these sheets of tetrahedra and octahedra (Gibbs 1966) are associated with the different space-group symmetries of the amphiboles. The space groups $P2_1/a$ and $P2_1/m$ are subgroups of $C2/m$ and involve the same bond topology, and hence we may consider only the space groups $C2/m$, $Pnma$ and $Pnmm$ in this regard. The stacking sequences are shown schematically in Figure 14. The apical O atoms of the tetrahedra provide the anions for the coordination of the octahedra, and hence there is a stagger of $\pm c/3$ between adjacent sheets of tetrahedra. For monoclinic amphiboles, this stagger is always in the same direction (Fig. 14a). For the orthorhombic amphiboles, a regular reversal of this stagger is necessary such that the periodicity in the a -direction is orthogonal to the plane of the sheets. For the $Pnma$ structure, the stagger between adjacent sheets of tetrahedra is $[+c/3, +c/3, -c/3, -c/3]$ (Fig. 14c), whereas for the $Pnmm$ structure type, the stagger between adjacent sheets of tetrahedra is $[+c/3, -c/3, +c/3, -c/3]$ (Fig. 14b).

BOND LENGTHS AND BOND VALENCES IN $^{[4]}\text{Al}$ -FREE AMPHIBOLES

This topic is examined extensively in Hawthorne (1983a) and will be treated only briefly here. Variations in bondlengths can be explained in terms of bond-valence theory (Brown 1981, 2002; Hawthorne 1992, 1994, 1997). Bond-valence tables for selected $^{[4]}\text{Al}$ -free amphiboles are shown in Table 5. The oxygen atoms at O(1), O(2) and O(3) are [4]-coordinated [O(3) is only [3]-coordinated where occupied by F, Cl or O], those at O(4), O(5) and O(6) are [3]-coordinated and O(7) is [4]-, [3]- or [2]-coordinated depending on the nature of the O(3) anion and the occupancy of the A site. The O(1), O(2) and O(4) oxygen atoms are linked to one Si cation. As O(1) and O(2) are [4]-coordinated, their bond-valence requirements are easily satisfied without any major deviations of the incident bondlengths from their mean values. However, O(4) is only [3]-coordinated and hence all bondlengths to O(4) are the shortest of their constituent polyhedra (Table 5). Where O(3) is occupied by (OH), the oxygen atom is bonded to 4 cations: $2 \times M(1) + M(3) + \text{H}$ and the incident bond-valence requirements are easily satisfied. The O(5), O(6) and O(7) oxygen atoms are each linked to two Si cations; in addition, O(5) and O(6) are linked to the $M(4)$ cation via long bonds in accord with their coordination by two Si cations. As a result, the bonds from Si to O(5) and O(6) are usually longer than the $\langle \text{Si-O} \rangle$ bondlengths [and the resulting bond-valences are < 1.00 vu]. The O(7) oxygen atom can be [2]-, [3]- or [4]-coordinated, depending on the type of O(3) anion present and whether the A site is occupied or vacant: [2]-coordinated: O(3) = (F,Cl,O), A = \square ; [3]-coordinated: O(3) = (F,Cl,O), A = (Na,K,Ca); [3]-coordinated: O(3) = (OH), A = \square ; [4]-coordinated: O(3) = (OH), A = (Na,K,Ca). The lower the coordination number of O(7), the shorter is the $T(1)$ -O(7) bond and the larger is its corresponding bond-valence (compare fluorotremolite, tremolite, fluororichterite and ferroglaucophane in Table 5). Thus it can be seen that the bond-valence requirements of the anions in the amphibole structure (together with the type of cations at the different cation sites in the structure) dictate the variations in bondlengths in the amphibole structure.

THE DOUBLE-CHAIN OF TETRAHEDRA IN $^{[4]}\text{Al}$ AMPHIBOLES

The substitution of $^{[4]}\text{Al}$ for Si is a major factor in the crystal chemistry of the amphiboles. Reported $^{[4]}\text{Al}$ contents vary between 0.0 and 3.55 apfu, although occurrences in which $^{[4]}\text{Al}$ exceeds 2.00 apfu are relatively uncommon, but not rare (Bunch and Okrusch 1973; Appleyard 1975; Hawthorne and Grundy 1977; Shimazaki et al. 1984; Mogessie et al. 1986; Sawaki 1989; Previde Massara 1990; Oberti et al. 1995a; Banno et al. 2004; Hawthorne and Harlow 2007; Nishio-Hamane pers. comm.). The $^{[4]}\text{Al}$ content of an amphibole is dependent on (1) bulk-rock composition, and (2) the pressure and temperature of crystal/equilibration of the amphibole (Oberti et al. 1995a).

Table 5. Bond-valence (vu) tables for selected ¹⁴¹Al-free C2/m amphiboles.

	<i>M</i> (1)	<i>M</i> (2)	<i>M</i> (3)	<i>M</i> (4)	<i>A</i>	<i>T</i> (1)	<i>T</i> (2)	Σ	Σ ^P
Cummingtonite: r.m.s. deviations are 3.2% and 9.6%, respectively.									
O(1)	0.375	0.312	0.346 ^{x2} ↓			1.008		2.041	2.000
O(2)	0.325	0.347		0.333			0.992	1.997	2.000
O(3)	0.353 ^{x2} →		0.367					1.073	1.000
O(4)		0.386		0.480			1.035	1.901	1.667
O(5)				(0.045)		1.021	0.956	1.977	2.000
O(6)				0.107		0.984	0.946	2.037	2.333
O(7)						1.024 ^{x2} →		2.048	2.000
Σ	2.103	2.090	2.160	1.840		4.037	3.929		
Tremolite: r.m.s. deviations are 4.4% and 11.3%, respectively.									
O(1)	0.356	0.309	0.351 ^{x2} ↓			1.055		2.071	2.000
O(2)	0.345	0.342		0.287			1.016	1.990	1.917
O(3)	0.342 ^{x2} →		0.361					1.064	1.000
O(4)		0.395		0.341			1.101	1.837	1.583
O(5)				0.133		0.974	0.922	2.029	2.250
O(6)				0.211		0.982	0.878	2.071	2.250
O(7)						1.016 ^{x2} →		2.032	2.000
Σ	2.086	2.092	2.146	1.944		4.027	3.917		
Fluorrichterite (34): r.m.s. deviations are 6.8% and 12.9%, respectively.									
O(1)	0.359	0.278	0.351 ^{x2} ↓			1.113		2.101	2.000
O(2)	0.381	0.359		0.236		0.992	0.992	1.968	1.854
O(3)	0.276 ^{x2} →		0.300			0.951		0.852	1.000
O(4)		0.398		0.273			1.125	1.796	1.521
O(5)				0.103	0.087 ^{x2} ↓		0.910	2.092	2.271
O(6)				0.166	0.061 ^{x2} ↓		0.858	2.036	2.271
O(7)					0.182	0.964 ^{x2} →		2.110	2.200
Σ	2.032	2.070	2.004	1.556	0.956	4.020	3.885		
Ferroglaucofane (69): r.m.s. deviations are 4.1% and 9.2%, respectively.									
O(1)	0.367	0.396	0.339 ^{x2} ↓			0.992		2.094	2.167
O(2)	0.361	0.476		0.193			0.977	1.947	1.958
O(3)	0.341 ^{x2} →		0.382					1.064	1.000
O(4)		0.605		0.220			1.072	1.897	1.625
O(5)				0.094		1.019	0.927	2.040	2.125
O(6)				0.175		0.997	0.917	2.089	2.125
O(7)						1.013 ^{x2} →		2.026	2.000
Σ	2.138	2.954	2.120	1.364		4.021	3.893		

^P Formal (Pauling) bond-strength

Variation in $\langle T-O \rangle$ bondlengths in $C2/m$ amphiboles

There have been numerous treatments of this issue (Papike et al. 1969; Hawthorne and Grundy 1973a,b, 1977; Robinson et al. 1973; Bocchio et al. 1978; Hawthorne 1981, 1983a,c; Oberti et al. 1995a), and although the relations between Al content and mean bondlengths have been improving, the current state of affairs is still far from ideal. Hawthorne (1976) and Ungaretti (1980) suggested that variations in $\langle T-O \rangle$ distances occur as a result of other cation substitutions in the amphibole structure. We may see this in the variation in $\langle T(1)-O \rangle$ and $\langle T(2)-O \rangle$ distances in $^{[4]}Al$ -free amphiboles (Fig. 15). If there is such a relation in $^{[4]}Al$ -free amphiboles, it seems probable that there is a similar relation in $^{[4]}Al$ -bearing amphiboles, particularly at the $T(2)$ site (Ungaretti 1980). Oberti et al. (1995a) incorporated such changes into a relation for the $T(2)$ site, but the relation does not work well for very Al-rich amphiboles. Consequently, it seemed desirable to reconsider this issue here. Data are taken from structure refinements selected from those listed in Appendix I; only about 50% of the structure refinements were used for this purpose as the remainder were identified as containing significant errors, particularly in the assigned site-populations.

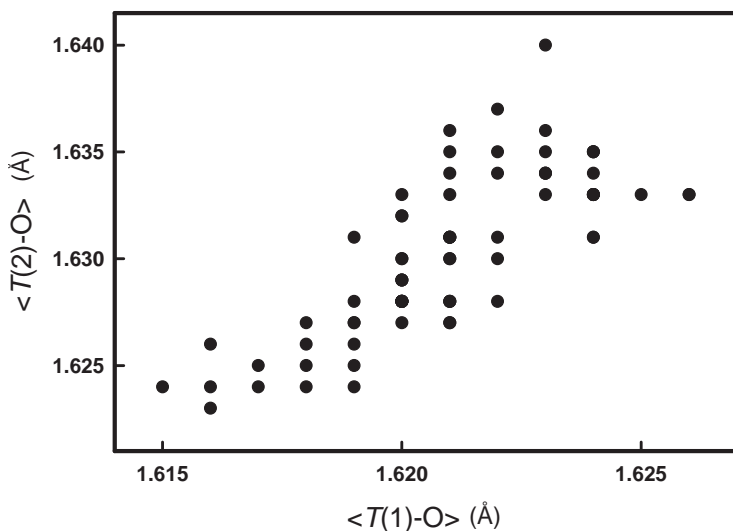


Figure 15. Variation in $\langle T(1)-O \rangle$ and $\langle T(2)-O \rangle$ distances for $C2/m$ amphiboles with $^{[4]}Al < 0.06$ apfu.

$\langle\langle T-O \rangle\rangle$ as a function of $^{[4]}Al$. The variation of $\langle\langle T-O \rangle\rangle$ as a function of $^{[4]}Al$ is shown in Figure 16a. Given that the average standard deviation of the mean bondlengths is of the order of 0.002 \AA , there is a well-developed linear relation above ~ 0.50 $^{[4]}Al$ apfu and much scatter of the data below ~ 0.50 $^{[4]}Al$ apfu. First, this general relation suggests that a single linear model for the variation of $\langle\langle T-O \rangle\rangle$ may not be appropriate. There is more than one way to approach this issue. We may consider just the data with $^{[4]}Al > 0.50$ apfu and fit a straight line to the data. The result of this is shown in Figure 16b and the resulting regression relations is given in Table 6; the standard error of estimate on the mean bondlength is similar to the estimated standard deviation, suggesting that the variation in $\langle\langle T-O \rangle\rangle$ is affected only by the total $^{[4]}Al$ content for $^{[4]}Al > 0.50$ apfu. Developing the inverse relation (Table 6) predicts the amount of $^{[4]}Al$ (greater than 0.50 apfu) with a standard error of the estimate of 0.08 apfu.

Such a simple model is obviously not adequate for small amounts of $^{[4]}Al$, and a more complicated model was investigated by stepwise multiple regression in the region $Al \leq 0.50$

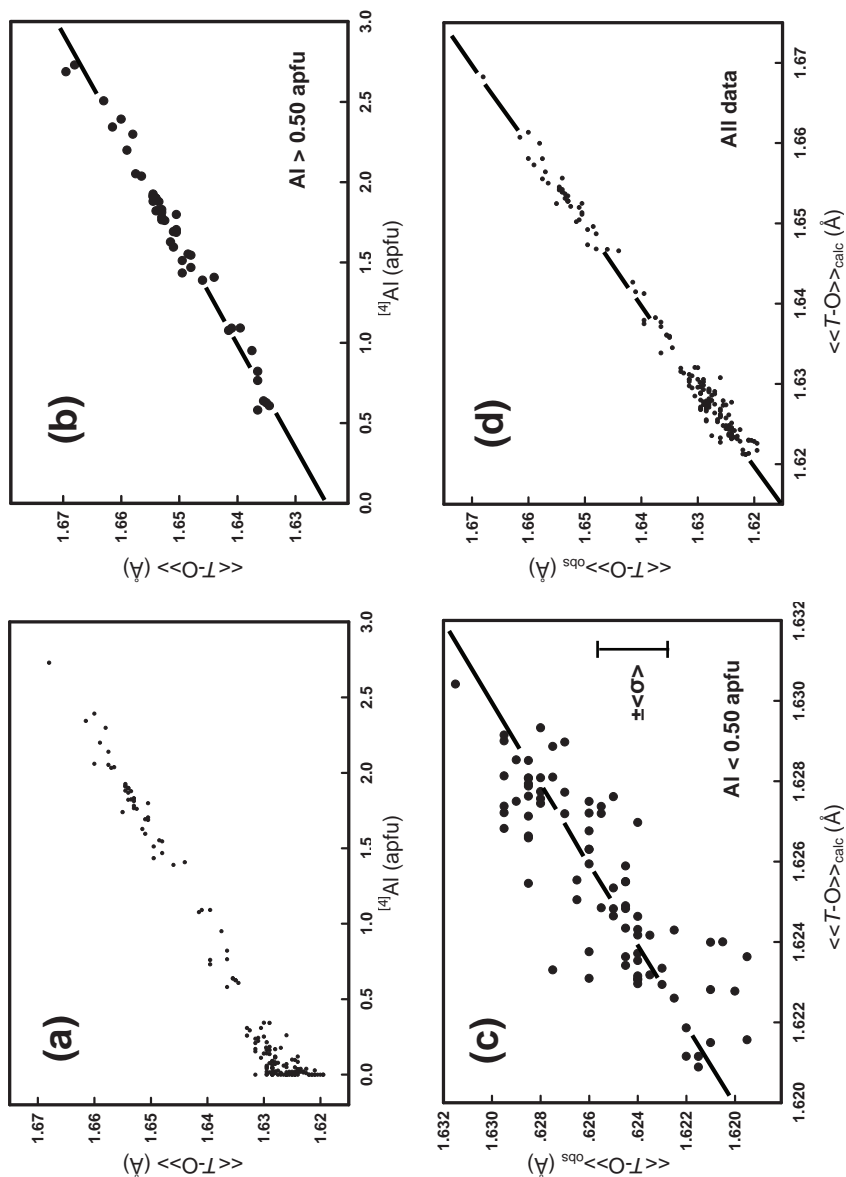


Figure 16. Relations between $\langle\langle T-O \rangle\rangle$ distance and $^{[4]}Al$ content in *C2/m* amphiboles; (a) $\langle\langle T-O \rangle\rangle$ as a function of $^{[4]}Al$ (all data); (b) $\langle\langle T-O \rangle\rangle$ as a function of $^{[4]}Al$ (where $^{[4]}Al > 0.50$ apfu); (c) observed *versus* calculated values of $\langle\langle T-O \rangle\rangle$ for amphiboles with $^{[4]}Al < 0.05$ apfu using the stepwise regression results of Table 5, where the 1:1 line is indicated; (d) observed *versus* calculated values of $\langle\langle T-O \rangle\rangle$ for all amphiboles using the stepwise regression results of Table 5, where the 1:1 line is indicated.

Table 6. Regression results for $\langle T-O \rangle$ (Å) and $^{[4]}Al$ contents (apfu) in $C2/m$ and $Pnma$ amphiboles.

y	x_i	y_o	a_i	R	s^* (Å or apfu)
<u>$C2/m$</u>					
$\langle\langle T-O \rangle\rangle$	$^{[4]}Al$ (>0.50 apfu)	1.6250(6)	0.0153(3)	0.989	0.0012
$^{[4]}Al$ (>0.50 apfu)	$\langle\langle T-O \rangle\rangle$	-102.26(2.26)	62.96(1.37)	0.990	0.08
$\langle\langle T-O \rangle\rangle$	$^{[4]}Al$ (<0.06 apfu)	1.5017	0.014(6)	0.879	0.0014
	$\langle\langle r_{M(1,2,3)} \rangle\rangle$		0.051(9)		
	$\langle r_{O(3)} \rangle$		0.045(14)		
	$\langle r_{M(4)} \rangle$		0.025(2)		
$\langle\langle T-O \rangle\rangle$	$^{[4]}Al$	1.522(11)	0.0156(2)	0.995	0.0013
	$\langle r_{M(1,2,3)} \rangle$		0.0416(6)		
	$\langle r_{O(3)} \rangle$		0.0304(8)		
	$\langle r_{M(4)} \rangle$		0.0246(17)		
	$\langle z_{M(4)} \rangle$		0.00129(41)		
$^{[4]}Al$	$\langle\langle T-O \rangle\rangle$	-94.4(1.4)	62.6(7)	0.995	0.08
	$\langle r_{M(1,2,3)} \rangle$		-3.69(38)		
	$\langle r_{O(3)} \rangle$		-2.3(5)		
	$\langle r_{M(4)} \rangle$		-1.43(9)		
<u>$C2/m$ for samples with $TAl > 0.50$ apfu</u>					
$\langle T(1)-O \rangle$	$T^{(1)}Al$	1.6202(6)	0.0308(4)	0.996	0.0012
$\langle T(2)-O \rangle$	$T^{(2)}Al$	1.6293(3)	0.0329(10)	0.981	0.0012
$T^{(1)}Al$	$\langle T(1)-O \rangle$	-52.120(699)**	32.177(420)	0.996	0.039
$T^{(2)}Al$	$\langle T(2)-O \rangle$	-47.613(1400)	29.228(856)	0.981	0.035
<u>$Pnma$</u>					
$\langle\langle T-O \rangle\rangle$	$^{[4]}Al$	1.6215(9)	0.0173(6)	0.985	0.0015
$^{[4]}Al$	$\langle\langle T-O \rangle\rangle$	-90.98(343)	56.1473(2085)	0.985	0.09

* s = standard error of estimate.

**Values are quoted to several digits in order to avoid significant termination errors.

apfu. The variables that have a significant effect on $\langle\langle T-O \rangle\rangle$ are $^{[4]}Al$, $\langle r_{M(4)} \rangle$ and $\langle r_{M(1,2,3)} \rangle$. The resulting regression equation is given in Table 6 and the observed and calculated $\langle\langle T-O \rangle\rangle$ values are compared in Figure 16c; at first sight, there is a lot of scatter in Figure 16c, but this is not significant in terms of the average standard deviation for the observed data. We also fitted a single model to all the data by stepwise linear regression; the results are given in Table 6 and a comparison of the observed and calculated data is given in Figure 16d. The fit is good, and the regression shows that $\langle\langle T-O \rangle\rangle$ is also affected by $\langle r_{M(1,2,3)} \rangle$, $\langle r_{O(3)} \rangle$ and $\langle r_{M(4)} \rangle$ in that order. We may also use $^{[4]}Al$ as the dependent variable in a stepwise regression to develop a predictive curve for $^{[4]}Al$; the result is given in Table 6.

$\langle T(1)-O \rangle$ and $\langle T(2)-O \rangle$ as a function of $^{[4]}Al$ content. Without independent measurement of the amounts of Al at $T(1)$ and $T(2)$ (e.g., by neutron diffraction or MAS NMR), it is not possible to rigorously assign site populations to $T(1)$ and $T(2)$. However, let us first try and get a sense of the behavior of $\langle T(1)-O \rangle$ and $\langle T(2)-O \rangle$ as a function of $^{[4]}Al$ content; Figure 17 shows this variation. It is immediately apparent from Figure 17 that there are two distinct regimes of behavior of the tetrahedra.

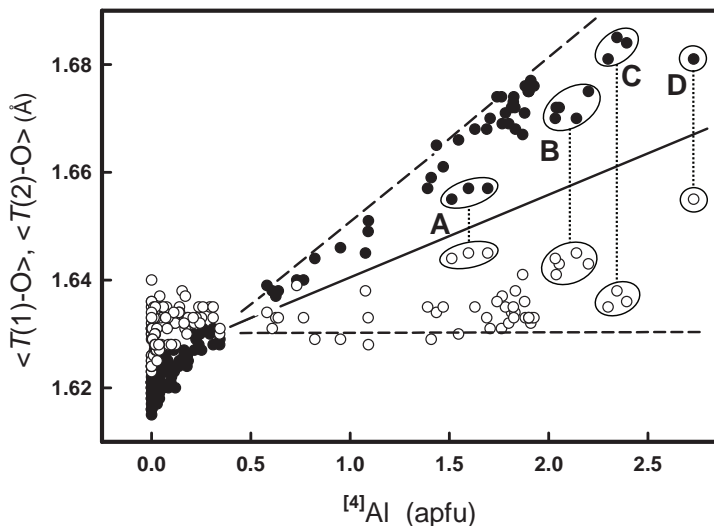


Figure 17. Variation in $\langle T(1)\text{-O} \rangle$ (black circles) and $\langle T(2)\text{-O} \rangle$ (white circles) as a function of $^{[4]}\text{Al}$ in C2/m amphiboles; the full line shows the regression relation from Fig. 16b, the upper dashed line is the limiting envelope for the $T(1)$ data, and the lower dashed line is the reflection of the upper dashed line through the full line parallel to the ordinate. The lines connect values for $T(1)$ (above the full line) and $T(2)$ (below the full line) for specific crystals. See text for the meanings of A, B, C and D.

- (1) below $^{[4]}\text{Al} = 0.40$ apfu, the data are densely clustered together; the maximum variation ($1.640 - 1.614 = 0.026$ Å) is at $^{[4]}\text{Al} = 0.0$ apfu, and the variation decreases with increasing $^{[4]}\text{Al}$ to extrapolate to 0.0 Å at ~ 0.045 $^{[4]}\text{Al}$. It is apparent that variation of both $\langle T(1)\text{-O} \rangle$ and $\langle T(2)\text{-O} \rangle$ are affected by aspects of the structure other than just $^{[4]}\text{Al}$ content (note that we already know this in terms of $\langle\langle T\text{-O} \rangle\rangle$ (the mean of $\langle T(1)\text{-O} \rangle$ and $\langle T(2)\text{-O} \rangle$) because of behavior shown in Fig. 16).
- (2) above $^{[4]}\text{Al} = 0.50$ apfu, the behavior changes drastically: $\langle T(1)\text{-O} \rangle$ increases strongly with increasing $^{[4]}\text{Al}$ content (with some scatter), whereas $\langle T(2)\text{-O} \rangle$ increases less strongly (but also with considerable scatter).

The solid line in Figure 17 is the regression line from Figure 16b, and Figure 16b also shows that $\langle\langle T\text{-O} \rangle\rangle$ values (i.e., $(\langle T(1)\text{-O} \rangle + \langle T(2)\text{-O} \rangle)/2$) follow this regression line very closely. In Figure 17, the pattern of data scatter about the $\langle\langle T\text{-O} \rangle\rangle$ line is extremely informative. Above ~ 0.45 $^{[4]}\text{Al}$ apfu, $\langle T(1)\text{-O} \rangle$ values fall above the line and $\langle T(2)\text{-O} \rangle$ values fall below the line (except for one datum point at $^{[4]}\text{Al} \approx 0.7$ apfu). Furthermore, the relative displacements of values on either side of the central line match for each structure. This feature is emphasized in Figure 17 by enclosing data points from specific structures or groups of structures by ellipses and connecting the corresponding $\langle T(1)\text{-O} \rangle$ and $\langle T(2)\text{-O} \rangle$ ellipses. Several points now become apparent from Figure 17: (1) the coupling of scatter of points about the line implies that their displacements from the central line are due to partial-to-complete order of $^{[4]}\text{Al}$ over $T(1)$ and $T(2)$; (2) the pattern of variation of $\langle T(1)\text{-O} \rangle$ shows a limiting envelope at higher values, shown by the upper dashed line; (3) the symmetrical equivalent line below the full line is a reasonable limiting envelope for the variation of $\langle T(2)\text{-O} \rangle$; (4) the slope of the upper limiting envelope (which was drawn 'by eye') is 0.992, i.e., not significantly different from 1.0, the ideal value for a hard-sphere model of $\text{Al} \leftrightarrow \text{Si}$ substitution; this suggests that this envelope provides the limiting line for complete order of $^{[4]}\text{Al}$ at $T(1)$; (5) correspondingly, the lower dashed line is the limiting line for zero $^{[4]}\text{Al}$ at $T(2)$.

Of course, one expects some scatter of data about a specific relation due to experimental error and inductive effects of the rest of the structure, and hence the two dashed lines might need to be moved slightly closer together (while maintaining the same slopes) to give the true limiting values. The origins of the amphiboles shown in Figure 17 also support this overall interpretation. The amphiboles labeled A are from Punta Falcone, a high-temperature leucogabbro where Oberti et al. (1995a) have identified significant disorder of Al over $T(1)$ and $T(2)$. The amphiboles labeled B are synthetic fluoropargasite (synthesized at 1240 °C for 1 h and cooled to 816 °C over a period of 332 h; Oberti et al. 1995b) and synthetic kaersutites (synthesized at 1270 °C for 1 h, cooled to 1070 °C at 0.5 °C/h, and then held at 1070 °C for 13h; Tiepolo et al. 1999). Synthetic fluoropargasites have a significant cannilloite component (Ca at the A site, a feature which favors incorporation of ^{41}Al at the $T(1)$ site beyond 2.0 apfu), and amphiboles labeled A and B have unusually high temperatures of synthesis. These features are in intuitive accord with some disorder of ^{41}Al over $T(1)$ and $T(2)$, and the observed mean bondlengths indicate Al at both $T(1)$ and $T(2)$. The amphiboles labeled C and D are fluorocannilloites and sadanagaite, all with high (> 2.1 apfu ^{41}Al), again in accord with the presence of ^{41}Al at $T(2)$; in fluorocannilloite, the presence of Ca at the A site allows ^{7}Al to exceed 2 apfu, whereas in sadanagaite, the lack of significant A-site Ca prevents ^{7}Al from significantly exceeding 2 apfu and requires the excess ^{41}Al beyond 2.0 apfu to occupy $T(2)$.

For amphiboles in which $^{41}\text{Al} > 0.50$ apfu, Figure 17 also suggests a method for predicting the occupancies of the $T(1)$ and $T(2)$ sites: (1) Consider the data for a single amphibole. The distance between the $T(1)$ datum-point and the upper broken line represents the amount of Al at the $T(1)$ site, and the distance between the $T(2)$ datum-point and the lower broken line represents the amount of Al at the $T(2)$ site. The equation of the upper broken line is $\langle T(1)\text{-O} \rangle = 1.620 + 0.0312 \text{ } ^{7}\text{Al}$ and this can be used to predict an initial estimate of ^{7}Al from the observed value of $\langle T(1)\text{-O} \rangle$. The relation between the two dashed lines and the central full line in Figure 17 implies that the analogous relation for the $T(2)$ site has the same slope as that for the $T(1)$ site; the intercept of this line can be read from Figure 17: 1.630 Å, and thus the analogous predictive equation for the $T(2)$ site is $\langle T(2)\text{-O} \rangle = 1.630 + 0.0312 \text{ } ^{7}\text{Al}$ and can be used to predict an initial estimate of ^{7}Al from the observed value of $\langle T(2)\text{-O} \rangle$.

We may then compare the sum of the predicted ^{41}Al ($= \text{}^{7}\text{Al}_{\text{pred}} + \text{}^{7}\text{Al}_{\text{pred}}$) with the observed value of ^{41}Al . We may take the difference between these two values and equally distribute the difference between the two values $\text{}^{7}\text{Al}_{\text{pred}} + \text{}^{7}\text{Al}_{\text{pred}}$ and re-examine the relation between $\langle T(1)\text{-O} \rangle$ and $\langle T(2)\text{-O} \rangle$ and the modified values of $\text{}^{7}\text{Al}_{\text{pred}} + \text{}^{7}\text{Al}_{\text{pred}}$. This is done in Figure 18, and the results of regression analysis are given in Table 6 for both $\langle T(1)\text{-O} \rangle$, $\langle T(2)\text{-O} \rangle$ in terms of $\text{}^{7}\text{Al}_{\text{pred}}$, $\text{}^{7}\text{Al}_{\text{pred}}$. We also did the inverse regressions to give $\text{}^{7}\text{Al}_{\text{pred}} + \text{}^{7}\text{Al}_{\text{pred}}$ as the dependent variables (Table 6). These relations may be used to give the Al contents of the $T(1)$ and $T(2)$ sites with standard errors of estimate of ~ 0.04 Al apfu for amphiboles with $^{7}\text{Al} > 0.50$ apfu. It is apparent from Figure 17 that for amphiboles with $^{7}\text{Al} < 0.50$ apfu, there are not any simple relations between $\langle T(1)\text{-O} \rangle$, $\langle T(2)\text{-O} \rangle$ and ^{7}Al , ^{7}Al . The regression with $\langle T\text{-O} \rangle$ as the dependent variable in Table 6 involves ^{41}Al , $\langle r^{M(1,2,3)} \rangle$, $\langle r^{O(3)} \rangle$, $\langle r^{M(4)} \rangle$ and $\langle Z^{M(4)} \rangle$ as independent variables, and there is no way of evaluating the different effects of $\langle r^{M(1,2,3)} \rangle$, $\langle r^{O(3)} \rangle$, $\langle r^{M(4)} \rangle$ and $\langle Z^{M(4)} \rangle$ on $\langle T(1)\text{-O} \rangle$ and $\langle T(2)\text{-O} \rangle$ separately. This issue will be addressed in Oberti et al. (2007b) based on regression analysis of the whole CNR-IGG-PV database; in this way, a predictive equation was obtained for ^{7}Al (but not for ^{7}Al) in all the compositional range.

Variation in $\langle T\text{-O} \rangle$ bondlengths in *Pnma* amphiboles

Until recently, there has not been much crystal-structure information available on amphiboles of the anthophyllite-gedrite group. Hawthorne (1983a) synthesized the available information, presented a relation between $\langle T\text{-O} \rangle$ distance and ^{41}Al content, and developed predictive curves for the four symmetrically distinct tetrahedrally coordinated sites: $T1A$, $T1B$,

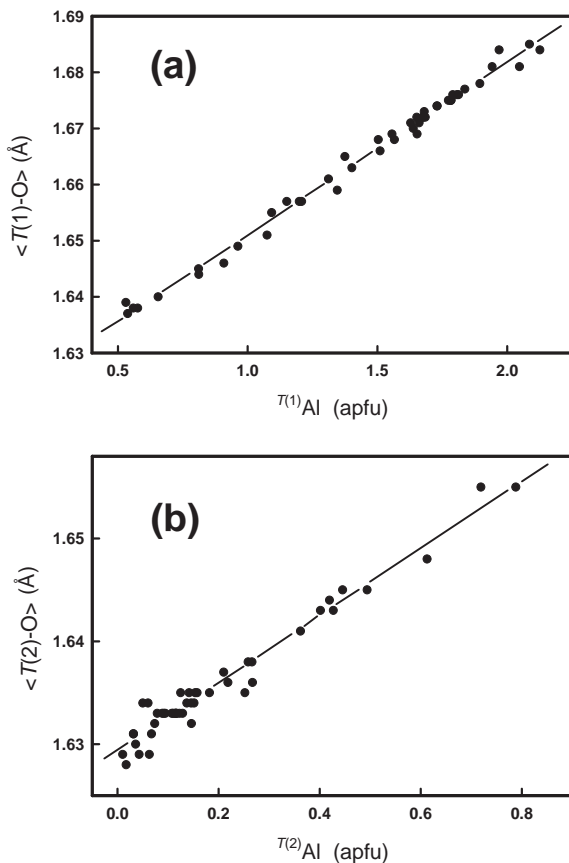


Figure 18. Relations between $\langle T-O \rangle$ distance and $^{[4]}\text{Al}$ content in $C2/m$ amphiboles; (a) $\langle T(1)-O \rangle$ as a function of $\tau^{(1)}\text{Al}$; (b) $\langle T(2)-O \rangle$ as a function of $\tau^{(2)}\text{Al}$.

$T2A$, $T2B$. Recently, Schindler et al. (2007) refined the structures of 26 anthophyllite-gedrite amphiboles and examined the stereochemistry of the $Pnma$ amphibole double-chain; these results are given below.

$\langle\langle T-O \rangle\rangle$ as a function of $^{[4]}\text{Al}$. The relation between $^{[4]}\text{Al}$ and the $\langle\langle T-O \rangle\rangle$ distance is shown in Figure 19. The data form a linear trend with a slope that is not significantly different from that characteristic of a hard-sphere model. Two of the data points in the central region fall 0.003–0.004 Å below the general trend. As crystals in this compositional range may be affected by unmixing, these two points were omitted from the linear regression, the results of which are given in Table 6.

$\langle T1A-O \rangle$, $\langle T1B-O \rangle$, $\langle T2A-O \rangle$ and $\langle T2B-O \rangle$ as a function of $^{[4]}\text{Al}$ content. There are four symmetrically distinct cation sites with tetrahedral coordination in the orthorhombic ($Pnma$) amphibole structure: $T1A$, $T2A$, $T1B$ and $T2B$ (Fig. 10). Hawthorne et al. (2007a) developed predictive curves relating the individual $\langle T-O \rangle$ distances to $^{[4]}\text{Al}$ content assuming that the slopes of the curves are the same.

The site occupancies predicted from the equations in Table 6 were adjusted slightly so as to accord exactly with the $^{[4]}\text{Al}$ determined by electron-microprobe analysis, and the $\langle T-O \rangle$

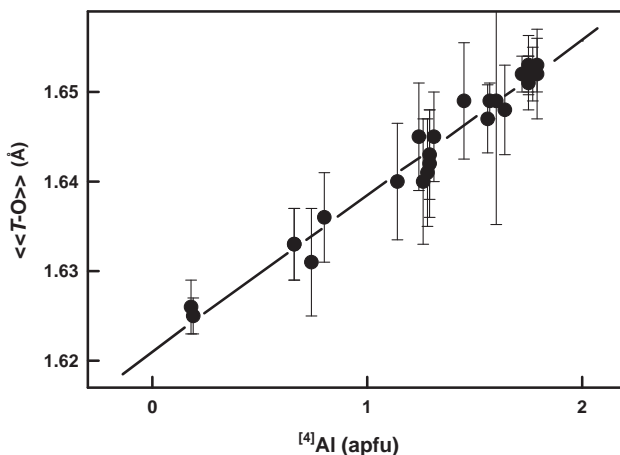


Figure 19. The relation between $\langle\langle T-O \rangle\rangle$ distance and $[4]Al$ in *Pnma* amphiboles.

distances are shown as a function of constituent Al in Figure 20, where the lines in the figures are the relevant equations of Table 6. As is apparent, $[4]Al$ is ordered over the non-equivalent *T* sites in the sequence $T1B > T1A > T2B > T2A$.

THE STEREOCHEMISTRY OF THE STRIP OF OCTAHEDRA

The strip of octahedra is the most compliant part of the amphibole structure and shows the greatest variation in size and valence of substituent cations and anions: it accepts cations from 0.535 Å ($[6]Al$) to 0.83 Å ($[6]Mn^{2+}$) and from 1⁺ (Li) to 4⁺ (Ti^{4+}) (and V^{5+} , Nb and Ta in synthetic samples), and the O(3) site can contain (OH), F, Cl and O. There are at least three octahedrally coordinated cation sites in all amphibole structures, and both long-range and short-range cation order can be important factors in their crystal chemistry. There has been an enormous amount of diffraction and spectroscopic work on the cation and anion order in amphiboles (Oberti et al. 2007a; Hawthorne and Della Ventura 2007), and here we examine the stereochemistry of the octahedron strip.

The *C2/m* amphiboles: variation in mean bondlengths

Variation in $\langle\langle M(1,2,3)-O \rangle\rangle$ distances. The variation in $\langle\langle M(1,2,3)-O \rangle\rangle$ bondlength as a function of the aggregate constituent *M*(1,2,3) cation radius is shown in Figure 21a, and the results of linear regression are shown in Table 7. There is quite a lot of scatter in Figure 21a and the standard error of estimate from the regression is 0.006 Å. The $\langle\langle M(1,2,3)-O \rangle\rangle$ bondlength will also be affected by the type of anion occupying the O(3) site, as the sizes of the constituent [3]-coordinated anions are significantly different: OH = 1.34, F = 1.30, O = 1.36 Å. In addition, there may be other inductive effects that also affect the $\langle\langle M(1,2,3)-O \rangle\rangle$ bondlength. This issue was examined by stepwise linear regression using the mean constituent ionic radii at the sites in the *C2/m* amphibole structure, and the results are given in Table 7. $\langle\langle M(1,2,3)-O \rangle\rangle$ is significantly affected by $\langle r^{M(1,2,3)} \rangle$ and $\langle r^{O(3)} \rangle$ as expected, but also is affected inductively by $\langle r^{M(4)} \rangle$, the mean radius of the cations at the *M*(4) site. The standard error of estimate is now 0.0028 Å and the correlation coefficient is 0.99; a comparison of the observed and calculated $\langle\langle M(1,2,3)-O \rangle\rangle$ distances is shown in Figure 21b.

Variation in $\langle M(2)-O \rangle$ distances. Figure 22b shows the variation in $\langle M(2)-O \rangle$ as a function of the aggregate size of the constituent cations, $\langle r^{M(2)} \rangle$. There is a well-developed

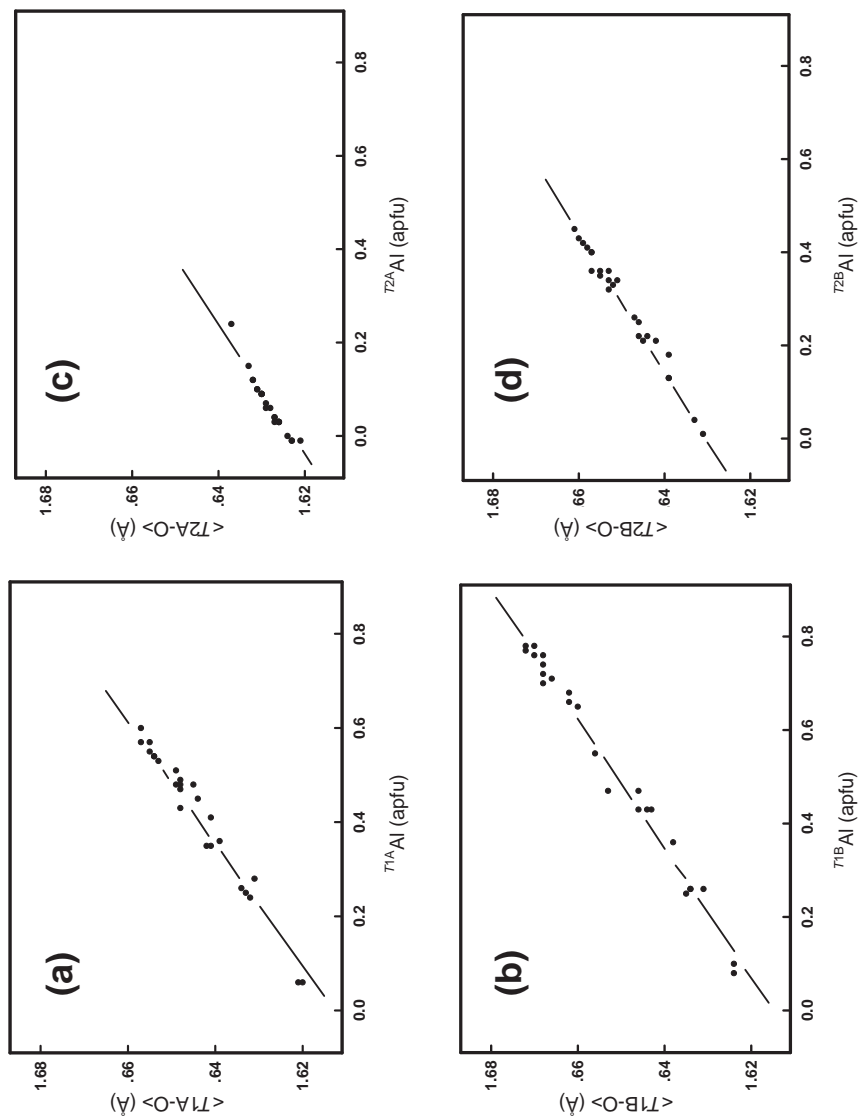


Figure 20. Relations between $\langle T-O \rangle$ distance and Al occupancy in *Pnma* amphiboles; (a) $T1A$; (b) $T1B$; (c) $T2A$; (d) $T2B$.

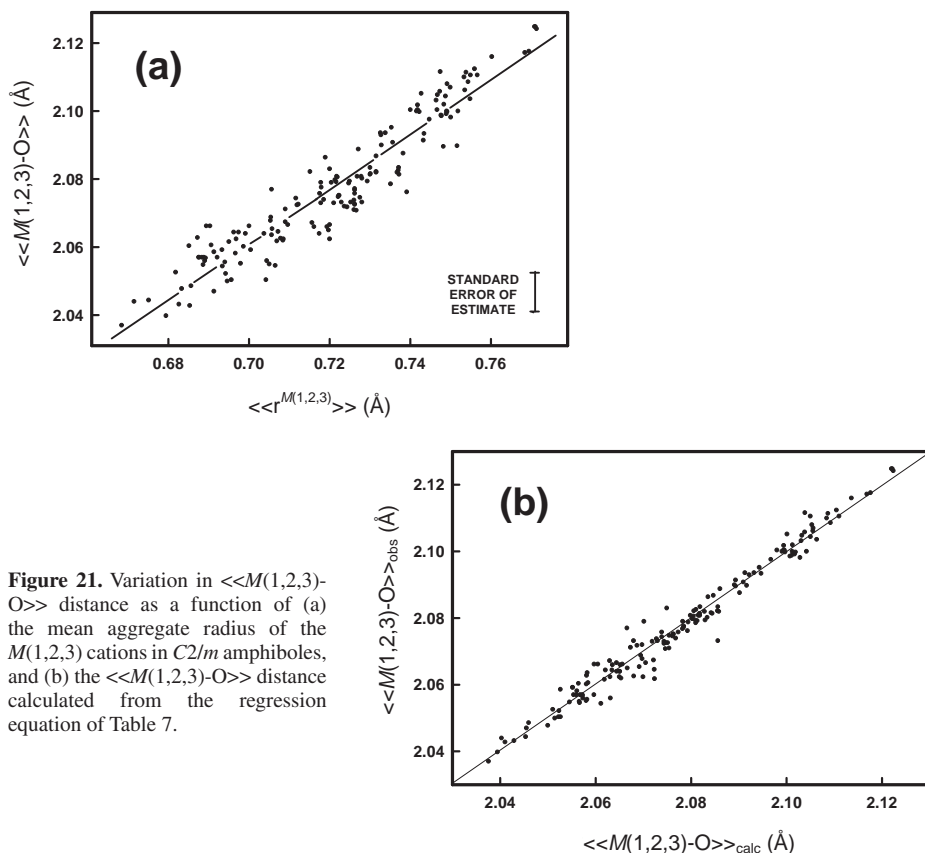


Figure 21. Variation in $\langle M(1,2,3)-O \rangle$ distance as a function of (a) the mean aggregate radius of the $M(1,2,3)$ cations in $C2/m$ amphiboles, and (b) the $\langle M(1,2,3)-O \rangle$ distance calculated from the regression equation of Table 7.

linear correlation, and the results of linear-regression analysis are given in Table 7. Possible inductive effects were investigated by stepwise linear regression using the ^7Al content, the mean radii at $M(1,3)$, $M(4)$ and $O(3)$ and the mean formal charges at the $M(4)$ and A sites, but none of these parameters had a significant effect. The regression equation is given in Table 7, and Figure 22e shows the comparison between the observed and predicted $\langle M(2)-O \rangle$ distances.

Variation in $\langle M(1)-O \rangle$ and $\langle M(3)-O \rangle$ distances. The situation for the $M(1)$ and $M(3)$ sites is somewhat more complicated than for the $M(2)$ site, as $M(1)$ and $M(3)$ are coordinated by the $O(3)$ site that shows variable occupancy of OH, F, Cl and O, all of which have significantly different radii: $^{13}\text{OH} = 1.34$, $^{13}\text{F} = 1.30$, $^{13}\text{O} = 1.36$ Å. Figures 22a and 22c show the variation in $\langle M(1)-O \rangle$ and $\langle M(3)-O \rangle$, respectively, as functions of $\langle r^{M(1)} \rangle$ and $\langle r^{M(3)} \rangle$. There is a lot of scatter in the relations, as expected as the graphs do not include the effects of different anions at the $O(3)$ site. In addition, there may be other inductive effects; this issue was examined by stepwise linear regression, and the results are given in Table 7. $\langle M(1)-O \rangle$ and $\langle M(3)-O \rangle$ are significantly affected by $\langle r^{M(1,2,3)} \rangle$, $\langle r^{O(3)} \rangle$ as expected, but inductively by the size of the $M(4)$ cation and the amount of tetrahedrally coordinated Al. The standard errors of estimate are 0.0027 Å and 0.0065 Å, respectively; comparisons of the observed and calculated $\langle M(1)-O \rangle$ and $\langle M(3)-O \rangle$ distances are shown in Figures 22d and 22f, respectively.

Indeed, Oberti et al. (2007c) compared the refined $\langle M(1)-O \rangle$ and $\langle M(3)-O \rangle$ bondlengths in glaucophane, nyböite, fluoronyböite, aluminotaramite, alumino-magnesiotalumite and fluoro-

Table 7. Regression results for ⁶M-sites and aggregate radii of cations at M-sites for C2/m and Pnma amphiboles.

y	x _i	y _o	a _i	R	s* (Å or apfu)
<u>C2/m</u>					
<<M(1,2,3)-O>>	<<r ^{M(1,2,3)} >>	1.497(15)	0.805(21)	0.950	0.0063
<<M(1,2,3)-O>>	<<r ^{M(1,2,3)} >>	1.0709(25)	0.784(14)	0.990	0.0028
	<r ^{O(3)} >		0.347(17)		
	<r ^{M(4)} >		-0.020(3)		
<M(1)-O>	<r ^{M(1)} >	0.932(24)	0.799(12)	0.990	0.0027
	<r ^{O(3)} >		0.467(16)		
	<r ^{M(4)} >		-0.0532(28)		
	⁴ Al		0.00358(30)		
<M(2)-O>	<r ^{M(2)} >	1.476(7)	0.845(9)	0.991	0.0053
<M(3)-O>	<r ^{M(3)} >	0.627(61)	0.775(19)	0.970	0.0058
	<r ^{O(3)} >		0.728(40)		
	<r ^{M(2)} >		-0.080(12)		
	<r ^{M(4)} >		-0.029(7)		
	Z ^A		0.0064(18)		
<u>Pnma^B(Mg,Fe,Mn)</u>					
<<M1,2,3-O>>	<<r ^{M1,2,3} >>	1.468(29)	0.855(42)	0.973	0.0024
<M1-O>	<r ^{M1} >	1.464(59)	0.862(79)	0.916	0.0028
<M2-O>	<r ^{M2} >	1.447(15)	0.899(24)	0.992	0.0039
<M3-O>	<r ^{M3} >	1.429(87)	0.87(12)	0.841	0.0044
<u>Pnma^B(Li)</u>					
<M1-O>	<r ^{M1} >	1.388(67)	0.954(91)	0.978	
<M2-O>	<r ^{M2} >	1.435(55)	0.908(99)	0.972	
<M3-O>	<r ^{M3} >	1.650(59)	0.597(79)	0.959	

* s = standard error of estimate.

alumino-magnesiotalamite. They concluded that the M(1) and M(3) octahedra are larger than expected based on their site populations, and that the difference in size increases with ^{T(1)}Al; in contrast, the individual M(1)-O(1) and M(3)-O(1) distances shorten with increasing ^{T(1)}Al, as expected by bond-strength requirements on the shared O(1) oxygen atom. It is possible that other inductive effects produce variations in mean bondlengths not described by the regression equations of Table 7. These could be investigated through examining structural strain as a function of amphibole composition. If structural strain is an issue here, one would expect deviations from the relations of Table 7 in compositions that approach the chemical limits of stability of the amphibole structure.

The Pnma amphiboles with ^B(Mg,Fe,Mn): variation in mean bondlengths

Hawthorne (1983) presented relations between the <M-O> distances and the aggregate radii of the constituent cations and anions at the M sites. However, not much data were available at that time. With the work of Evans et al. (2001) and Schindler et al. (2007) and Hawthorne et al. (2007), this situation has now changed, and more accurate relations are now available for anthophyllite-gedrite amphiboles.

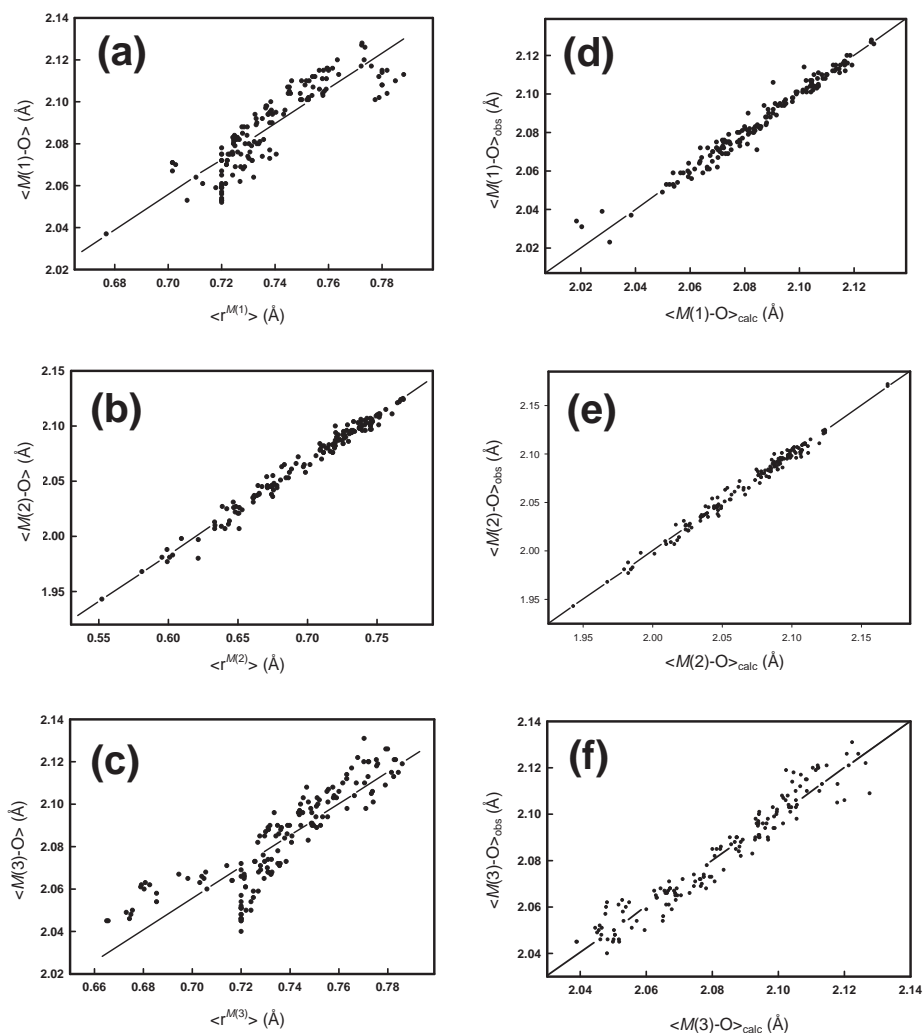


Figure 22. (a,b,c): Variation in $\langle M-O \rangle$ distance as a function of the mean aggregate radius of the M cations in $C2/m$ amphiboles: (a) $M(1)$; (b) $M(2)$; (c) $M(3)$; comparison of observed and calculated (from the regression relations of Table 5) $\langle M-O \rangle$ distances: (d) $M(1)$; (e) $M(2)$; (f) $M(3)$.

Variation in $\langle\langle M1,2,3-O \rangle\rangle$ distances. The variation in $\langle\langle M1,2,3-O \rangle\rangle$ bondlength as a function of the aggregate constituent $M1,2,3$ cation radius for amphiboles of the anthophyllite-gedrite series is shown in Figure 23, and the results of linear regression are shown in Table 7. The data are quite linear, given the large standard deviations in the intermediate range of composition (where the refinements are affected by exsolution), and the values are not materially affected by the small amounts of F occupying the O(3) site in these crystals. In the $C2/m$ amphiboles, the $\langle\langle M(1,2,3)-O \rangle\rangle$ distances were inductively affected by variation in the aggregate size of the cations occupying the $M(4)$ site. There is no sign of such an effect in the $Pnma$ amphiboles, which is not surprising, given the small amount of variation in $\langle r^{M4} \rangle$ relative to the analogous variation in the $C2/m$ amphiboles.

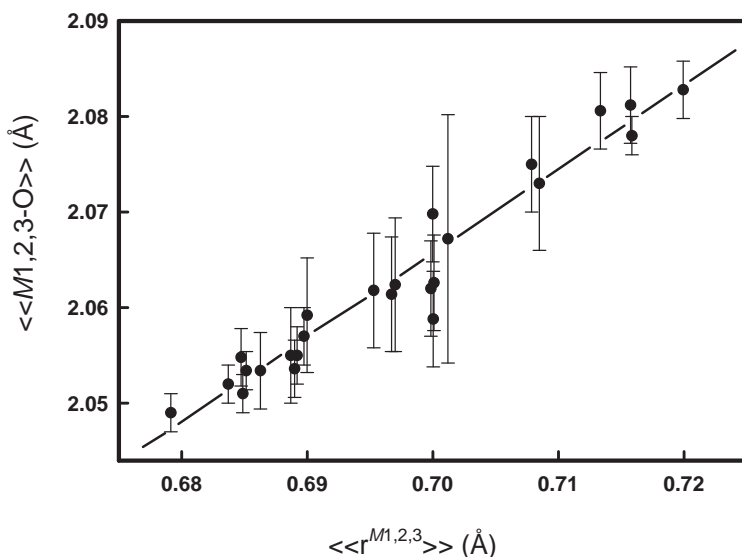


Figure 23. Variation in $\langle\langle M1,2,3-O \rangle\rangle$ distance as a function of the mean aggregate radius of the $M1,2,3$ cations in $Pnma$ amphiboles with $^B(Mg,Fe,Mn)$.

The $M1$ and $M3$ sites. The $M1$ and $M3$ sites are occupied predominantly by Mg and Fe^{2+} . In principle, the mean bond-lengths at these sites are dependent not only on the cation site-populations, but also on the anion site-populations at the $O3A$ and $O3B$ sites (cf. monoclinic amphiboles, Table 7). However, the $Pnma$ amphiboles generally contain only minor F , and we may omit consideration of the monovalent-anion content and focus just on the site populations of $M1$ and $M3$. Figures 24a, c show the variation of $\langle M1-O \rangle$ and $\langle M3-O \rangle$ as functions of mean constituent-cation radii for amphiboles of the anthophyllite-gedrite series. The variations are linear for each site, and no data deviate significantly (> 2.7 standard deviations) from the least-squares line. The regression curves are given in Table 7. The correlation coefficients are much lower for the $M1$ and $M3$ sites than that for the $M2$ site, a result of the much smaller spread of the data for the former two sites (where the standard deviation for each data point is proportionately much greater relative to the total range of the data for the $M1$ and $M3$ sites compared to the $M2$ site).

The $M2$ site. The $M2$ site is occupied predominantly by Mg , Al , Fe^{2+} and small amounts of Ti^{4+} and Fe^{3+} . The relation between $\langle M2-O \rangle$ and the mean constituent-cation radius is shown in Figure 24b, and the equation of the linear-regression curve is given in Table 7. The slope and intercept of the curve are reasonably similar to the analogous values for the $M(2)$ site in the $C2/m$ amphiboles.

The $Pnma$ amphiboles with $^B Li$: variation in mean bondlengths

The behavior observed in holmquistites is significantly different from that of the other $Pnma$ amphiboles discussed above. The crucial point in holmquistite crystal-chemistry is the presence of two monovalent cations pfu at the $M4$ site, which implies the presence of two trivalent cations pfu at the $M2$ site. The geometry of the strip of octahedra, does not allow incorporation of Al into the double chain of tetrahedra. Holmquistite, ideally $A\Box^+B Li_2^C(Mg_3Al_2)^T Si_8 O_{22} (OH)_2$, is actually the amphibole composition composed of the smallest possible structural modules. Crystallization in $Pnma$ symmetry, where the two double-chains of tetrahedra can assume different conformations, is probably required by the need to obtain a more suitable [5 + 1]-

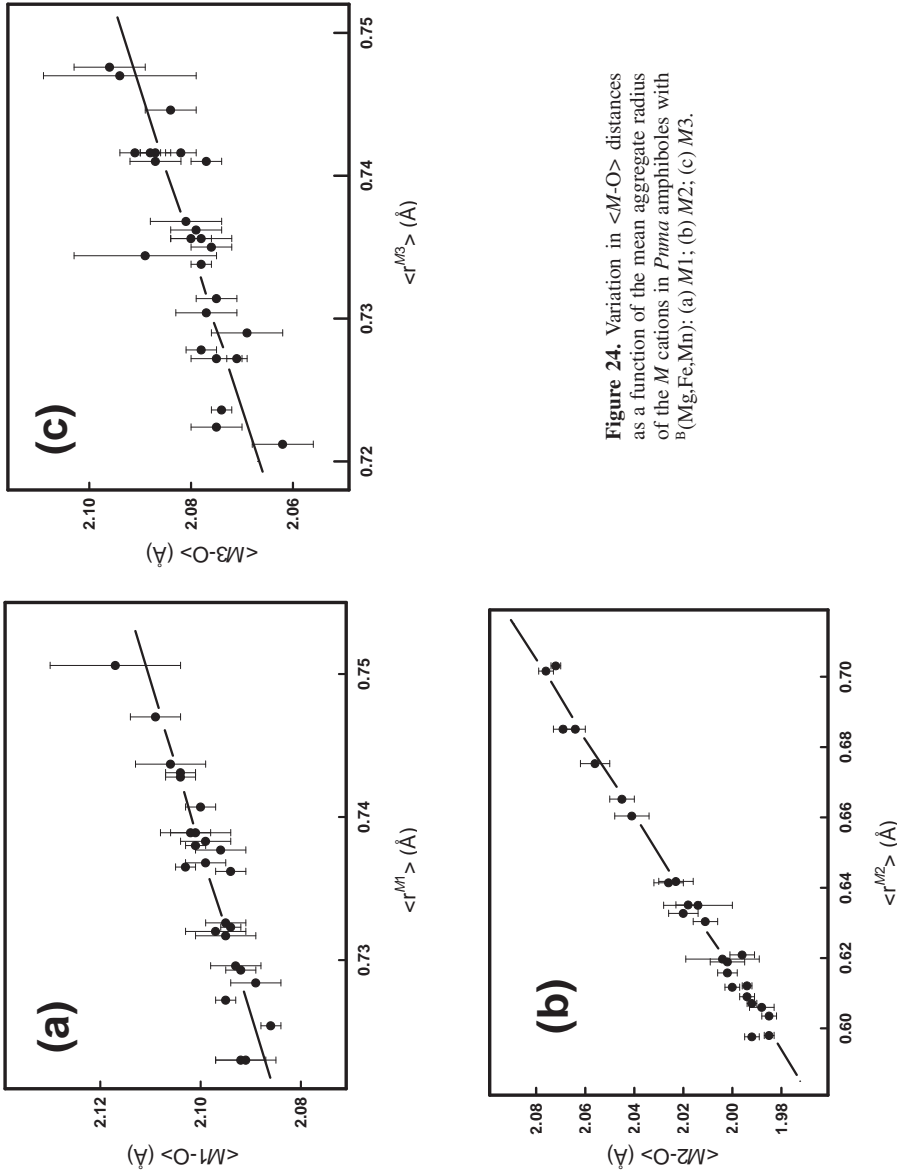


Figure 24. Variation in $\langle M-O \rangle$ distances as a function of the mean aggregate radius of the M cations in $Pima$ amphiboles with $B(Mg,Fe,Mn)$: (a) $M1$; (b) $M2$; (c) $M3$.

coordination for ${}^B\text{Li}$, and to shrink the cation-cation distances. This arrangement does not allow extensive incorporation of larger homovalent substituents, which are hosted via mechanisms implying distortion of the octahedra. Actually, only one occurrence of ferroholmquistite has been reported so far (Cámara and Oberti 2005).

Cámara and Oberti (2005) also provided structure refinements and complete chemical analyses of samples from reported occurrences of holmquistite. The observed trends are reported in Figure 25, and the relevant regression equations are given in Table 6. Comparison with those reported for *Pnma* amphiboles with ${}^B(\text{Mg},\text{Fe},\text{Mn})$ confirms the different relations between composition and geometry in the two series.

THE STEREOCHEMISTRY OF THE $M(4)$ SITE

The $M(4)$ site occurs at the junction of the strip of octahedra and the double-chain of tetrahedra in all amphibole structure types, and is occupied by B cations (Na , Li , Ca , Mn^{2+} , Fe^{2+} , Mg). The B cation bonds to oxygen atoms of both the strip of octahedra and the double-chain of tetrahedra, and is the primary link between these two parts of the structure. As a result, this site and its constituent cations are a major influence on the symmetry, crystal chemistry and chemical composition of the amphiboles (Warren 1930; Whittaker 1960; Papike et al. 1969). In monoclinic amphiboles, the nature of the B cation significantly affects the β angle, and thus the periodicity along the stacking direction, a^* ($= a \sin \beta$). Within compositional series with homovalent B cations, there is a reasonable linear correlation (with obvious systematic scatter) between the aggregate ionic radius at $M(4)$ [$\langle r^{M(4)} \rangle$] and the β angle. We may investigate

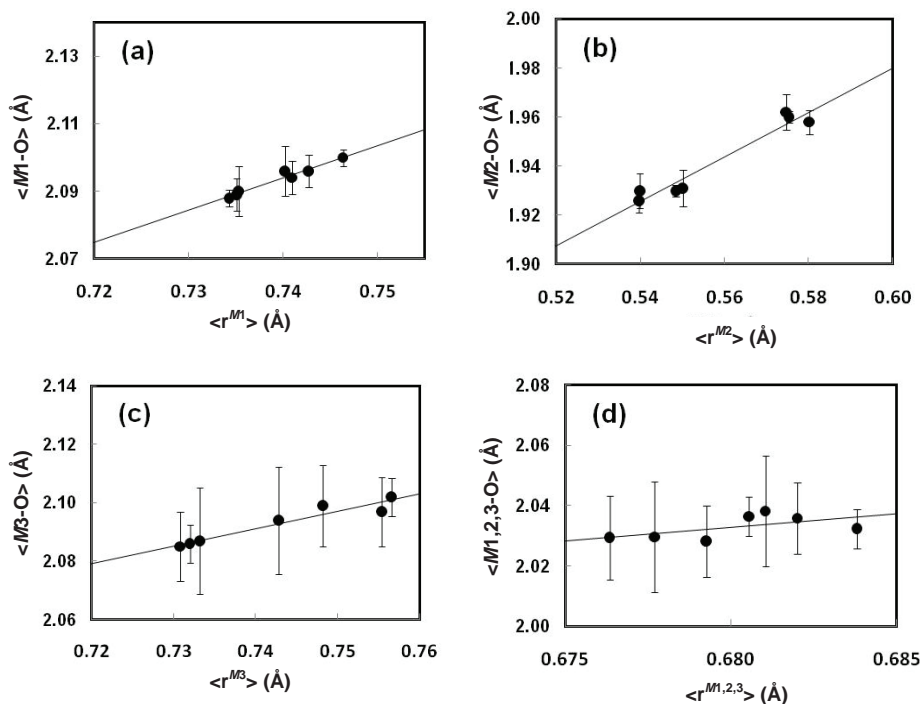


Figure 25. Variation in $\langle M-O \rangle$ distances as a function of the mean aggregate radius of the M cations in *Pnma* amphiboles with ${}^B\text{Li}$: (a) $M1$; (b) $M2$; (c) $M3$; (d) $M1,2,3$.

the origin of the scatter in Figure 26 by stepwise regression analysis, the results of which are given in Table 8. After the aggregate size of the $M(4)$ cations, the following parameters correlate significantly with the β angle: the aggregate formal charge, Z , of the $M(4)$ cations, the aggregate size of the $M(1,2,3)$ cations, and the $^{[4]}Al$ content. This behavior is in accord with the β angle being controlled by the linkage requirements of the double-chain of tetrahedra and the strip of octahedra.

The calcic, sodic-calcic and sodic amphiboles

These amphiboles have space-group symmetry $C2/m$; the $M(4)$ site has point symmetry 2 and is surrounded by eight O atoms. In these groups with large B cations, the $M(4)$ site occupies a position at $0 \sim 0.28 \frac{1}{2}$. In $C2/m$ amphiboles with small B cations, the $M(4')$ site

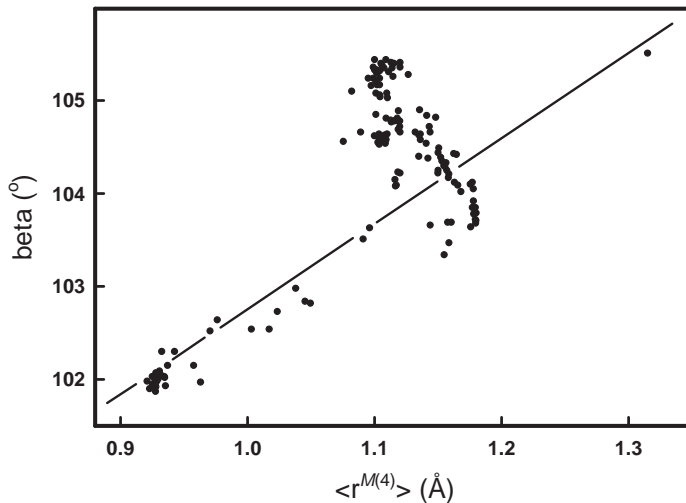


Figure 26. Variation in the β angle in as a function of the aggregate radius of the $M(4)$ cations for selected $C2/m$ amphiboles.

Table 8. Regression results for the $M(4)$ -sites in $C2/m$ amphiboles and $^{[6]}M4$ in $Pnma$ amphiboles.

Y	x_j	y_o	a_i	R	s^* (° or Å)
β	$\langle r^{M(4)} \rangle$	92.8(1.3)	1.86(36)	0.965	0.31
	$Z^{M(4)}$		1.33(9)		
	$\langle r^{M(1,2,3)} \rangle$		-5.7(1.8)		
	$^{[4]}Al$		0.33(6)		
$\langle M(4)-O \rangle$	$^{[4]}Al$	1.306	-0.0262(17)	0.934	0.011
	$\langle r^{M(1,2,3)} \rangle$		0.68(6)		
	$\langle r^{O(3)} \rangle$		0.446(78)		
	$\langle r^{M(4)} \rangle$		0.106(14)		
	Z^A		0.049(4)		
$\langle M4-O \rangle$	$\langle r^{M1,2,3} \rangle$	1.363(74)	1.37(11)	0.938	0.006

* s = standard error of estimate.

occupies a position at $0 \sim 0.26 \frac{1}{2}$, and in calcic, sodic-calcic and sodic amphiboles with a significant component of $^B(\text{Mg}, \text{Fe}, \text{Mn})$, both sites can be identified (Rossi et al. 1987; Oberti and Ghose 1993). A detailed discussion of the coordination at the $M(4)$ site is given by Hawthorne (1983a). The size of the $M(4)$ polyhedron increases from $M(4) = \text{Ca}_2 \rightarrow \text{CaNa} \rightarrow \text{Na}_2$, but is also strongly affected by the size of the $M(2)$ polyhedron (cation), $\langle M(4)\text{-O} \rangle$ increasing with increasing $\langle M(2)\text{-O} \rangle$ for a fixed size of the $M(4)$ cation.

Amphiboles with small B cations (magnesium-iron-manganese-lithium, magnesium-sodium and lithium-sodium)

The orthorhombic amphiboles have space-group symmetries $Pnma$ and $Pnmm$, and the $M4$ sites have point symmetries 1 and 2, respectively. The monoclinic amphiboles have space-group symmetries $C2/m$ and $P2_1/m$, and the $M(4)$ sites have point symmetries 2 and 1, respectively. As in the $C2/m$ amphiboles, with large B cations, the $M(4)$ site occupies a position at $0 \sim 0.28 \frac{1}{2}$, whereas with small B cations, the $M(4')$ site occupies a position at $0 \sim 0.26 \frac{1}{2}$. In $^B\text{Na-}^B\text{Li}$ solid-solutions, both sites can be identified by crystal-structure refinement (Oberti et al. 2004).

The $C2/m$ amphiboles: variation in $\langle M(4)\text{-O} \rangle$ bondlengths

In the $C2/m$ amphiboles, the $M(4)$ site can be occupied by a wide variety of cations of different charge and size: Li, Mg, Fe^{2+} , Mn^{2+} , Ca, Na (and even K and Sr in various synthetic amphiboles), and the $\langle M(4)\text{-O} \rangle$ distance shows considerable variation in these amphiboles: 2.45–2.62 Å. However, within the calcic, sodic-calcic, sodic, and magnesium-iron-manganese-lithium amphibole groups, there is no significant simple correlation between $\langle M(4)\text{-O} \rangle$ and $\langle r^{M(4)} \rangle$. The amphiboles of the magnesium-iron-manganese-lithium group show a significant correlation of $\langle M(4)\text{-O} \rangle$ and $\langle r^{M(1,2,3)} \rangle$ (Fig. 27a, Table 7). This relation suggests that $\langle M(4)\text{-O} \rangle$ is significantly affected by the articulation requirements of the strip of octahedra and the double-chain of tetrahedra. As the size of the strip of octahedra increases (i.e., increasing $\langle r^{M(1,2,3)} \rangle$), the double-chain straightens to maintain linkage, and the $M(4)\text{-O}$ bonds lengthen accordingly, thereby increasing $\langle M(4)\text{-O} \rangle$.

The factors affecting $\langle M(4)\text{-O} \rangle$ in the $C2/m$ amphiboles as a whole were investigated using stepwise linear regression with $\langle M(4)\text{-O} \rangle$ as the dependent variable and the following sets of independent variables: (1) $^{[4]}\text{Al}$, $\langle r^{M(1)} \rangle$, $\langle r^{M(2)} \rangle$, $\langle r^{M(3)} \rangle$, $\langle r^{M(4)} \rangle$, $\langle r^{O(3)} \rangle$, $Z^{M(4)}$ and Z^A (where $Z^{M(4)}$ and Z^A are the formal charges of the $M(4)$ - and A -site cations, respectively); (2) $^{[4]}\text{Al}$, $\langle r^{M(1,2,3)} \rangle$, $\langle r^{M(4)} \rangle$, $\langle r^{O(3)} \rangle$, $Z^{M(4)}$ and Z^A . The second option gave the more significant fit and the results are given in Table 8. The most important parameters are $^{[4]}\text{Al}$, $\langle r^{M(1,2,3)} \rangle$ and Z^A . These are the principal parameters affecting the relative sizes of the double-chain of tetrahedra ($^{[4]}\text{Al}$) and the strip of octahedra ($\langle r^{M(1,2,3)} \rangle$), and ability of the double chain to vary its $\text{T-O}_{\text{bridging}}\text{-T}$ distances (Z^A , a measure of the occupancy of the A site), and are in accord with the idea that the stereochemistry of the $M(4)$ site has a major influence on the crystal chemistry and bulk composition of the amphiboles.

The $Pnma$ amphiboles: variation in $\langle M4\text{-O} \rangle$ bondlengths

The $M4$ site is occupied predominantly by Fe^{2+} , Mn^{2+} , Mg and Li; however, there is no significant correlation between $\langle M4\text{-O} \rangle$ and $\langle r^{M4} \rangle$, the mean radius of the constituent $M4$ cations. However, as with the monoclinic magnesium-iron-manganese-lithium amphiboles, there is a strong correlation between $\langle M4\text{-O} \rangle$ and the mean constituent-cation radius of the $M(1,2,3)$ sites (Fig. 27b): the equation of the linear-regression relation is given in Table 8. The slope and intercept of the curve are reasonably similar to the analogous values for the $M(4)$ site in the monoclinic magnesium-iron-manganese-lithium amphiboles (Fig. 27a, Table 8), indicating the same cause for this relation.

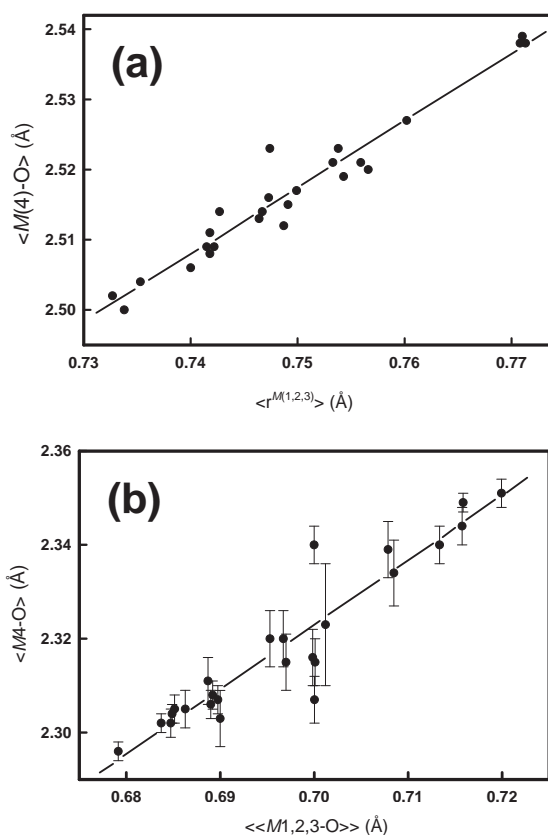


Figure 27. (a) Variation in $\langle M(4)-O \rangle$ distance in $C2/m$ Mg-Fe-Mn-Li amphiboles as a function of the aggregate radius of the $M(1,2,3)$ cations; (b) variation in $\langle M4-O \rangle$ distance in $Pnma$ Mg-Fe-Mn-Li amphiboles as a function of the aggregate radius of the $M1,2,3$ cations.

THE STEREOCHEMISTRY OF THE A SITE

The A site occurs in the large cavity between the back-to-back chains of tetrahedra in the amphibole structure. This site may be occupied or vacant, and like the $M(4)$ site, the details of this occupancy are very dependent on structure type (i.e., space group) as the relative displacement of the back-to-back chains is dependent on space-group symmetry and stacking of the layers (Fig. 14). The A cavity may be occupied by monovalent (Na, K, Li) or divalent (Ca, Pb^{2+}) cations, and the siting of these cations are strongly influenced by short-range bond-valence constraints. It is notable that in the $P2_1/m$ and $Pnmm$ structures, the A site is vacant in natural amphiboles, but may be occupied by $B(NaMg)$ in synthetic $P2_1/m$ amphiboles (Oberti et al. 2007b; Welch et al. 2007).

The $C2/m$ amphiboles

The arrangement of polyhedra around the A site is shown in Figure 28, and typical A-O distances for different amphiboles are shown in Table 9. The pattern of distances is similar in each structure, but the variation is considerable (up to 0.3 Å) for each individual distance. This variation is accompanied by rotation of the chains [variation in the O(5)-O(6)-O(5) angle] that moves the O(5), O(6) and O(7) anions relative to the central A position].

Figure 28. The arrangement of polyhedra around the A cavity and the A sites in the $C2/m$ amphibole structure.

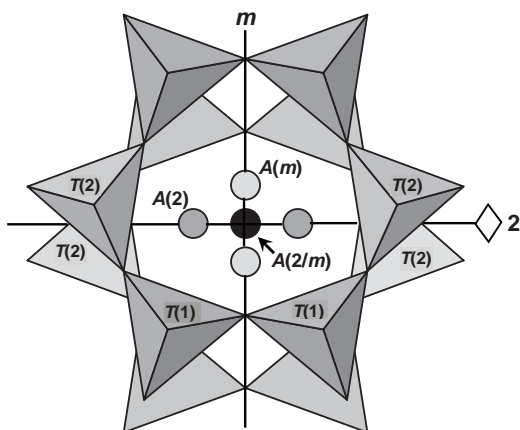


Table 9. A–O distances (Å) in selected $C2/m$ amphiboles.

		Cumm	Trem	Parg	Winch	Taram
A–O(5)	×4	2.824	2.970	3.045	2.77	3.008
A–O(6)	×4	3.278	3.156	3.068	3.13	3.152
A–O(7)	×2	2.295	2.486	2.432	2.539	2.520
<A–O>		2.900	2.948	2.932	2.87	2.968
		Nyb	Kato	Arf	Glauc	Rieb
A–O(5)	×4	2.913	2.970	2.755	2.814	2.832
A–O(6)	×4	3.137	3.108	3.212	3.216	3.252
A–O(7)	×2	2.446	2.419	2.629	2.519	2.550
<A–O>		2.909	3.091	2.913	2.916	2.944

Refs: Cumm: Ghose (1961), Hawthorne (1983a); Trem: Papike et al. (1969); Parg: Bocchio et al. (1978); Winch: Sokolova et al. (2001); Taram: Hawthorne and Grundy (1978); Nyb: Hawthorne et al. (1996a); Kato: Oberti et al. (1998); Arf: Hawthorne (1976); Glauc: Hawthorne (1979); Rieb: Hawthorne (1978).

The A cations do not occupy the central site $[A(2/m)]$ at $(0, \frac{1}{2}, 0)$ (notation from Hawthorne and Grundy 1972). Figure 28 shows the sites that are actually occupied in the many hundreds of amphibole structures refined to the present time; a few studies have put cations at a general site $[A(1): x, y, z]$, but further work has shown that these assignments are not warranted. Where the A cation is K, the electron density occurs at the $A(m)$ site (Papike et al. 1969; Cameron et al. 1983). The maxima of the electron density are confined to the mirror plane through $(0, \frac{1}{2}, 0)$ and occur on both sides of the $A(2/m)$ site with the density elongated in the general direction of the nearer O(7) anions. The distance between the two maxima is of the order of 0.29 Å, too short for simultaneous occupancy of both sites in a single A cavity, and hence K may be considered as positionally disordered off the central position with only one (or sometimes neither if $K < 1$ apfu) position occupied in a specific cavity.

The situation where $A = Na$ is much more complicated as electron density can occur at $A(m)$, $A(2)$ or both. As indicated in Figure 29, where distributed over the $A(m)$ and $A(2)$ sites, the electron density is best shown in a difference-Fourier map parallel to $(\bar{2}01)$ and through $(0, \frac{1}{2}, 0)$. Figure 30 shows the distribution of electron density for a series of amphiboles with $^A Na$ cations ≈ 1 apfu. It is apparent from Figure 30 that Na may occur only at $A(m)$, only at $A(2)$, or disordered over $A(m)$ and $A(2)$. There has been a considerable amount of work trying to

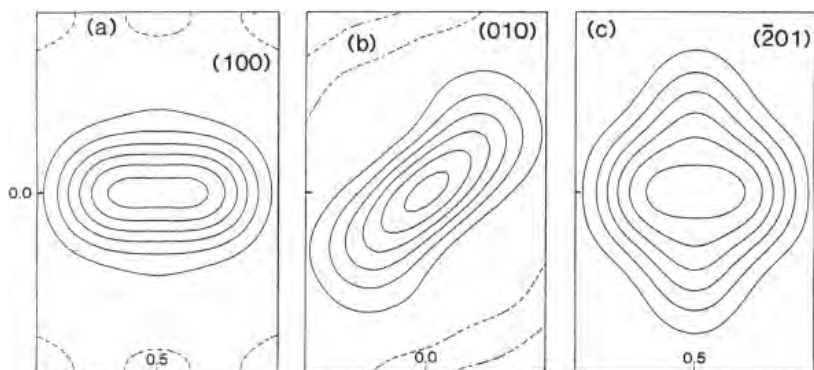


Figure 29. The electron density in the A cavity for nyböite with $A \approx \text{Na}$; (a) section parallel to (100); (b) section parallel to (010); (c) section parallel to $(\bar{2}01)$; the contour interval is $1 e/\text{\AA}^3$ and the broken line is the zero contour (from Hawthorne et al. 1996a).

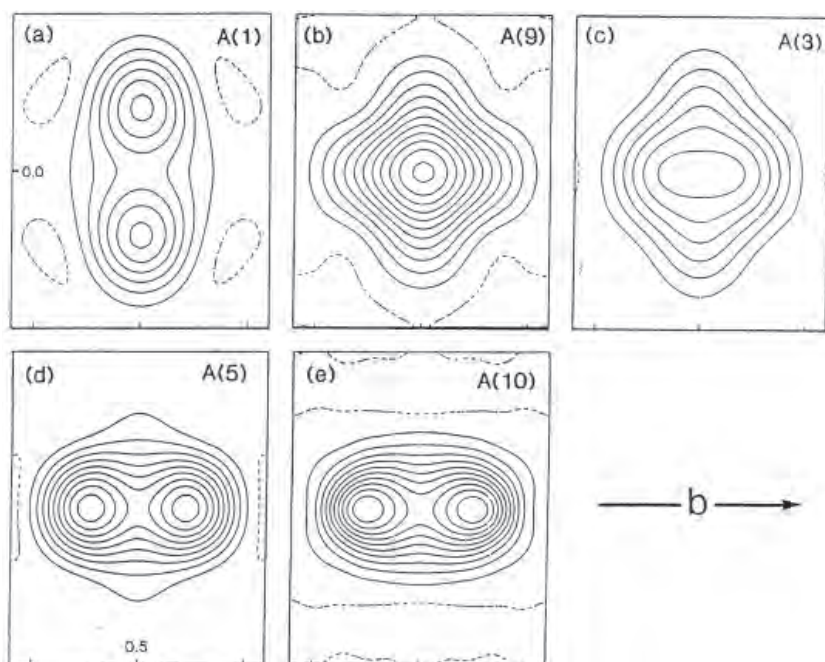


Figure 30. Sections parallel to $\bar{2}01$ showing the electron density in the A cavity for a series of $C2/m$ amphiboles with $A \approx \text{Na}$; legend as in Fig. 28 (from Hawthorne et al. 1996a); (a) fluoronyböite; (b) pargasite; (c) nyböite; (d) taramite; (e) pargasite.

understand the details of this disorder, often focusing on variations in bond valence (and hence bond lengths) (see summary by Hawthorne 1983a). However, Hawthorne et al. (1996a) showed that the order-disorder relations within the A cavity are actually controlled by short-range bond-valence requirements; these will be dealt with by Hawthorne and Della Ventura (2007).

The $P2_1a$ amphibole

The polyhedra arrangement around the *A* site is shown in Figure 31, and the A-O distances and analogous bond-valences for joesmithite are shown in Table 10. Moore (1969) suggested that the occurrence of Pb^{2+} may be fortuitous, but Hawthorne (1983a) noted that the off-centered arrangement of Pb^{2+} indicates lone-pair stereoactivity. As discussed by Moore (1969) and Moore et al. (1993), Pb^{2+} is displaced off the central position toward the *T*(1)B site occupied by Be, suggesting that bond-valence requirements are driving this arrangement (Oberti et al. 2007b).

The $Pnma$ amphiboles

The arrangement of polyhedra around the *A* site is shown in Figure 32. Comparison with the arrangement in the $C2/m$ amphiboles (Fig. 28) shows significant differences. First, the chains in the $Pnma$ structure are more displaced relative to each other than the chains in the $C2/m$ structure (cf. Figs. 28 and 32). Second, the difference in degree of rotation of the *A*- and *B*-chains in the $Pnma$ structure significantly affects the A-O distances; thirdly, the *A* site does not occur in the center of the cavity (Fig. 32). The collective result of these factors is that the arrangement of anions around the *A* site in the $Pnma$ structure is more compact than the analogous arrangement in the $C2/m$ structure. As a result of the difference in symmetry, there is no longer a center of symmetry at the centre of the *A* cavity (as there is for the $C2/m$ structure). The only symmetry involving the *A* cavity is the mirror plane parallel to the *b*-axis. In all structures so far refined, the *A* site is confined to this mirror plane with coordinates (*x*, $-\frac{1}{4}$, *z*). Typical A-O distances in $Pnma$ amphiboles with *A* cations are shown in Table 11 (Fe-

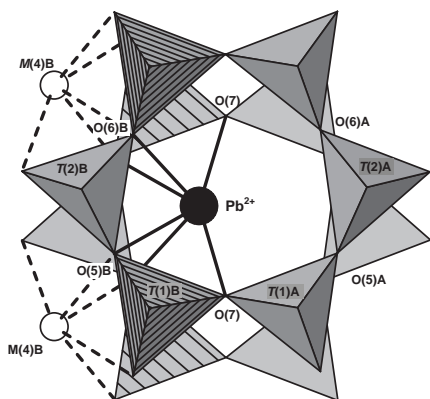


Figure 31. The arrangement of polyhedra around the *A* cavity and the *A* site in the $P2_1a$ amphibole structure.

Table 10. A–O distances (Å) in joesmithite*.

A–O(5)A	3.517(5)
A–O(5)B	2.589(5)
A–O(6)A	2.568(4)
A–O(6)B	3.433(5)
A–O(7)	2.580(6)
<A–O>	2.937

* from Moore et al. (1993)

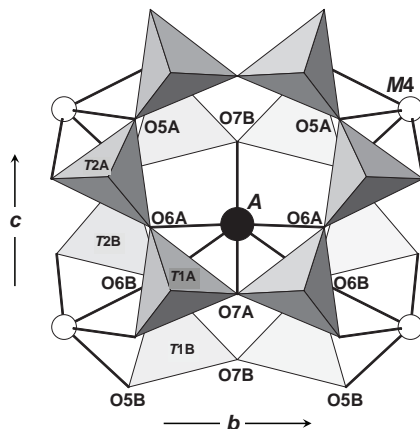


Figure 32. The arrangement of polyhedra around the *A* cavity and the *A* site in the $Pnma$ amphibole structure.

Table 11. A–O distances (Å) in antophyllite and sodicgedrite.

$^{[4]}Al$ (apfu)	0.17	1.79
A–O6A ×2	2.677	2.654
A–O6B ×2	2.808	2.624
A–O7A	2.287	2.387
A–O7B	2.370	2.378

* from Schindler et al. (2007)

poor anthophyllite and holmquistite have very low *A*-site occupancies (e.g., Robinson et al. 1971; Cámara and Oberti 2005).

The *Pnmm* amphiboles

In the synthetic protoamphibole reported by Gibbs (1969), the chemical analysis (Gibbs et al. 1960) indicated Li at the *A* site, but Li could not be located by structure refinement. Sueno et al. (1998) reported the occurrence and structures of proto-ferro-anthophyllite and proto-mangano-ferro-anthophyllite, but in both these structures, the *A* site is vacant.

THE STEREOCHEMISTRY OF THE O(3) SITE

The O(3) site is located at the center of the strip of *M*(1,2,3) octahedra and can be occupied by monovalent [(OH), F, Cl] and divalent (O) anions that are bonded to two *M*(1) and one *M*(3) cations (Fig. 33a; the siting of the O(3) site in other amphibole structure types is analogous to that in the *C2/m* structure). Where occupied by (OH), the associated H atom is situated ~ 1 Å away from the O(3) site with the O-H bond orthogonal to the plane of the strip of *M*(1,2,3) octahedra.

The *C2/m* amphiboles

O(3) = (OH). The arrangement of atoms around the O(3) site [where O(3) = (OH)] in the *C2/m* amphibole structure is shown in Figure 33b. The position of the H atom in tremolite was located by Hawthorne and Grundy (1976) [O(3)-H = 0.957(6) Å] and Hanisch (1966) showed by polarized infrared spectroscopy that the O-H bond is orthogonal to (100). It is notable that the H atom hydrogen-bonds only to one O(7) atom [H...O(7) = 2.775 Å in tremolite, Hawthorne and Grundy 1976], although this situation may change for short-range arrangements in ^[4]Al-bearing amphiboles.

O(3) = F. Above, we note that there is a hydrogen bond to the O(7) anion. Where O(3) = F, this hydrogen bond is no longer present, and as a consequence, the valence-sum rule (Brown 1981, 2002; Hawthorne 1994, 2006) predicts that the *T*(1)-O(7) distance should be slightly shorter in fluorotremolite than in tremolite. This conclusion is in accord with the *T*(1)-O(7) distances in tremolite (1.622 Å, Evans and Yang 1998, sample 11B, Si = 7.997 apfu) and synthetic fluorotremolite (1.606 Å, Cameron and Gibbs 1973, Si = 8 apfu).

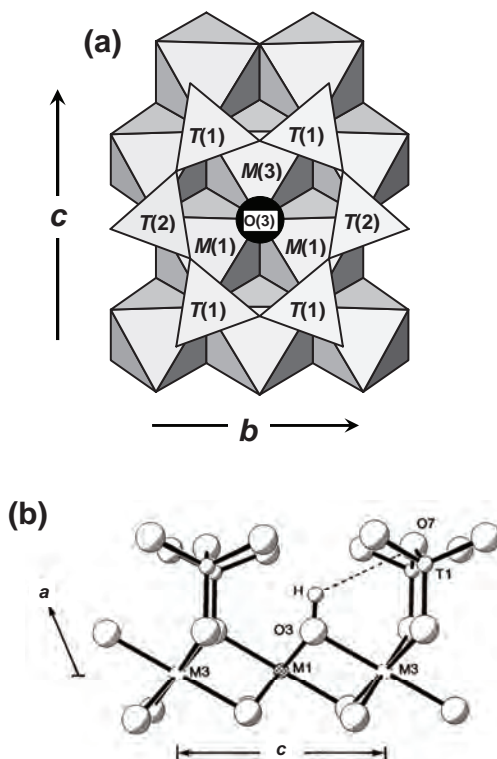


Figure 33. The O(3) site in the *C2/m* amphibole structure; the O(3) site is shown by a black circle; (a) projected onto (100); (b) projected onto (010) with perspective and with the *T*(2) sites omitted for clarity, the H atom is shown by a small circle, and the H...O(7) hydrogen bond is shown by a dashed line. [Used by permission of Schweizerbart'sche Verlagsbuchhandlung, from Della Ventura et al. (1999), *European Journal of Mineralogy*, Vol. 11, Fig. 7, p. 88.]

O(3) = Cl. Where O(3) = Cl, the site is significantly displaced with reference to the strip of $M(1,2,3)$ octahedra relative to where O(3) = (OH). Figure 34 shows the electron density through the O(3) site for a series of amphiboles with increasing Cl content. The Cl atom is displaced from the position of the O atom, in accord with the much larger radius of Cl relative to that of O [$r(\text{Cl}) = 1.81$, $r(\text{O}) = 1.36 \text{ \AA}$, Shannon 1976]. Indeed, for the crystal with Cl = 0.98 apfu, the distances from the M cations to Cl are much greater than the corresponding distances to O at O(3): $M(1)\text{-O}(3) = 2.147$, $M(1)\text{-Cl} = 2.462$; $M(3)\text{-O}(3) = 2.105$, $M(3)\text{-Cl} = 2.400 \text{ \AA}$ (Oberti et al. 1993); similar values are reported by Rastsvetaeva et al. (1996).

There are two possible mechanisms whereby Cl can replace (OH) at O(3) in the amphibole structure: (1) the strip of octahedra could expand to incorporate the larger anion (as suggested by Volfinger et al. 1985), and (2) the larger anion could take up a position displaced from the plane of the O anions of the octahedron strip into the A cavity. Oberti et al. (1993) show that both mechanisms are operative, and that mechanism (2) is more important than mechanism (1). Cl-rich amphiboles are generally rich in Fe^{2+} and K (Krutov 1936; Dick and Robinson 1979; Volfinger et al. 1985; Vanko 1986; Suwa et al. 1987; Castelli 1988; Morrison 1991; Enami et al. 1992; Zhu et al. 1994; Kullerud 1996; Leger et al. 1996; Sato et al. 1997; McCormick and McDonald 1999), indicating the effect of increasing Fe^{2+} in increasing the dimensions of the strip of octahedra, and increasing K promoting the bonding between K at the $A(m)$ site and Cl at O(3) (see also Oberti et al. 2007b).

O(3) = O. The occurrence of O at O(3) places considerable restrictions on occupancy of the adjacent $M(1)$ and $M(3)$ sites as the bond-valence requirements of the oxygen atom at O(3) must be satisfied by the three adjacent $M(1)$ and $M(3)$ cations. In turn, this requirement places considerable restrictions on the chemical composition of the amphibole. At least some of the $M(1)$ and $M(3)$ cations must be of high charge in order to provide sufficient bond-valence to O(3). Thus the compositions of oxygenian amphiboles tend to be characterized by Ti^{4+} as a prominent C cation. However, this is not always the case: ungarrettiite is characterized by $M(1) = M(3) = \text{Mn}^{3+}$, where the Jahn-Teller distortion of the constituent polyhedra provides sufficiently short bondlengths to O(3) to satisfy local bond-valence requirements (Hawthorne et al. 1995). These amphiboles are discussed in more detail by Oberti et al. (2007a).

UNIT-CELL PARAMETERS AND COMPOSITION IN $C2/m$ AMPHIBOLES

We have shown above that the geometry (size and distortion) of each module of the amphibole structure is significantly affected by its constituent site-population, and by the composition of the other modules. The unit-cell parameters are a measure of the volume occupied by the complete structure, and thus must be sensitive to (1) the intrinsic geometry of the strip of octahedra and of the double-chain of tetrahedra; (2) the geometry of their connections through the shared oxygen atoms to form what is usually called an I-beam; (3) the geometry of the connections between the I-beams through the $M(4)$ site; (4) the size of the A cation. Therefore, variations in chemical composition and cation ordering are expected to strongly affect unit-cell parameters. It may also be expected that some combinations of site populations will not allow articulation of the structure modules, and thus cannot occur, at least under specific P and T conditions.

An understanding of the relations between the composition and unit-cell parameters in amphiboles would, in principle, help to understand the structural constraints on amphibole stability. Several statistical studies have been made (beginning with Whittaker 1960 and Colville et al. 1966). However, none of these have been truly comprehensive. Four factors have hampered this analysis: (1) lack of reliable site-populations; (2) lack of precise and accurate unit-cell dimensions obtained with a reasonably similar procedure; (3) lack of reliable site-

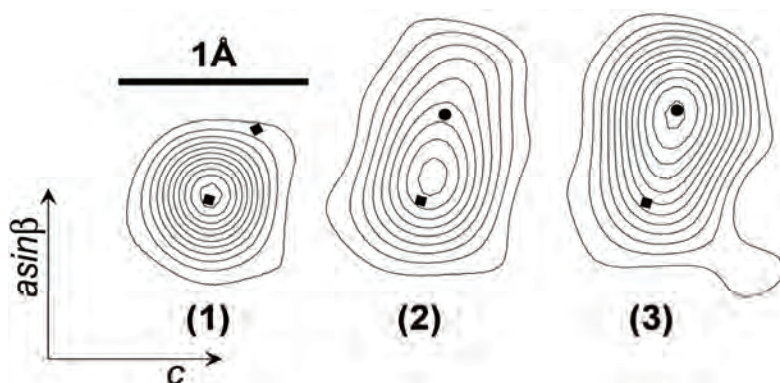


Figure 34. The electron density through the O(3) site in amphiboles with different amounts of Cl at the O(3) site, showing the displacement of the positions of O, H and Cl at this site; (a) Cl = 0.00 apfu; (b) Cl = 0.56 apfu; (c) Cl = 0.98 apfu; Circle: O atom; diamond: H atom; square: Cl atom; contours are drawn at 5, 10, 15, 20 and 25 e/Å³ (from Oberti et al. 1993).

populations and chemical compositions for synthetic amphiboles; (4) the observation that a fixed cation-O distance (for instance, as calculated from constituent ionic radii) cannot be used for all amphibole compositions. The latter two points make the determination of site populations a difficult task, as it will be further discussed in Oberti et al. (2007a).

The crystal-chemical database for amphiboles at the IGG-CNR-PV satisfies all the above requirements. It contains unit formulae and structural data representative of every known *C2/m* amphibole composition (but sadanagaite), and were obtained by the same procedure. In particular, site populations were optimized by combining chemical analyses with quantitative models of structural change as a function of composition (a peculiar case of structure modeling) in the COMAMPH procedure, as described in more detail by Oberti et al. (2007a). The ranges of variation observed in the data base are: $a = 9.357\text{--}10.143$ Å, $b = 17.580\text{--}18.402$ Å, $c = 5.262\text{--}5.365$ Å, $\beta = 101.84\text{--}105.71^\circ$, $V = 846.21\text{--}948.23$ Å³.

As a first step, the unit-cell parameters were plotted one against the other to understand whether there are forbidden zones for their combination. Figure 35 shows that amphiboles do not occupy all available space, and that discrete populations can be identified which are mainly related to the nature of the B cations. Multiple stepwise linear regression was then done using the unit-cell parameters as dependent variables. Due to the constraint of the full occupancy of the *T* and *M* sites, only the following independent chemical constituents were used: ^AK, ^ANa, ^BNa, ^B(Fe,Mn)²⁺, ^BLi, ^BMg, ^CAl, ^CTi, ^CFe²⁺, ^CFe³⁺, ^CLi, ^TAl, ^WF, ^WO²⁻. In this way, the equations predict deviations from ideal tremolite, □Ca₂Mg₅Si₈O₂₂(OH)₂. Four regression equations were obtained, which allow calculation of the unit-cell parameters starting from the unit-formula (Table 12). For a , b and β , multiple correlation coefficients are higher than 0.99, and the lower value obtained for the c edge (0.930) is justified by its far smaller variance. The y_0 values given in Table 12 represent the unit-cell parameters extrapolated for pure tremolite: $a = 9.873(15)$, $b = 18.057(11)$, $c = 5.268(5)$ Å, $\beta = 104.94(8)^\circ$, giving $V = 907.4$ Å³. They are consistent with those extrapolated by Gottschalk et al. (1999) based on Rietveld analysis of a series of samples in the much simpler synthetic system tremolite-cummingtonite: $a = 9.8354(18)$, $b = 18.0562(14)$, $c = 5.2768(6)$ Å, $\beta = 104.74(2)^\circ$, $V = 906.3$ Å³.

It is not easy to interpret the relative importance of the various chemical descriptors on the variation of the dependent variable because the regression coefficient must be weighted for the possible abundance of each cation/anion. For the a edge, the key role is played by ^AK and by the incorporation of highly charged cations at the *M*(1,2,3) sites. However, each

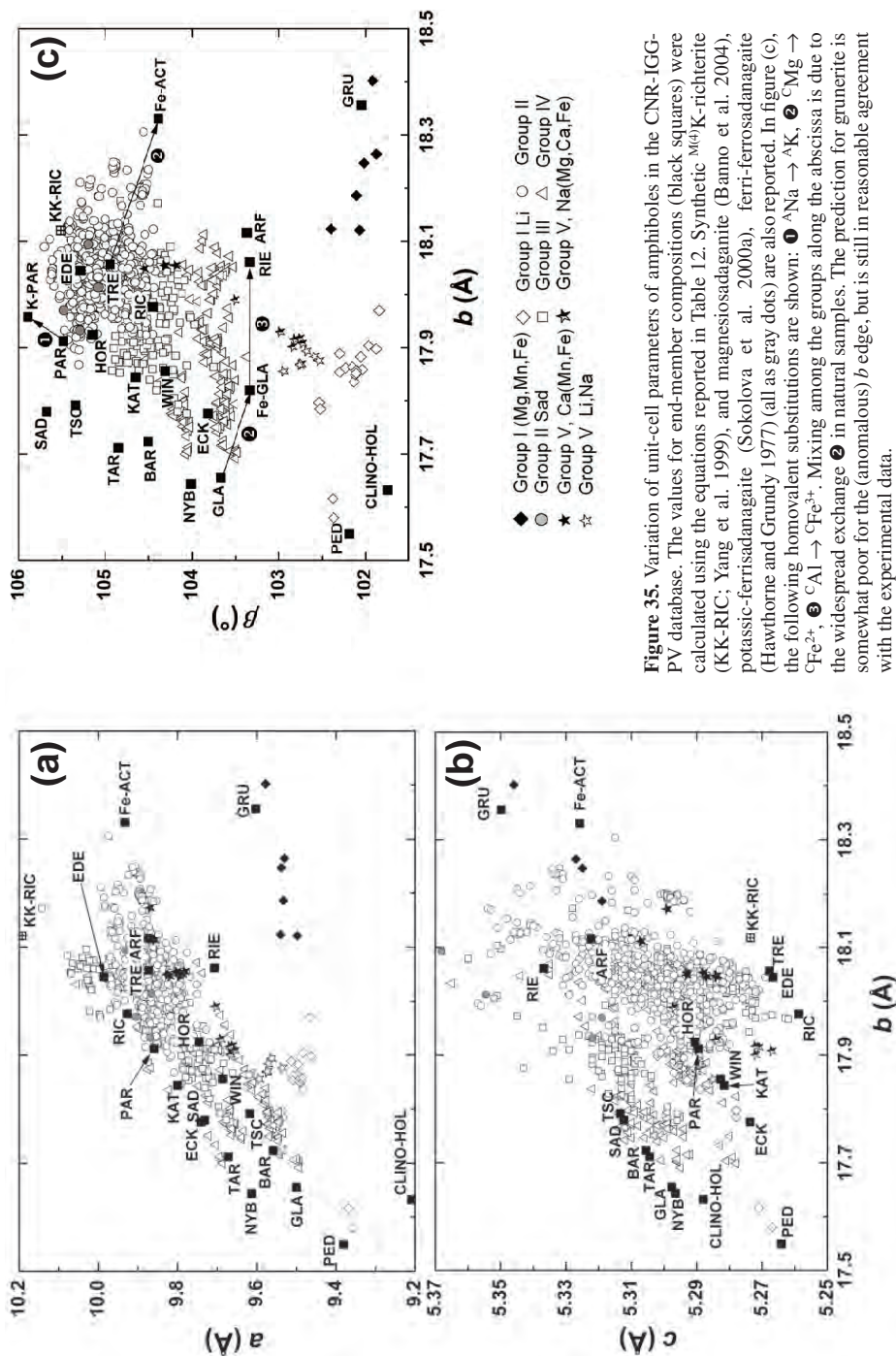


Table 12. Predictive equations for the unit-cell parameters obtained by multiple regression analysis of the CNR-JGG-PV data base.

x_i	a (Å)			b (Å)			c (Å)			β (°)		
	a_i	x_i	a_i	a_i	x_i	a_i	x_i	a_i	x_i	a_i	x_i	a_i
^A K	0.2030(58)	^C Al	-0.1207(25)	^C Ti	0.0093(18)	^B Li	-1.5980(245)					
^C Ti	-0.1968(126)	^C Li	-0.0828(75)	^A Na	-0.0239(14)	^B Mg	-1.2021(1082)					
^C Al	-0.1866(25)	^B Li	-0.0915(37)	^T Al	0.0228(8)	^B (Fe,Mn)	-1.1678(166)					
^B (Fe,Mn)	-0.1652(69)	^B Na	-0.0800(22)	^B Na	0.0149(8)	^B Na	-0.6355(116)					
^B Li	-0.1453(41)	^C Fe ²⁺	0.0548(9)	^B (Fe,Mn)	0.0120(22)	^A K	0.5539(235)					
^C Li	0.1174(120)	^A K	0.0456(42)	^C Fe ²⁺	0.0116(4)	^C Li	0.2992(505)					
^B Mg	-0.1083(215)	^W F	-0.0207(17)	^B Li	0.0101(14)	^T Al	0.1979(132)					
^C Fe ³⁺	-0.1010(34)	^W O ²⁻	0.0192(20)	^A K	-0.0062(17)	^A Na	0.1422(247)					
^A Na	0.0543(44)	^B (Fe,Mn)	0.0126(49)	^C Fe ³⁺	0.0022(8)	^C Fe ²⁺	-0.1119(71)					
^T Al	0.0591(17)	^T Al	-0.0119(18)									
^W F	-0.0439(24)											
^W O ²⁻	0.0416(65)											
^C Fe ²⁺	0.0120(14)											
^A K	0.2030(58)											
y_0	9.8728	y_0	18.0569	y_0	5.2678	y_0	104.944					
R	0.991	R	0.994	R	0.930	R	0.992					
s^*	0.015	s	0.011	s	0.0050	s	0.083					

* s = standard error of estimate

of these substitutions (heterovalent with respect to tremolite) implies a coupled heterovalent substitution, which also affects the dependent variable in a different and sometimes inverse way. For the *b* edge, substitutions at the *M*(1,2,3) and the O(3) site are particularly significant. For the β angle, the results confirm the regression done in a previous section based on aggregate ionic radius: the most important factors are the type of B cation and the amount of $^{\text{T}}\text{Al}$.

These equations can provide a rapid tool to (1) verify whether or not the structure predicted for amphibole compositions not found in Nature falls in an allowed region, (2) calculate the molar volume of pure end-members, (3) detect the occurrence or the effects of anomalous site-partitioning. They can also be used as a check for anomalous or incomplete chemical analyses.

SUMMARY

In the last 25 years, there have been major advances in our knowledge of both long-range and short-range order of both cations and anions. Experimental procedures for characterizing order and chemical composition of amphiboles have made major strides, and we now see widespread use of SREF, SIMS and infrared spectroscopy. In the future, we need to focus much more on the difficult-to-measure constituents: H (in particular), $\text{Fe}^{3+}/\text{Fe}^{2+}$ and Li, until their accurate measurement becomes routine in the same way that electron-microprobe analysis and SREF are today. Most of the advances discussed here have been experimental. Bond-valence requirements exert major control on short-range order of heterovalent cations and anions in amphiboles (and therefore on long-range order as well, as long-range order is the average of all short-range-order arrangements in a structure). However, the effects of temperature and pressure on SRO and bond-valence requirements are almost unknown. We still lack much understanding of the mechanistic controls on order-disorder of homovalent cations, particularly Mg and Fe^{2+} ; this is particularly unfortunate, as order-disorder of Mg and Fe^{2+} in many minerals is commonly quite sensitive to differences in temperature of equilibration. Thus there is much theoretical work and structure modeling to be done to understand temperature- and pressure-dependent ordering in amphiboles.

The range of chemical composition occupied by amphibole structures has widened significantly since the last Amphibole Short Course. Then, there was no knowledge either of the richness of the crystal chemistry of Li in amphiboles, or the occurrence of exotic oxygenian amphiboles. In the last 10 years, this state of affairs has changed radically. Monoclinic Li-dominant amphiboles have been discovered, and a new group of amphiboles has been recognized: the (Mg-Fe-Mn-Na-Li) amphiboles, with solid solution of Na and Li at the *M*(4) site in the *C2/m* structure. It is tempting to say that we have drawn bounds around the possible compositions of amphiboles, but we thought that 25 years ago, and it was patently untrue; perhaps the future holds more new and exotic chemistries, maybe in the area of synthetic amphiboles where novel compositions and structures are being discovered. In summary, the last 25 years have produced a lot of new knowledge about amphiboles; undoubtedly the next 25 years will do the same.

ACKNOWLEDGMENTS

FCH was supported by a Canada Research Chair in Crystallography and Mineralogy, and by a Discovery grant, both from NSERC, the Natural Sciences and Engineering Research Council of Canada. In addition, much of the work reviewed here was also supported by NSERC Major Equipment Grants and by grants from the Canada Foundation for Innovation. RO was supported by the Italian Consiglio Nazionale delle Ricerche through the project TAP01.004.002.

REFERENCES

- Appleyard EC (1975) Silica-poor hastingsitic amphiboles from the metasomatic alkaline gneisses at Wolfe, eastern Ontario. *Can Mineral* 13:342-351
- Bancroft GM (1973) Mössbauer Spectroscopy. An Introduction for Inorganic Chemists and Geochemists. McGraw-Hill, New York
- Bancroft GM, Brown JR (1975) A Mössbauer study of coexisting hornblendes and biotites: quantitative Fe³⁺/Fe²⁺ ratios. *Am Mineral* 60:265-272
- Banno Y, Miyawaki R, Matsubara S, Makino K, Bunno M, Yamada S, Kamiya T (2004) Magnesiosadanagaite, a new member of the amphibole group from Kasuga-mura, Gifu Prefecture, central Japan. *Eur J Mineral* 16:177-183
- Bocchio R, Ungaretti L, Rossi G (1978) Crystal chemical study of eclogitic amphiboles from Alpe Arami, Lepontine Alps, Southern Switzerland. *Rend Soc Ital Mineral Petrol* 34:453-470
- Brese NE, O'Keeffe M (1991) Bond-valence parameters for solids. *Acta Crystallogr* B47:192-197
- Brown ID (1981) The bond valence method. An empirical approach to chemical structure and bonding. *In: Structure and Bonding in Crystals II*. O'Keeffe M, Navrotsky A (eds) Academic Press, New York, p 1-30
- Brown ID (2002) The Chemical Bond in Inorganic Chemistry. The Bond Valence Model. Oxford University Press
- Brown ID, Altermatt D (1985) Bond-valence parameters obtained from a systematic analysis of the inorganic crystal structure database. *Acta Crystallogr* B41:244-247
- Bunch TE, Okrusch M (1973) Al-rich pargasite. *Am Mineral* 58:721-726
- Caballero JM, Monge A, La Iglesia A, Tornos F (1998) Ferri-clinoholmquistite, Li₂(Fe²⁺,Mg)₃Fe³⁺₂Si₈O₂₂(OH)₂, a new ⁶Li clin amphibole from the Pedriz Massif, Sierra de Guadarrama, Spanish Central System. *Am Mineral* 83:167-171
- Caballero JM, Oberti R, Ottolini L (2002) Ferripedrizite, a new monoclinic ⁶Li amphibole end-member from the Eastern Pedriz Massif, Sierra de Guadarrama, Spain, and a restatement of the nomenclature of Mg-Fe-Mn-Li amphiboles. *Am Mineral* 87:976-982
- Cámara F, Oberti R, Iezzi G, Della Ventura G (2003) The P2₁/m ↔ C2/m phase transition in synthetic amphibole NaNaMg Mg₅ Si₈ O₂₂ (OH)₂: thermodynamic and crystal-chemical evaluation. *Phys Chem Mineral* 30:570-581
- Cámara F, Oberti R, Della Ventura G, Welch MD, Maresch WV (2004) The crystal-structure of synthetic NaNa₂Mg₅Si₈O₂₁(OH)₃, a triclinic C $\bar{1}$ amphibole with a triple-cell and excess hydrogen. *Am Mineral* 89:1464-1473
- Cámara F, Oberti R (2005) The crystal-chemistry of holmquistites: Ferroholmquistite from Greenbushes (Western Australia) and hints for compositional constraints in ⁶Li amphiboles. *Am Mineral* 90:1167-1176
- Cameron M, Gibbs GV (1973) The crystal structure and bonding of fluor-tremolite: a comparison with hydroxyl tremolite. *Am Mineral* 58:879-888
- Cameron M, Sueno S, Papike JJ, Prewitt CT (1983) High temperature crystal chemistry of K and Na fluor-rich richterites. *Am Mineral* 68:924-943
- Castelli D (1988) Chlorpotassium ferro-pargasite from Sesia-Lanzo marbles (Western Italian Alps): A record of highly saline fluids. *Rend Soc Ital Mineral Petrol* 43:129-138
- Colville PA, Ernst WG, Gilbert MC (1966) Relationships between cell parameters and chemical compositions of monoclinic amphiboles. *Am Mineral* 51:1727-1754
- Cosca MA, Essene EJ, Bowman JR (1991) Complete chemical analyses of metamorphic hornblendes: implications for normalizations, calculated H₂O activities, and thermobarometry. *Contrib Mineral Petrol* 108:472-484
- Delaney JS, Bajt S, Sutton SR, Dyar MD (1996) In situ microanalysis of Fe³⁺/ΣFe in amphibole by X-ray absorption near edge structure (XANES) spectroscopy. *In: Mineral Spectroscopy: A Tribute to Roger G. Burns*. Dyar MD, McCammon C, Schaefer MW (eds). Geochemical Society Special Publication 5:165-171
- Della Ventura G, Hawthorne FC, Robert J-L, Delbove F, Welch MF, Raudsepp M (1999) Short-range order of cations in synthetic amphiboles along the richterite-pargasite join. *Eur J Mineral* 11:79-94
- Dick LA, Robinson GW (1979) Chlorine-bearing potassian hastingsite from a sphalerite skarn in southern Yukon. *Can Mineral* 17:25-26
- Dyar MD, McGuire AV, Mackwell SJ (1992) Fe³⁺/H⁺ and D/H in kaersutites: Misleading indicators of mantle source fugacities. *Geol* 20:565-568
- Dyar MD, Mackwell SJ, McGuire AV, Cross LR, Robertson JD (1993) Crystal chemistry of Fe³⁺ and H⁺ in mantle kaersutite: Implications for mantle metasomatism. *Am Mineral* 78:968-979
- Dyar MD, Gunter ME, Delaney JS, Lanzarotti A, Sutton SR (2002) Systematics in the structure and XANES spectra of pyroxenes, amphiboles, and micas as derived from oriented single crystals. *Can Mineral* 40:1375-1393

- Dyar MD, Agresti DG, Schaefer MW, Grant CA, Sklute EC (2006) Mössbauer Spectroscopy of Earth and Planetary Materials. *Ann Rev Earth Planet Sci* 34:83-125
- Eeckhout SG, De Grave E (2003) Evaluation of ferrous and ferric Mössbauer fractions. Part II. *Phys Chem Mineral* 30:142-146
- Enami M, Liou JG, Bird DK (1992) Cl-bearing amphibole in the Salton Sea geothermal system, California. *Can Mineral* 30:1077-1092
- Enders M, Speer D, Maresch WV, McCammon CA (2000) Ferric/ferrous iron ratios in sodic amphiboles: Mössbauer analysis, stoichiometry-based model calculations and the high-resolution microanalytical flank method. *Contrib Mineral Petrol* 140:135-147
- Evans BW, Yang H (1998) Fe-Mg order-disorder in tremolite-actinolite-ferro-actinolite at ambient and high temperature. *Am Mineral* 83:458-475
- Evans BW, Ghiroso MS, Yang H, Medenbach O (2001) Thermodynamics of the amphiboles: Anthophyllite-ferroanthophyllite and the ortho-clino phase loop. *Am Mineral* 86:640-651
- Garvie LAJ, Buseck PR (1998) Ratios of ferrous to ferric iron from nanometer-sized areas in minerals. *Nature* 396:667-670
- Garvie LAJ, Zega TJ, Rez P, Buseck PR (2004) Nanometer-scale measurements of $\text{Fe}^{3+}/\Sigma\text{Fe}$ by electron energy-loss spectroscopy: A cautionary note. *Am Mineral* 89:1610-1616
- Ghose S (1961) The crystal structure of cummingtonite. *Acta Crystallogr* 14:622-627
- Gibbs GV (1966) Untitled article. In: AGI Short Course Lecture Notes on Chain Silicates. p 1-23
- Gibbs GV (1969) The crystal structure of protoamphibole. *Mineral Soc Am Spec Pap* 2:101-110
- Gibbs GV, Bloss FD, Shell HR (1960) Protoamphibole, a new polytype. *Am Mineral* 45:974-989
- Gottschalk M, Andrut M, Melzer S (1999) The determination of the cummingtonite content of synthetic tremolite. *Eur J Mineral* 11:967-982
- Gunter ME, Dyar MD, Twamley B, Foit FF Jr, Cornelius S (2003) Composition, $\text{Fe}^{3+}/\Sigma\text{Fe}$, and crystal structure of non-asbestiform and asbestiform amphiboles from Libby, Montana, U.S.A. *Am Mineral* 88:1970-1978
- Hanisch K (1966) Messung des Ultrarot-Pleochroismus von Mineralen. VI. Der Pleochroismus des OH-Streckfrequenz in Riebeckit. *N Jahrb Mineral Monatsh* 109-112
- Hawthorne FC (1976) The crystal chemistry of the amphiboles. V. The structure and chemistry of arfvedsonite. *Can Mineral* 14:346-356
- Hawthorne FC (1978) The crystal chemistry of the amphiboles. VIII. The crystal structure and site-chemistry of fluor-riebeckite. *Can Mineral* 16:187-194
- Hawthorne FC (1979) The crystal chemistry of the amphiboles. X. Refinement of the crystal structure of ferroglaucophane and an ideal polyhedral model for clinoamphiboles. *Can Mineral* 17:1-10
- Hawthorne FC (1981) Crystal chemistry of the amphiboles. *Rev Mineral* 9A:1-102
- Hawthorne FC (1983a) The crystal chemistry of the amphiboles. *Can Mineral* 21:173-480
- Hawthorne FC (1983b) Quantitative characterization of site occupancies in minerals. *Am Mineral* 68:287-306
- Hawthorne FC (1983c) Characterization of the average structure of natural and synthetic amphiboles. *Per Mineral Roma* 52:543-581
- Hawthorne FC (1988) Mössbauer spectroscopy. *Rev Mineral* 18:255-340
- Hawthorne FC (1992) The role of OH and H_2O in oxide and oxysalt minerals. *Z Kristallogr* 201:183-206
- Hawthorne FC (1994) Structural aspects of oxides and oxysalt crystals. *Acta Crystallogr B* 50:481-510
- Hawthorne FC (1997) Short-range order in amphiboles: a bond-valence approach. *Can Mineral* 35:201-216
- Hawthorne FC (2006) Landmark Papers: Structure Topology. Mineralogical Society of Great Britain and Ireland, London
- Hawthorne FC, Della Ventura G (2007) Short-range order in amphiboles. *Rev Mineral* 67:xxx-yyy
- Hawthorne FC, Grundy HD (1972) Positional disorder in the A-site of clino-amphiboles. *Nature* 235:72
- Hawthorne FC, Grundy HD (1973a) The crystal chemistry of the amphiboles. I. Refinement of the crystal structure of ferrotschermakite. *Mineral Mag* 39:36-48
- Hawthorne FC, Grundy HD (1973b) The crystal chemistry of the amphiboles. II. Refinement of the crystal structure of oxykaersutite. *Mineral Mag* 39:390-400
- Hawthorne FC, Grundy HD (1976) The crystal chemistry of the amphiboles. IV. X-ray and neutron refinements of the crystal structure of tremolite. *Can Mineral* 14:334-345
- Hawthorne FC, Grundy HD (1977) The crystal chemistry of the amphiboles. III. Refinement of the crystal structure of a sub-silicic hastingsite. *Mineral Mag* 41:43-50
- Hawthorne FC, Grundy HD (1978) The crystal chemistry of the amphiboles. VII. The crystal structure and site chemistry of potassium ferri-taramite. *Can Mineral* 16:53-62
- Hawthorne FC, Harlow GE (2007) The crystal chemistry of Al-rich amphiboles: sadanagaite and potassic-ferrisadanagaite. *Can Mineral* (submitted)
- Hawthorne FC, Oberti R (2007) The crystal chemistry of the amphiboles. *Rev Mineral* 67:xxx-yyy
- Hawthorne FC, Oberti R, Ungaretti L, Grice JD (1992) Leakeite, $\text{Na Na}_2(\text{Mg}_2\text{Fe}^{3+}_2)\text{Si}_8\text{O}_{22}(\text{OH})_2$, a new alkali amphibole from the Kajlidongri manganese mine, Jhabua district, Madhya Pradesh, India. *Am Mineral* 77:1112-1115

- Hawthorne FC, Ungaretti L, Oberti R, Bottazzi P, Czamanske GK (1993) Li: An important component in igneous alkali amphiboles. *Am Mineral* 78:733-745
- Hawthorne FC, Ungaretti L, Oberti R, Cannillo E, Smelik EA (1994) The mechanism of ^{6}Li incorporation in amphiboles. *Am Mineral* 79:443-451
- Hawthorne FC, Oberti R, Cannillo E, Sardone N, Zanetti A, Grice JD, Ashley PM (1995) A new anhydrous amphibole from the Hoskins mine, Grenfell, New South Wales, Australia: Description and crystal structure of ungarettiite, $\text{Na Na}_2(\text{Mn}^{2+}_2\text{Mn}^{3+}_3)\text{Si}_8\text{O}_{22}\text{O}_2$. *Am Mineral* 80:165-172
- Hawthorne FC, Oberti R, Sardone N (1996a) Sodium at the A site in clin amphiboles: the effects of composition on patterns of order. *Can Mineral* 34:577-593
- Hawthorne FC, Oberti R, Ottolini L, Foord EE (1996b) Lithium-bearing fluor-arfvedsonite from Hurricane Mountain, New Hampshire: a crystal-chemical study. *Can Mineral* 34:1015-1019
- Hawthorne FC, Oberti R, Ungaretti L, Ottolini L, Grice JD, Czamanske GK (1996c) Fluor-ferro-leakeite, $\text{Na Na}_2(\text{Fe}_2^{2+}\text{Fe}_3^{2+}\text{Li})\text{Si}_8\text{O}_{22}\text{F}_2$, a new alkali amphibole from the Cañada Pinabete pluton, Questa, New Mexico, U.S.A. *Am Mineral* 81:226-228
- Hawthorne FC, Oberti R, Zanetti A, Czamanske GK (1998) The role of Ti in hydrogen-deficient amphiboles: Sodic-calcic and sodic amphiboles from Coyote Peak, California. *Can Mineral* 36:1253-1265
- Hawthorne FC, Cooper MA, Grice JD, Ottolini L (2000) A new anhydrous amphibole from the Eifel region, Germany: Description and crystal structure of obertiite, $\text{Na Na}_2(\text{Mg}_3\text{Fe}^{3+}\text{Ti}^{4+})\text{Si}_8\text{O}_{22}\text{O}_2$. *Am Mineral* 85:236-241
- Hawthorne FC, Oberti R, Cannillo E, Ottolini L, Roelofsen J, Martin RM (2001) Li-bearing arfvedsonitic amphiboles from the Strange Lake peralkaline granite, Quebec. *Can Mineral* 39:1161-1170
- Hawthorne FC, Schindler M, Sokolova E, Abdu J, Evans BW, Ishida K (2007) The crystal chemistry of the gedrite-group amphiboles: II: Stereochemistry and chemical relations. *Can Mineral* (submitted)
- Höfer HE, Brey GP, Schulz-Dobrick B, Oberhänsli R (1994) The determination of the iron oxidation state by the electron microprobe. *Eur J Mineral* 6:407-418
- King PL, Hervig RL, Holloway JR, Vennemann TW, Righter K (1999) Oxy-substitution and dehydrogenation in mantle-derived amphibole megacrysts. *Geochim Cosmochim Acta* 62:3635-3651
- King PL, Hervig RL, Holloway JR, Delaney JS, Dyar MD (2000) Partitioning of $\text{Fe}^{3+}/\text{Fe}^{\text{total}}$ between amphibole and basanitic melt as a function of oxygen fugacity. *Earth Planet Sci Lett* 178:97-112
- Krutov GA (1936) Dashkesanite, a new chlorine-bearing amphibole of the hastingsite group. *Izv Akad Nauk Ser Geol* 341-373 (in Russian)
- Kullerød K (1996) Chlorine-rich amphiboles: interplay between amphibole compositions and an evolving fluid. *Eur J Mineral* 8:355-370
- Leake BE (1968) A catalog of analyzed calciferous and subcalciferous amphiboles together with their nomenclature and associated minerals. *Geol Soc Am Spec Pap* 98
- Léger A, Rebbert C, Webster J (1996) Cl-rich biotite and amphibole from Black Rock Forest, Cornwall, New York. *Am Mineral* 81:495-504
- Maresch WV, Miede G, Czank M, Fuess H, Schreyer W (1991) Triclinic amphibole. *Eur J Mineral* 3:899-903
- McCammon CA (1994) A Mössbauer milliprobe: Practical considerations. *Hyperfine Interactions* 92:1235-1239
- McCormick KA, McDonald AM (1999) Chlorine-bearing amphiboles from the Fraser mine, Sudbury, Ontario, Canada: Description and crystal chemistry. *Can Mineral* 37:1385-1403
- McGuire AV, Dyar MD, Ward KW (1989) Neglected $\text{Fe}^{3+}/\text{Fe}^{2+}$ ratios: A study of Fe^{3+} content of megacrysts from alkali basalts. *Geol* 17:687-690
- McGuire AV, Dyar MD, Nielson JE (1991) Metasomatic oxidation of upper mantle peridotite. *Contrib Mineral Petrol* 107:252-264
- Mogessie A, Purtscheller F, Tessadri R (1986) High alumina calcic amphiboles (alumino pargasite-magnesio sadanagaite) from metabasites and metacarbonates of Central Oetzal, Eastern Alps (Northern Tyrol, Austria). *N Jahrb Mineral Abh* 154:21-39
- Moore PB (1969) Joesmithite: a novel amphibole crystal chemistry. *Mineral Soc Am Spec Pap* 2:111-115
- Moore PB, Davis AM, Van Derveer DG, Sen Gupta PK (1993) Joesmithite, a plumbous amphibole revisited and comments on bond valences. *Mineral Petrol* 48:97-113
- Morrison J (1991) Compositional constraints on the incorporation of Cl into amphiboles. *Am Mineral* 76:1920-1930
- Murad E, Cashion J (2004) Mössbauer Spectroscopy of Environmental Materials and Their Industrial Utilization. Kluwer, Dordrecht
- Nasir S, Al-Rawas AD (2006) Mössbauer characterization of upper mantle ferrikaersutite. *Am Mineral* 91:1163-1169
- Oberti R, Ghose S (1993) Crystal-chemistry of a complex Mn-bearing alkali amphibole ("tirodite") on the verge of exsolution. *Eur J Mineral* 5:1153-1160
- Oberti R, Ungaretti L, Cannillo E, Hawthorne FC (1993) The mechanism of Cl incorporation in amphibole. *Am Mineral* 78:746-752

- Oberti R, Ungaretti L, Cannillo E, Hawthorne FC, Memmi I (1995a) Temperature-dependent Al order-disorder in the tetrahedral double-chain of *C2/m* amphiboles. *Eur J Mineral* 7:1049-1063
- Oberti R, Sardone N, Hawthorne FC, Raudsepp M, Turnock AC (1995b) Synthesis and crystal-structure refinement of synthetic fluor-pargasite. *Can Mineral* 33:25-31
- Oberti R, Hawthorne FC, Cámara F, Raudsepp M (1998) Synthetic fluoro-amphiboles: site preferences of Al, Ga, Sc and inductive effects on mean bond-lengths of octahedra. *Can Mineral* 36:1245-1252
- Oberti R, Caballero JM, Ottolini L, López-Andrés S, Herreros V (2000) Sodic-ferripedrizite, a new monoclinic amphibole bridging the magnesium-manganese-lithium and the sodium-calcium groups. *Am Mineral* 85:578-585
- Oberti R, Cámara F, Caballero JM, Ottolini L (2003a) Sodic-ferri-ferropedrizite and ferri-clinoferroholmquistite: Mineral data and degree of order of the A-site cations in Li-rich amphiboles. *Can Mineral* 41:1345-1354
- Oberti R, Cámara F, Ottolini L, Caballero JM (2003b) Lithium in amphiboles: detection, quantification and incorporation mechanisms in the compositional space bridging sodic and ⁶Li amphiboles. *Eur J Mineral* 15:309-319
- Oberti R, Cámara F, Caballero JM (2004) Ferri-ottoliniite and ferriwhittakerite, two new end-members of the new Group 5 for monoclinic amphiboles. *Am Mineral* 89:888-893
- Oberti R, Hawthorne FC, Cannillo E, Cámara F (2007a) Long-range order in amphiboles. *Rev Mineral* 67:xxx-yyy
- Oberti R, Della Ventura G, Cámara F (2007b) New amphibole compositions. *Rev Mineral* 67:xxx-yyy
- Oberti R, Boiocchi M, Smith DC, Medenbach O (2007c) Aluminotaramite, alumino-magnesiotaramite, and fluoro-alumino-magnesiotaramite: mineral data and crystal chemistry. *Am Mineral* 92:1428-1435
- Ottolini L, Hawthorne FC (2001) SIMS ionization of hydrogen in silicates: A case study of kornepupine. *J Anal Atomic Spectrom* 16:1266-1270
- Ottolini L, Oberti R (2000) Accurate quantification of H, Li, Be, B, F, Ba, REE, Y, Th and U in complex matrices: a combined approach based on SIMS and single-crystal structure refinement. *Anal Chem* 72(16):3731-3738
- Ottolini L, Bottazzi P, Vannucci R (1993) Quantification of Li, Be and B in silicates by secondary ion mass spectrometry using conventional energy filtering. *Anal Chem* 65:1960-1968
- Ottolini L, Bottazzi P, Zanetti A, Vannucci R (1995) Determination of hydrogen in silicates by secondary ion mass spectrometry. *Analyst* 120:1309-1313
- Papike JJ, Ross M, Clarke JR (1969) Crystal chemical characterization of clinoamphiboles based on five new structure refinements. *Mineral Soc Am Spec Pap* 2:117-136
- Papike JJ, Cameron KL, Baldwin K (1974) Amphiboles and pyroxenes: characterization of OTHER than quadrilateral components and estimates of ferric iron from microprobe data. *Geol Soc Am Abstr Prog* 6:1053-1054
- Popp RK, Virgo D, Yoder HS Jr, Hoering TC, Phillips MW (1995) An experimental study of phase equilibria and Fe oxy-component in kaersutitic amphibole: implications for the f_{H_2} and $a_{\text{H}_2\text{O}}$ in the upper mantle. *Am Mineral* 80:534-548
- Popp RK, Hibbert HA, Lamb WM (2006) Oxy-amphibole equilibria in Ti-bearing calcic amphiboles: Experimental investigation and petrologic implications for mantle-derived amphiboles. *Am Mineral* 91:54-66
- Previde Massara E (1990) Studio cristallografico delle principali fasi mineralogiche delle eclogiti di Liset (Western Gneiss Region, Norvegia). PhD Dissertation, Università di Pavia, Italy
- Rastsvetaeva RK, Puscharovskii DY, Vinogradova RA, Pekov IV (1996) Crystal structure of dashkesanite. *Crystallogr Rep* 41(1):58-62
- Robinson K, Gibbs GV, Ribbe PH, Hall MR (1973) Cation distributions in three hornblendes. *Am J Sci* 273A:522-535
- Robinson P, Ross M, Jaffe HW (1971) Composition of the anthophyllite-gedrite series, comparisons of gedrite-hornblende, and the anthophyllite-gedrite solvus. *Am Mineral* 56:1004-1041
- Rossi G, Oberti R, Dal Negro A, Molin GM, Mellini M (1987) Residual electron density at the M2 site in *C2/c* clinopyroxenes: relationships with bulk chemistry and sub-solidus evolution. *Phys Chem Mineral* 14:514-520
- Sato H, Yamaguchi Y, Makino K (1997) Cl incorporation into successively zoned amphiboles from the Ramnes cauldron, Norway. *Am Mineral* 82:316-324
- Sawaki T (1989) Sadanagaite and subsilicic ferroan pargasite from thermally metamorphosed rocks in the Nogo-Hakusan area, central Japan. *Mineral Mag* 53:99-106
- Schindler M, Sokolova E, Abdu J, Hawthorne FC, Evans BW, Ishida K (2007) The crystal chemistry of the gedrite-group amphiboles. I: Crystal structure and site populations. *Can Mineral* (submitted)
- Schumacher JC (1991) Empirical ferric iron corrections: necessity, assumptions, and effects on selected geothermobarometers. *Mineral Mag* 55:3-18

- Schumacher JC (1997) Appendix 2. The estimation of the proportion of ferric iron in the electron-microprobe analysis of amphiboles. *Can Mineral* 35:238-246
- Schumacher JC (2007) *Metamorphic amphiboles: compositions and coexistence*. *Rev Mineral* 67: xxx-yyy
- Shannon RD (1976) Revised effective ionic radii and systematic studies of interatomic distances in halides and chalcogenides. *Acta Crystallogr A* 32:751-767
- Shimazaki H, Bunno M, Ozawa T (1984) Sadanagaite and magnesio-sadanagaite, new silica-poor members of calcic amphibole from Japan. *Am Mineral* 69:465-471
- Sokolova EV, Hawthorne FC, Kabalov Y, Schneider J, McCammon C (2000a) The crystal chemistry of potassic-ferrisadanagaite. *Can Mineral* 38:669-674
- Sokolova EV, Kabalov YuK, McCammon C, Schneider J, Konev, AA (2000b) Cation partitioning in an unusual strontian potassicrichterite from Siberia: Rietveld structure refinement and Mössbauer spectroscopy. *Mineral Mag* 64:19-24
- Sokolova EV, Hawthorne FC, Gorbatoa V, McCammon C, Schneider J (2001) Ferrian winchite from the Ilmen Mountains, Southern Urals, Russia, and some problems with the current scheme for amphibole nomenclature. *Can Mineral* 39:171-177
- Stout JH (1972) Phase petrology and mineral chemistry of coexisting amphiboles from Telemark, Norway. *J Petrol* 13:99-145
- Sueno S, Matsubara S, Gibbs GV, Boisen MB Jr (1998) A crystal chemical study of protoanthophyllite: orthoamphiboles with the protoamphibole structure. *Phys Chem Mineral* 25:366-377
- Suwa K, Enami M, Horiuchi T (1987) Chlorine-rich potassium hastingsite from West Ongul Island, Lützow-Holm Bay, East Antarctica. *Mineral Mag* 51:709-714
- Tait KT, Hawthorne FC, Grice JD, Ottolini L, Nayak VK (2005) Dellaventuraite, Na Na₂ (MgMn³⁺2Ti⁴⁺Li) Si₈O₂₂O₂, a new anhydrous amphibole from the Kajlidongri Manganese Mine, Jhabua District, Madhya Pradesh, India. *Am Mineral* 90:304-309
- Tiepolo M, Zanetti A, Oberti R (1999) Detection, crystal-chemical mechanisms and petrological implications of ¹⁶Ti⁴⁺ partitioning in pargasite and kaersutite. *Eur J Mineral* 11:345-354
- Tiepolo M, Zanetti A, Vannucci R (2005) Determination of lithium, beryllium and boron at trace levels by laser ablation-inductively couple plasma-sector field mass spectrometry. *Geostandards Geoanalytical Res* 29:211-224
- Ungaretti L (1980) Recent developments in X-ray single crystal diffractometry applied to the crystal-chemical study of amphiboles. *God Jugosl Cent Krist* 15:29-65
- Uvarova Y, McCammon C, Sokolova E, Hawthorne FC, Lobanov KV, Kazansky VI (2005) Fe³⁺ content and Ti⁴⁺ ordering in amphiboles from the Kola Superdeep Borehole: Correlation of crystal-chemical and Mössbauer measurements. GAC-MAC-CSPG-CSSS Joint Meeting, Halifax, Abstracts 30:197
- van Aken PA, Liebscher B (2002) Quantification of ferrous/ferric ratios in minerals: new evaluation schemes of Fe L_{2,3} electron energy-loss near-edge spectra. *Phys Chem Mineral* 29:188-200
- Vanko DA (1986) High-chlorine amphiboles from oceanic rocks: product of highly saline hydrothermal fluids? *Am Mineral* 71:51-59
- Völtinger M, Robert JL, Vielzeuf D, Neiva AMR (1985) Structural control of the chlorine content of OH-bearing silicates (micas and amphiboles). *Geochim Cosmochim Acta* 49:37-48
- Warren BE (1930) The crystal structure and chemical composition of the monoclinic amphiboles. *Z Kristallogr* 72:493-517
- Welch MD, Cámara F, Della Ventura G, Iezzi G (2007) Non-ambient *in situ* studies of amphiboles. *Rev Mineral* 67: xxx-yyy
- Whittaker EJW (1960) The crystal chemistry of the amphiboles. *Acta Crystallogr* 13:291-298
- Zanetti A, Vannucci R, Bottazzi P, Oberti R, Ottolini L (1996) Infiltration metasomatism at Lherz as monitored by systematic ion-microprobe investigations close to a hornblende vein. *Chem Geol* 134:113-133
- Zhu C, Xu H, Ilton ES, Veblen DR, Henry DJ, Tivey MK, Thompson G (1994) TEM-AEM observations of Cl-rich amphibole and biotite and possible petrologic implications. *Am Mineral* 79:909-920

APPENDIX 1: CRYSTAL-STRUCTURE REFINEMENTS OF AMPHIBOLE

- Bocchio R, Ungaretti L, Rossi G (1978) Crystal chemical study of eclogitic amphiboles from Alpe Arami, Lepontine Alps, Southern Switzerland. *Rend Soc Ital Mineral Petrol* 34:453-470
- Bojar H-P, Walitz F (2006) Fluor-magnesiohastingsite from Dealul Uroi (Hunedoara county, Romania): Mineral data and crystal structure of a new amphibole end-member. *Eur J Mineral* 18:503-508
- Boschmann K, Burns PC, Hawthorne FC, Raudsepp M, Turnock AC (1994) A-site disorder in synthetic fluor-edenite, a crystal structure study. *Can Mineral* 32:21-30
- Caballero JM, Monge A, La Iglesia A, Tornos F (1998) Ferri-clinoholmquistite, Li₂(Fe²⁺,Mg)₃Fe³⁺₂Si₈O₂₂(OH)₂, a new ⁶Li clin amphibole from the Pedriz Massif, Sierra de Guadarrama, Spanish Central System. *Am Mineral* 83:167-171

- Caballero JM, Oberti R, Ottolini L (2002) Ferripedrizite, a new monoclinic ^BLi amphibole end-member from the Eastern Pedriza Massif, Sierra de Guadarrama, Spain, and a restatement of the nomenclature of Mg-Fe-Mn-Li amphiboles. *Am Mineral* 87:976-982
- Cámara F, Oberti R (2005) The crystal-chemistry of holmquistites: Ferroholmquistite from Greenbushes (Western Australia) and hints for compositional constraints in ^BLi amphiboles. *Am Mineral* 90:1167-1176
- Cámara F, Oberti R, Iezzi G, Della Ventura G (2003) The $P2_1/m \leftrightarrow C2/m$ phase transition in synthetic amphibole Na NaMg Mg₅ Si₈ O₂₂ (OH)₂: thermodynamic and crystal-chemical evaluation. *Phys Chem Mineral* 30:570-581
- Cámara F, Oberti F, Della Ventura G, Welch MD, Mareschi WV (2004) The crystal-structure of synthetic NaNa₂Mg₅Si₈O₂₁(OH)₃, a triclinic $C\bar{1}$ amphibole with a triple-cell and excess hydrogen. *Am Mineral* 89:1464-1473
- Cameron M, Gibbs GV (1971) Refinement of the crystal structure of two synthetic fluor-richterites. *Carnegie Inst Wash Year Book* 70:150-153
- Cameron M, Gibbs GV (1973) The crystal structure and bonding of fluor-tremolite: a comparison with hydroxyl tremolite. *Am Mineral* 58:879-888
- Cameron M, Sueno S, Papike JJ, Prewitt CT (1983) High temperature crystal chemistry of K and Na fluor-richterites. *Am Mineral* 68:924-943
- Evans BW, Yang H (1998) Fe-Mg order-disorder in tremolite-actinolite-ferro-actinolite at ambient and high temperature. *Am Mineral* 83:458-475
- Evans BW, Ghiorso MS, Yang H, Medenbach O (2001) Thermodynamics of the amphiboles: Anthophyllite-ferroanthophyllite and the ortho-clino phase loop. *Am Mineral* 86:640-651
- Ghose S (1961) The crystal structure of cummingtonite. *Acta Crystallogr* 14:622-627
- Gibbs GV (1969) The crystal structure of protoamphibole. *Mineral Soc Am Spec Pap* 2:101-110
- Gunter ME, Dyar MD, Twamley B, Foit FF Jr, Cornelius S (2003) Composition, Fe³⁺/ΣFe, and crystal structure of non-asbestiform and asbestiform amphiboles from Libby, Montana, U.S.A. *Am Mineral* 88:1970-1978
- Hawthorne FC (1976) The crystal chemistry of the amphiboles. V. The structure and chemistry of arfvedsonite. *Can Mineral* 14:346-356
- Hawthorne FC (1978) The crystal chemistry of the amphiboles. VIII. The crystal structure and site-chemistry of fluor-riebeckite. *Can Mineral* 16:187-194
- Hawthorne FC (1979) The crystal chemistry of the amphiboles. X. Refinement of the crystal structure of ferroglaucophane and an ideal polyhedral model for clinoamphiboles. *Can Mineral* 17:1-10
- Hawthorne FC (1983) The crystal chemistry of the amphiboles. *Can Mineral* 21:173-480
- Hawthorne FC, Grundy HD (1973a) The crystal chemistry of the amphiboles. I. Refinement of the crystal structure of ferrotschermakite. *Mineral Mag* 39:36-48
- Hawthorne FC, Grundy HD (1973b) The crystal chemistry of the amphiboles. II. Refinement of the crystal structure of oxykaersutite. *Mineral Mag* 39:390-400
- Hawthorne FC, Grundy HD (1976) The crystal chemistry of the amphiboles. IV. X-ray and neutron refinements of the crystal structure of tremolite. *Can Mineral* 14:334-345
- Hawthorne FC, Grundy HD (1977) The crystal chemistry of the amphiboles. III. Refinement of the crystal structure of a sub-silicic hastingsite. *Mineral Mag* 41:43-50
- Hawthorne FC, Grundy HD (1978) The crystal chemistry of the amphiboles. VII. The crystal structure and site chemistry of potassian ferri-taramite. *Can Mineral* 16:53-62
- Hawthorne FC, Harlow GE (2007) The crystal chemistry of Al-rich amphiboles: sadanagaite and potassic-ferrisadanagaite. *Can Mineral* (submitted)
- Hawthorne FC, Griep JL, Curtis L (1980) A three amphibole assemblage from the Tallan Lake sill, Peterborough County, Ontario. *Can Mineral* 18:275-284
- Hawthorne FC, Oberti R, Ungaretti L, Grice JD (1992) Leakeite, NaNa₂(Mg₂Fe³⁺)₂Si₈O₂₂(OH)₂, a new alkali amphibole from the Kajlidongri manganese mine, Jhabua district, Madhya Pradesh, India. *Am Mineral* 77:1112-1115
- Hawthorne FC, Ungaretti L, Oberti R, Bottazzi P, Czamanske GK (1993) Li: An important component in igneous alkali amphiboles. *Am Mineral* 78:733-745
- Hawthorne FC, Ungaretti L, Oberti R, Cannillo E, Smelik EA (1994) The mechanism of ⁶Li incorporation in amphiboles. *Am Mineral* 79:443-451
- Hawthorne FC, Oberti R, Cannillo E, Sardone N, Zanetti A, Grice JD, Ashley PM (1995) A new anhydrous amphibole from the Hoskins mine, Grenfell, New South Wales, Australia: Description and crystal structure of ungarettiite, NaNa₂(Mn²⁺₂Mn³⁺₃)Si₈O₂₂O₂. *Am Mineral* 80:165-172
- Hawthorne FC, Oberti R, Sardone N (1996a) Sodium at the A site in clinoamphiboles: the effects of composition on patterns of order. *Can Mineral* 34:577-593
- Hawthorne FC, Oberti R, Ottolini L, Foord EE (1996b) Lithium-bearing fluor-arfvedsonite from Hurricane Mountain, New Hampshire: a crystal-chemical study. *Can Mineral* 34:1015-1019

- Hawthorne FC, Oberti R, Ungaretti L, Ottolini L, Grice JD, Czamanske GK (1996c) Fluor-ferro-leakeite, $\text{NaNa}_2(\text{Fe}_2^{2+}\text{Fe}_3^{2+}\text{Li})\text{Si}_8\text{O}_{22}\text{F}_2$, a new alkali amphibole from the Cañada Pinabete pluton, Questa, New Mexico, U.S.A. *Am Mineral* 81:226-228
- Hawthorne FC, Oberti R, Ungaretti L, Grice JD (1996d) A new hyper-calcic amphibole with Ca at the A site: Fluor-cannilloite from Pargas, Finland. *Am Mineral* 81:995-1002
- Hawthorne FC, Oberti R, Zanetti A, Czamanske GK (1998) The role of Ti in hydrogen-deficient amphiboles: Sodic-calcic and sodic amphiboles from Coyote Peak, California. *Can Mineral* 36:1253-1265
- Hawthorne FC, Cooper MA, Grice JD, Ottolini L (2000) A new anhydrous amphibole from the Eifel region, Germany: Description and crystal structure of obertiite, $\text{NaNa}_2(\text{Mg}_3\text{Fe}^{3+}\text{Ti}^{4+})\text{Si}_8\text{O}_{22}\text{O}_2$. *Am Mineral* 85:236-241
- Hawthorne FC, Oberti R, Cannillo E, Ottolini L, Roelofsen J, Martin RM (2001) Li-bearing arfvedsonitic amphiboles from the Strange Lake peralkaline granite, Quebec. *Can Mineral* 39:1161-1170
- Hawthorne FC, Oberti R, Martin RF (2006) Short-range order in amphiboles from the Bear Lake diggings, Ontario. *Can Mineral* 44:1171-1179
- Hawthorne FC, Schindler M, Sokolova E, Abdu J, Evans BW, Ishida K (2007) The crystal chemistry of the gedrite-group amphiboles: II: Stereochemistry and chemical relations. *Can Mineral* (submitted)
- Karanovic LJ, Krstanovic I, Ungaretti L (1990) Crystal structure and cation distribution in hornblendes. *Bulletin, Academie Serbe des Sciences et des Arts, Classe des Sciences Mathematiques et Naturelles, Sciences Naturelles* 32:21-28
- Makino K, Tomita K (1989) Cation distribution in the octahedral sites of hornblendes. *Am Mineral* 74:1097-1105
- Mancini F, Sillanpää R, Marshall B, Papunen H (1996) Magnesian hornblende from a metamorphosed ultramafic body in Southwestern Finland: crystal chemistry and petrological implications. *Can Mineral* 34:835-844
- Matsubara S, Miyawaki R, Kurosawa M, Suzuki Y (2002) Potassicleakeite, a new amphibole from the Tanohata mine, Iwate prefecture, Japan. *J Mineral Petrol Sci* 97:177-184
- Mitchell JT, Bloss FD, Gibbs GV (1971) Examination of the actinolite structure and four other $C2/m$ amphiboles in terms of double bonding. *Z Kristallogr* 133:273-300
- Moore PB (1969) Joesmithite: a novel amphibole crystal chemistry. *Mineral Soc Am Spec Pap* 2:111-115
- Moore PB, Davis AM, Van Derveer DG, Sen Gupta PK (1993) Joesmithite, a plumbous amphibole revisited and comments on bond valences. *Mineral Petrol* 48:97-113
- Oberti R, Ghose S (1993) Crystal-chemistry of a complex Mn-bearing alkali amphibole ("tirodite") on the verge of exsolution. *Eur J Mineral* 5:1153-1160
- Oberti R, Ungaretti L, Cannillo E, Hawthorne FC (1992) The behaviour of Ti in amphiboles. I. Four- and six-coordinate Ti in richterite. *Eur J Mineral* 3:425-439
- Oberti R, Ungaretti L, Cannillo E, Hawthorne FC (1993a) The mechanism of Cl incorporation in amphibole. *Am Mineral* 78:746-752
- Oberti R, Hawthorne FC, Ungaretti L, Cannillo E (1993b) The behaviour of Mn in amphiboles: Mn in richterite. *Eur J Mineral* 5:43-52
- Oberti R, Hawthorne FC, Ungaretti L, Cannillo E (1995a) ⁶Al disorder in amphiboles from mantle peridotites. *Can Mineral* 33:867-878
- Oberti R, Ungaretti L, Cannillo E, Hawthorne FC, Memmi I (1995b) Temperature-dependent Al order-disorder in the tetrahedral double-chain of $C2/m$ amphiboles. *Eur J Mineral* 7:1049-1063
- Oberti R, Sardone N, Hawthorne FC, Raudsepp M, Turnock AC (1995c) Synthesis and crystal-structure refinement of synthetic fluor-pargasite. *Can Mineral* 33:25-31
- Oberti R, Hawthorne FC, Raudsepp M (1997) The behaviour of Mn in amphiboles: Mn in synthetic fluor-edenite and synthetic fluor-pargasite. *Eur J Mineral* 9:115-122
- Oberti R, Hawthorne FC, Cámara F, Raudsepp M (1998) Synthetic fluoro-amphiboles: site preferences of Al, Ga, Sc and inductive effects on mean bond-lengths of octahedra. *Can Mineral* 36:1245-1252
- Oberti R, Hawthorne FC, Cámara F, Raudsepp M (1999) Unusual ⁶M³⁺ cations in synthetic amphiboles with nominal fluoro-eckermannite composition: Deviations from stoichiometry and structural effects of the cummingtonite component. *Am Mineral* 84:102-111
- Oberti R, Caballero JM, Ottolini L, López-Andrés S, Herreros V (2000) Sodic-ferripedrizite, a new monoclinic amphibole bridging the magnesium-manganese-lithium and the sodium-calcium groups. *Am Mineral* 85:578-585
- Oberti R, Cámara F, Caballero JM, Ottolini L (2003a) Sodic-ferri-ferropedrizite and ferri-clinoferroholmquistite: Mineral data and degree of order of the A-site cations in Li-rich amphiboles. *Can Mineral* 41:1345-1354
- Oberti R, Cámara F, Ottolini L, Caballero JM (2003b) Lithium in amphiboles: detection, quantification and incorporation mechanisms in the compositional space bridging sodic and ⁶Li amphiboles. *Eur J Mineral* 15:309-319
- Oberti R, Boiocchi M, Smith DC (2003c) Fluoronyböite from Jianchang (Su-Lu, China) and nyböite from Nybø (Nordfjord, Norway): description and comparison of two high-pressure amphibole end-members. *Mineral Mag* 67:769-782

- Oberti R, Cámara F, Caballero JM (2004) Ferri-ottoliniite and ferriwhittakerite, two new end-members of the new Group 5 for monoclinic amphiboles. *Am Mineral* 89:888-893
- Oberti R, Boiocchi M, Smith DC, Medenbach O (2007) Aluminotaramite, alumino-magnesirotaramite, and fluoro-alumino-magnesirotaramite: Mineral data and crystal chemistry. *Am Mineral* 92:1428-1435
- Papike JJ, Ross M, Clarke JR (1969) Crystal chemical characterization of clinoamphiboles based on five new structure refinements. *Mineral Soc Am Spec Pap* 2:117-136
- Pechar F, Fuess H, Joswig W (1989) Refinement of the crystal structure of kaersutite (Vlci Hora Bohemia) from neutron diffraction. *N Jahrb Mineral Mh* 1989:137-143
- Phillips MW, Popp RK, Clowe CA (1988) Structural adjustments accompanying oxidation-dehydrogenation in amphiboles. *Am Mineral* 73:500-506
- Phillips MW, Draheim JE, Popp RK, Clowe CA, Pinkerton AA (1989) Effects of oxidation-dehydrogenation in tschermakitic hornblende. *Am Mineral* 74:764-773
- Pushcharovskii DYu, Lebedeva YuS, Pekov IV, Ferraris G, Novakova AA, Ivaldi G (2003) Crystal structure of magnesiokatophorite. *Crystallogr Rep* 48:16-23
- Rastsvetaeva RK, Puscharovskii DY, Vinogradova RA, Pekov IV (1996) Crystal structure of dashkesanite. *Crystallogr Rep* 41:58-62
- Redhammer GJ, Roth G (2002) Crystal structure and Mössbauer spectroscopy of the synthetic amphibole potassic-ferri-ferrorichterite at 298 K and low temperatures (80–110 K). *Eur J Mineral* 14:105-114
- Robinson GW, Grice JD, Gault RA, Lalonde AE (1997) Potassicpargasite, a new member of the amphibole group from Pargas, Turku-Pori, Finland. *Can Mineral* 35:1535-1540
- Robinson K, Gibbs GV, Ribbe PH, Hall MR (1973) Cation distributions in three hornblendes. *Am J Sci* 273A:522-535
- Schindler M, Sokolova E, Abdu J, Hawthorne FC, Evans BW, Ishida K (2007) The crystal chemistry of the gedrite-group amphiboles: I: Crystal structure and site populations. *Can Mineral* (submitted)
- Sokolova EV, Hawthorne FC, Kabalov Y, Schneider J, McCammon C (2000a) The crystal chemistry of potassic-ferrisadanagaite. *Can Mineral* 38:669-674
- Sokolova EV, Kabalov YuK, McCammon C, Schneider J, Konev, AA (2000b) Cation partitioning in an unusual stromian potassicrichterite from Siberia: Rietveld structure refinement and Mössbauer spectroscopy. *Mineral Mag* 64:19-24
- Sokolova EV, Hawthorne FC, Gorbatova V, McCammon C, Schneider J (2001) Ferrian winchite from the Ilmen Mountains, Southern Urals, Russia, and some problems with the current scheme for amphibole nomenclature. *Can Mineral* 39:171-177
- Sueno S, Matsubara S, Gibbs GV, Boisen MB Jr (1998) A crystal chemical study of protoanthophyllite: orthoamphiboles with the protoamphibole structure. *Phys Chem Mineral* 25:366-377
- Tait T, Hawthorne FC, Grice JD, Ottolini L, Nayak VK (2005) Dellaventurite, $\text{NaNa}_2(\text{MgMn}^{3+}_2\text{Ti}^{4+}\text{Li})\text{Si}_8\text{O}_{22}\text{O}_2$, a new anhydrous amphibole from the Kajlidongri Manganese Mine, Jhabua District, Madhya Pradesh, India. *Am Mineral* 90:304-309
- Tartarotti P, Caucia F (1993) Coexisting cummingtonite - sodic amphibole pair in metaquartzites from the ophiolite's sedimentary cover (St. Marcel Valley, Italian Western Alps): A X-ray structure refinement and petrology study. *N Jahrb Mineral Abh* 165:223-243
- Tiepolo M, Zanetti A, Oberti R (1999) Detection, crystal-chemical mechanisms and petrological implications of $^{63}\text{Ti}^{4+}$ partitioning in pargasite and kaersutite. *Eur J Mineral* 11:345-354
- Ungaretti L (1980) Recent developments in X-ray single crystal diffractometry applied to the crystal-chemical study of amphiboles. *God Jugosl Cent Krist* 15:29-65
- Walitzi EM, Walter F (1981) Verfeinerung der Kristallstruktur eines basaltischen Magnesio-Hastingsites. *Z Kristallogr* 156:197-208
- Walitzi EM, Ettinger K (1986) Verfeinerung der Kristallstruktur eines Tremolites vom Ochsenkogel (Gleinalpe/Steiermark), Oesterreich. *N Jahrb Mineral Mh* 1986:360-366
- Warren BE (1930) The crystal structure and chemical composition of the monoclinic amphiboles. *Z Kristallogr* 72:493-517
- Yang H, Evans BW (1996) X-ray structure refinements of tremolite at 140 and 295K: Crystal chemistry and petrologic implications. *Am Mineral* 81:1117-1125
- Yang H, Konzett J, Prewitt CT, Fei Y (1999) Single-crystal structure refinement of synthetic $^{\text{M4}}\text{K}$ -substituted potassic richterite, $\text{K}(\text{KCa})\text{Mg}_5\text{Si}_8\text{O}_{22}(\text{OH})_2$. *Am Mineral* 84:681-684